BIOPROTA

Key Issues in Biosphere Aspects of Assessment of the Long-term Impact of Contaminant Releases Associated with Radioactive Waste Management

C-14 in the Biosphere: Terrestrial Model-Data Comparisons and Review of Carbon Uptake by Fish

Mike Thorne, Karen Smith, Ivan Kovalets, Rodolfo Avila, Russell Walke

QRS-1769B-1, Version 2.0, August 2018

PREFACE

BIOPROTA is an international collaboration forum which seeks to address key uncertainties in the assessment of environmental and human health impacts in the long term arising from release of radionuclides and other contaminants as a result of radioactive waste management practices. It is understood that there are radio-ecological and other data and information issues that are common to specific assessments required in many countries. The mutual support within a commonly focused project is intended to make more efficient use of skills and resources, and to provide a transparent and traceable basis for the choices of parameter values, as well as for the wider interpretation of information used in assessments. A list of sponsors of BIOPROTA and other information is available at www.bioprota.org.

The general objectives of BIOPROTA are to make available the best sources of information to justify modelling assumptions made within radiological and related assessments of radioactive waste management. Particular emphasis is placed on key data required for the assessment of long-lived radionuclide migration and accumulation in the biosphere, and the associated radiological impact, following discharge to the environment or release from solid waste disposal facilities. The programme of activities is driven by assessment needs identified from previous and on-going assessment projects. Where common needs are identified within different assessment projects in different countries, a common effort can be applied to finding solutions.

This report describes model-data comparisons for radiocarbon measurements in Finnish boreal forest and a Canadian swamp. Analysis of the boreal forest dataset shows that isotopic signatures arising from the soil are rapidly damped in the first few metres of the atmosphere above the soil and that this can be readily represented in a simple dispersion model using physically reasonable parameter values. Analysis of the data for the Canadian swamp emphasises the need for a two-layer model, with groundwater-driven transport in the lower layer, where biological activity is limited, contrasting with dominance of uptake in biomass, effects of mineralisation and losses by volatilisation in the upper layer.

The report also presents a review of carbon uptake in freshwater lacustrine environments. The review emphasises the importance of considering both terrestrial and aquatic sources of carbon, and distinctions in the use of these different sources at different trophic levels and by functionally distinct components of lacustrine food-webs.

The financial support provided for the project by French National Radioactive Waste Management Agency (ANDRA), National Cooperative for the Disposal of Radioactive Waste (Nagra, Switzerland), Nuclear Waste Management Organization of Japan (NUMO), Nuclear Waste Management Organization (NWMO, Canada), Posiva Oy (Finland), Swedish Nuclear Fuel and Waste Management Company (SKB) and the Swedish Radiation Safety Authority (SSM) is gratefully acknowledged.

The report is presented as working material for information. The content may not be taken to represent the official position of the organisations involved. All material is made available entirely at the user's risk.

Version History

Version 1.0: First full draft compiled by Russell Walke based on input from Mike Thorne, Karen Smith, Ivan Kovalets and Rodolfo Avila. Distributed to BIOPROTA project sponsor organisations for comment on 11 May 2018.

Version 2.0: Revised to address comments from G M Smith, M A Pogson and from BIOPROTA project sponsor and participant organisations. Distributed to BIOPROTA members on 9 August 2018.

CONTENTS

1. INTRODUCTION

C-14 can be a radionuclide of importance in assessing the safety of discharges to the environment from operating facilities (including nuclear power plants and existing waste disposal facilities), historical facilities (including historical waste disposals) and potential future facilities (e.g. planned or proposed power plants and waste disposal facilities). The behaviour of C-14 in the biosphere has, therefore, been a topic of interest to the international collaborative BIOPROTA forum for more than a decade.

In the context of disposal of solid radioactive wastes in geological repositories, releases of C-14 are likely to enter the biosphere dissolved in groundwater or incorporated in bulk gases such as hydrogen and methane originating in corrosion of metals in the repository or in microbial degradation of organic materials. This contrasts with more usual routes of release of C-14 from operating nuclear installations, as these releases are typically either to surface waters or direct to atmosphere.

When C-14 enters the soil zone, either dissolved in groundwater or in gaseous form, it is subject to metabolism by microbial communities and uptake by plants both through the roots and through the foliage. It can then be incorporated in the biomass by photosynthesis. The degree to which different chemical forms of C-14 are incorporated into biomass by these processes has been investigated in the context of agricultural ecosystems and this work has been reviewed previously within BIOPROTA (see below). In this report, a similar analysis is undertaken for a forest ecosystem, using natural variations in isotopic ratios of C-13 and C-14 relative to C-12 to investigate the processes of transport through both the soil and the overlying plant canopy (Section 2). Thus, the work reported here is a natural extension of previous analyses, as well as drawing on the existing, extensive understanding of processes of temperature, momentum and contaminant transport in forest ecosystems.

If C-14 is transported in a groundwater plume, it is typically subject to very little retardation. However, if that plume then encounters a system rich in organic matter, the C-14 may be either incorporated into the biomass or volatilised and lost to the atmosphere. The Duke Swamp study, described in Section 3, provides a valuable field test of the processes governing C-14 transport, accumulation and loss in such a system. In the Duke Swamp system, C-14 is being leached from a near-surface waste-disposal facility, transported downslope in solution in groundwater flowing through mineral sediments and is then being accumulated in the biomass of a wetland at the base of the slope. As data are available on the rate of release from the wastes, on concentrations in the groundwater plume, and on concentrations in vegetation in the wetland, a basis existed for developing a quantitative model of the processes involved. Development of such a model is the focus of Section 3. It is intended that this model should be of use in the formulation and application of assessment models for other contexts in which plumes of groundwater contaminated with C-14 are projected to interact with wetland vegetation, particularly where the wetland constitutes a discharge area for the contaminant plume.

Previously, discharge to surface-water bodies of C-14 being transported in a groundwater plume has been given only limited attention within BIOPROTA, though it has been of interest in some national programmes for solid radioactive waste management. In this report, an initial review is presented in Section 4 of the cycling of carbon in freshwater lakes and the sources of carbon used by various types of biota, and specifically by freshwater fish. This review is intended to provide a basis for future modelling studies of how C-14 entering a freshwater lake or its associated catchment in a contaminated, discharging groundwater plume is distributed between the various terrestrial and aquatic carbon ‘pools’ in the environment, how the specific activities of those pools change with time, and how this, in turn, affects the specific activities of biota and of humans consuming aquatic foods from the contaminated environment.

This report presents the results of a BIOPROTA project undertaken during 2017-18, with the support of seven sponsors from amongst the forum, as described in the preface. The project has been co-ordinated by a Technical Support Team comprising Quintessa Limited, Mike Thorne and Associates Limited and RadEcol Consulting Limited. Contribution to the project has been invited from the BIOPROTA membership, whereby Posiva supported the provision of input by Facilia AB.

Previous studies, the project objectives and the report structure are described in the sub-sections below.

1.1 BACKGROUND

The previous BIOPROTA projects and workshops concerning C-14 in the biosphere are listed below.

- A review of C-14 assessment models [Sheppard and Thorne, 2005].
- Modelling of C-14 uptake in agricultural crops [Limer et al., 2012; Norris et al., 2011; Mobbs et al., 2013].
- A series of workshops focussing on C-14 behaviour [Smith and Smith, 2014; Smith, 2015].
- Terrestrial model-data comparisons for operational atmospheric and long-term sub-surface releases [Limer et al., 2017].

Independently of the BIOPROTA studies, several waste management and research organisations have been conducting research, further developing their in-house C-14 modelling capabilities, and testing their conceptual models against real world datasets.

- Radioactive Waste Management Limited in the United Kingdom has undertaken a multi-year field and laboratory research programme, with associated modelling, relating to sub-surface C-14 release to agricultural soils and potential uptake into crops [Hoch et al., 2014].

- Institut de Radioprotection et de Sûreté Nucléaire (IRSN) have further developed and applied models for C-14 uptake by plants following atmospheric releases [Aulagnier et al., 2012; 2013; Le Dizès et al., 2012].

- The Swedish Nuclear Fuel and Waste Management Company (SKB) has further developed its models for C-14 release and behaviour in mire and agricultural ecosystems in support of assessments for radioactive waste disposal [Saetre et al., 2013].

- The Swedish Radiation Safety Authority (SSM) have developed a modelling capability for uptake by plants for both sub-surface and atmospheric release contexts [Limer et al., 2013; 2015].

1.2 OBJECTIVES

The objectives of the project reported here were to develop further understanding of the behaviour of C-14 in the biosphere and to build further confidence in its representation within assessment models. Specifically, attention is focused on the transport of C-14 in groundwater and in the gas phase, accumulation of that C-14 in biota and losses of C-14 from the local biosphere by various volatilisation processes. The project included the following activities.

- Modelling of C-14 within a Finnish boreal forest system and comparison against high resolution observational data.
- Further modelling of C-14 from an historical near-surface waste disposal facility and its migration to the Duke Swamp area within the Chalk River site in Canada, along with comparison against observational data.
- Review of carbon uptake by fish, including timescales for potential equilibrium with the surrounding water/sediment environment and their food source.

1.3 REPORT STRUCTURE

The report is structured in the following way.

- The Finnish forest modelling model-data comparison exercise is covered in Section 2.
- The Duke Swamp modelling model-data comparison scenario is described in Section 3.
- An initial review of carbon sources for freshwater lakes is presented in Section 4.
- Conclusions are then presented in Section 5.
- References are provided in Section 6.

The data set used as a basis for the Duke Swamp modelling is presented in Appendix A.

2. FINNISH FOREST SCENARIO

The data for the Finnish forest case are described in Section 2.1. Modelling of the scenario undertaken on behalf of Posiva is then described in Section 2.2. Calculations exploring the data and scenario that have been undertaken by the project Technical Support Team are described in Section 2.3. Conclusions from the exercise are summarised in Section 2.4. Throughout, the focus is on whether the model can explain the observed naturally occurring C-13 and C-14 to C-12 ratios in air (including the soil atmosphere, below-canopy atmosphere and above-canopy atmosphere) and on characterising CO_2 emission from the soil, transmission through the forest canopy, and uptake into that canopy for use in photosynthesis.

2.1 FINNISH FOREST DATA SET

The University of Helsinki has been monitoring material and energy flows in atmosphere-vegetation-soils at different spatial and temporal scales at four locations in Finland (see Figure 1) for more than twenty years [Vesala et al., 1998]. The "Station for Measuring Ecosystem-Atmosphere Relations" programme (SMEAR) programme provides a data set for research understanding.

Figure 1: Location of the four SMEAR research stations in Finland.

The SMEAR II station (see Figure 2), established in 1995, is in Hyytiälä, Southern Finland (61° 51' N, 24° 17' E, 181 m above sea level). The terrain around the station is representative of the boreal coniferous forest. The 55-year old (in 2017) Scots pine (*Pinus sylvestris* L.) dominated stand is homogenous for about 200 m in all directions, extending to the north for about 1.2 km. The terrain is subject to modest height variation. The annual mean temperature is 3 °C and precipitation is 700 mm. It has several operational units that reach into and above the stand canopy: a 128 m high tower for atmospheric and flux measurements, one 18 m tower for irradiation and flux measurements, another for tree physiology measurements and a 35 m walk-up tower for aerosol measurements.

The station is run in co-operation of the Division of Atmospheric Sciences (from the Department of Physical Sciences) and the department of Forest Ecology in the University of Helsinki. The institutes cooperate in research on ecosystem-atmosphere relations, and are part of the Research Unit on

Physics, Chemistry and Biology of Atmospheric Composition and Climate Change, which is a Center of Excellence of the Academy of Finland, as well as the Nordic Center of Excellence Research unit BACCI (Biosphere-Aerosol-Cloud-Climate Interactions). Staff from the University of Helsinki have performed soil and soil-water measurements on two water catchment areas. Near the station, solar irradiance from 280 to 800 nm is measured with a radio spectrometer.

Atmospheric and soil CO_2 samples were collected using sieve cartridges [Palonen, 2015] from April 2012 to April 2013. The atmospheric samples were collected monthly from 1, 16, 67 and 125 m altitudes with a short collection time of 10 minutes, at 10-12 am (local time). Some samples were also taken between the monthly samples to increase the time resolution at selected time intervals. Soil CO_2 samples were taken roughly monthly from April to October in the afternoon from soil heights of 0.1, 0.04, -0.02, -0.08, -0.028, -0.48, -0.69 m (from the mineral-organic boundary), and from an 8-litre soil chamber.

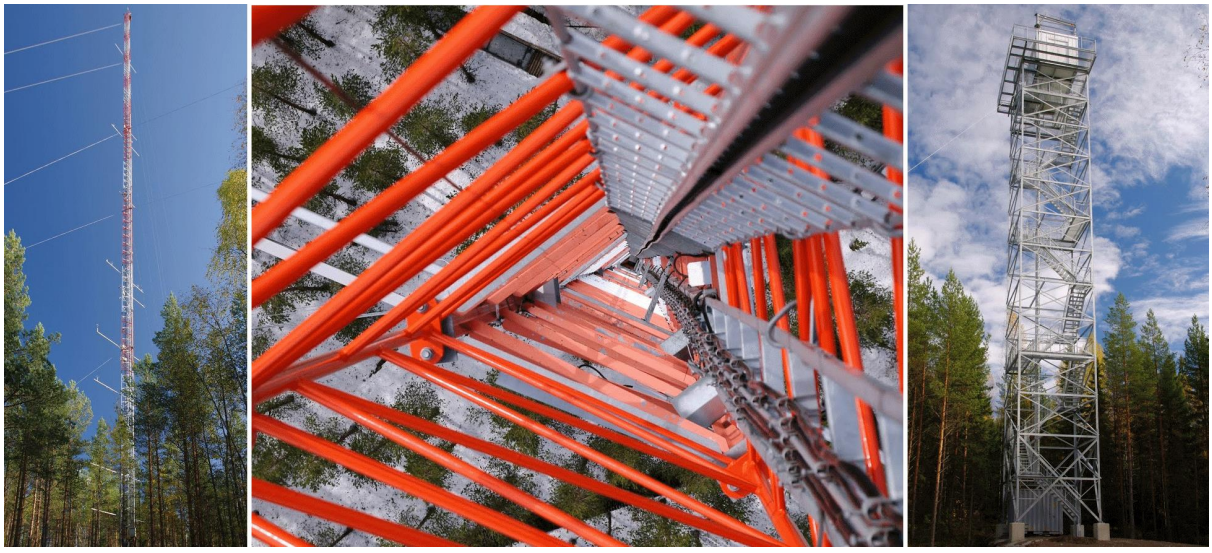

Figure 2: SMEAR II mast and measurement tower.

The soil profile chambers were first scrubbed from CO_2, after which the accumulation of CO_2 was monitored for 20-30 minutes to check that enough CO_2 had accumulated. After this, the sample gas was circulated through the molecular sieve sampling cartridge, which traps all the CO_2 in the gas flow. Some of the profile tubes had accumulated too much water for an acceptable sample to be taken. This was especially the case with profile tubing at depth 0.028 m, and also with other lower depths in late autumn and early spring. In some cases, the sample size was enough for the AMS C-14 measurement, but no separate fraction for $\delta^{13}C$ measurement could be taken. For these samples the $\delta^{13}C$ based fractionation correction was made with the assumed $\delta^{13}C$ value of -20 ‰ that is typical of plant biomass.

The collected samples were graphitized in the Laboratory of Chronology, University of Helsinki, and measured at three AMS laboratories. The laboratories were the Vienna Environmental Research Accelerator (VERA), the Tandem Laboratory at the University of Uppsala, and Ion beam analysis laboratory, University of Helsinki.

The C-14 fluxes, given as $\Delta^{14}C$, are calculated using:

$$\Delta^{14}C = \left[F^{14}C \times e^{-\lambda(y-1950)}\right] \times 1000 \quad (1)$$

Here, the fraction of modern C-14, $F^{14}C = Rsample/Rstandard$ [Reimer et al., 2004], denotes the ratio of $\delta^{13}C$ -corrected measured C-14/C-13 ratios of a sample and a standard concentration, y is the year

of measurement and λ = 1/8267 y^{-1} is the decay rate of radiocarbon. The standard concentration, $R_{standard}$, represents the atmospheric radiocarbon concentration in 1950, and is slightly decayed relative to the present.

Palonen et al. [2018] note that, while the $F^{14}C$ is suitable for radiocarbon age determination and calibration purposes, as an old sample and the standard decay at the same rate and hence the ratio remains constant irrespective of the time of measurement, the $\Delta^{14}C$ is absolute as defined and represents the difference of sample C-14 concentration from the 1950 atmospheric C-14 concentration [Stuiver and Polach, 1977], the value of which does not change with time even though the international standard representing it has already decayed slightly. Positive $\Delta^{14}C$ values hence indicate larger C-14 concentrations than the 1950 atmosphere had at the time. Negative $\Delta^{14}C$ values indicate lower C-14 concentrations, e.g. that the bulk of the carbon has been isolated from the active carbon cycle long enough for significant radioactive decay to have occurred.

2.2 MODELLING AND INTERPRETATION UNDERTAKEN ON BEHALF OF POSIVA

The following sub-section describes work undertaken on behalf of Posiva by Kovalets and Avila [2018]. This work used a detailed, 1D, physically based model to simulate CO_2 profiles and isotopic ratio variations with height within and above the forest canopy. Results were reported relating the C-14 flux at the soil surface to variations in C-14 concentration with height.

2.2.1 Setting Basic Model Parameters for Simulation of CO_2 Profiles

The simulations were performed in a domain extending vertically up to reference height z_r = 50 m from which measured CO_2 concentrations were taken as reference values and were used to specify the upper boundary condition.

The average value of the frontal area per unit volume $\bar{a}$ has been estimated using the dependence of that parameter on LAI derived in [Kovalets et al., 2018] and was estimated equal to $\bar{a} \approx 0.045$ m^{-1}. The values of the micrometeorological parameters r, c_d, c_σ, β_1, c_1 were taken to be the same as in previous work [Kovalets et al., 2018]: r = 0.1 and c_d = 0.25, c_σ = 1.3, c_1 = 4.86, β_1 = 1.3. The value of β_N was specified using measurements of friction velocity and horizontal velocity interpolated to canopy height, available in the SMEAR database. The average value obtained was β_N = 0.285, which is close to the reference value β_N = 0.3 provided by [Harman and Finnigan, 2008]. For the turbulent Schmidt number S_∞ inside the canopy, the formula in [Kovalets et al., 2018] was used, with parameter values S^n_∞ = 0.52, s_g = 0.16 (for unstable conditions), s_g = 0.2 (for stable conditions) obtained from fitting concentration profiles to measurements at the Norunda station.

Photosynthesis and respiration fluxes were assigned using a similar approach to that in [Kovalets et al., 2018]. The net respiration flux was parameterized using empirical relationships obtained based on measurements performed at a SMEAR-II station by [Markkanen et al., 2001] as a function of air and soil temperatures (t_a and t_s):

$$R_F = 0.25\, t_s + 0.27\, exp(0.14\, t_a). \quad (2)$$

Here R_F is in μmol m^{-2} s^{-1}, and t_s and t_a are in °C. There was no information found in the literature regarding partitioning of respiration fluxes. However, the conditions affecting partitioning of the respiration flux are like those at the Norunda site, where most of the respiration comes from soil. Therefore, it was assumed that 50% of the respiration flux originates from the soil surface ($R_F^0 = 0.5R_F$) and the other 50% is uniformly distributed through the canopy height.

According to the approach presented in [Kovalets et al., 2018], the net photosynthesis flux (P_F) is taken as the difference between the net CO_2 flux measured through the upper boundary of the canopy (F_N)

and the net respiration flux calculated with Equation 2. The distribution of the net photosynthesis flux with height was calculated using the same approach as in [Kovalets et al., 2018], with the extinction coefficient taken as that for the site of the SMEAR-II station [Mäkelä et al., 2006] and equal to $k_e \approx 0.18$. Four layers inside the canopy were identified in which photosynthesis was assumed to occur: δ_1 = (0 m,8 m), δ_2 = (8 m,10 m), δ_3 = (10 m,13 m), δ_4 = (13 m,14 m), which produced the following fractions of the net photosynthesis flux: $\alpha_1 = 0.19$, $\alpha_2 = 0.23$, $\alpha_3 = 0.42$, $\alpha_4 = 0.16$. Within each specified layer the photosynthesis source rate was assumed constant.

2.2.2 Setting Model Parameters for Simulations of $^{14}CO_2$ Vertical Profiles

Measurements of $^{14}CO_2$ concentration profiles are available in [Palonen et al., 2018] only for selected dates and times. Table 1 presents dates and times for which both measurements of $^{14}CO_2$ in air and soil were available. The concentrations of C-14 presented in [Palonen et al., 2018] in the form of $\Delta^{14}C$ [‰] were converted to specific concentrations A [Bq/kg C] according to the formula [Stenström et al., 2011]:

$$A = \frac{226\left[\frac{\Delta^{14}C}{1000}+1\right]\left[1+\frac{\delta^{13}C}{1000}\right]^2}{0.95063} \qquad (3)$$

Measurements of isotope fractionation $\delta^{13}C$ [‰] are also provided by [Palonen et al., 2018] for the same dates and times and at the same levels. So, conversion of $\Delta^{14}C$ to specific concentration A using Equation 3 is straightforward.

Measurements of $\Delta^{14}C$ are provided at heights 124, 67, 16 and 1 m (with some exceptions), but the height of the computational domain of the simulations was set to 50.4 m, since the relationships relating to the atmospheric surface layer used in the model are frequently violated at higher altitudes. Therefore, the upper boundary conditions for C-14 concentration were calculated by linear interpolation of the measured values from the 16 m and 67 m levels to 50.4 m height.

Accurate estimation of C-14 fluxes from the soil is not possible by using only measurements of $\Delta^{14}C$ (or equivalently specific concentrations) at different soil layers. Therefore, release rates of C-14 from the soil Q_0 [Bq/m^{2}s] were estimated by multiplying the CO_2 flux R_F^0 from the ground surface (Equation 2) by the measured value of C-14 specific concentration in soil:

$$Q_0 = 12 \times 10^{-9} R_F^0 A_s(0). \qquad (4)$$

The constant in the right-hand side is used for conversion of R_F^0 from [μmol m^{-2} s^{-1}] to [kg m^{-2} s^{-1}], $A_s(0)$ [Bq kg[C]$^{-1}$] is the C-14 specific concentration at the soil surface.

It should be noted that the times of measurement of surface soil concentrations, reported in Table 1, are shifted by a few hours with respect to the times of measurement of air concentrations.

Table 1 presents micrometeorological conditions during measurements of C-14 concentrations. Since C-14 concentrations were measured at somewhat different times, Table 1 also provides the respective 'reference' times at which measurements of input micrometeorological parameters were taken for the simulations. The measurements used in the simulations were 30-minute averaged.

Table 1: Measurement dates and times available for simulations (containing both soil and atmospheric measurements of C-14) and corresponding micrometeorological parameters measured and estimated as explained in text at the reference time used in the simulations.

Date	Time (meas. in air)	Time (meas. in soil surface)	Ref. time	U_h, m s^{-1}	U^* m s^{-1}	MOL m	F_N, µmol m^{-2} s^{-1}	R_F, µmol m^{-2} s^{-1}
20120503	11:25-12:35	19:00	12:30	2.32	0.94	-352	-6.3	1.49
20120606	10:15-11:00	12:45	10:30	1.84	0.59	-88	-18.3	3.67
20120704	10:35-11:24	13:14	-	1.26	0.36	-13.9	-14.8	7.77
20120830	12:00-13:05	14:01	12:30	0.76	0.35	-48.7	-12.94	4.21
20120831	01:00-01:47	2:35	01:30	1.16	0.36	203	3.79	3.79
20121018	10:41-11:30	13:15	11:00	2.25	0.56	301	-1.83	2.5
20130425	10:20-11:09	12:44	10:30	2.54	1.12	-360.6	-4.98	1.08

Notes:
Row in red denotes conditions which could not be simulated (see text).
Row in grey denotes night time conditions.

One date (July 4, 2012) was characterized by an extremely small value of the Monin-Obukhov length (-13.9 m), corresponding to an extremely unstable stratification for which the relationships applied to the atmospheric surface layer in the model do not apply. In addition, measurements of CO_2 concentrations were absent for that date. Therefore, the conditions for that date were not calculated.

One measurement profile (Aug 31, 2013) was taken at night, when photosynthesis does not occur. In such a case, there is no sense in using the empirical parameterisation in Equation 1 for respiration flux R_F. Instead, measurements of net eddy covariance flux F_N at 23 m height were used as respiration flux for that date. For day-time conditions, measurements of F_N were used together with the estimated respiration flux R_F in the same way as described in [Kovalets et al., 2018].

2.2.3 Simulation Results

Results of simulations together with measurements processed from [Palonen et al., 2018] are shown in Figure 3 and Figure 4. As explained above, the upper boundary condition was set at 50.4 m and measurements of C-14 were interpolated to this height. Therefore, the measurements at 67 m are located above the simulated profile.

In most cases, the simulated profiles agree reasonably well with measurements. According to Table 1, in most cases the net flux is negative, and the absolute value is greater than the respiration flux. Therefore, the integrated photosynthesis uptake of C-14 is greater than the release from the ground surface. This leads to a decrease of simulated volumetric concentrations (Figure 3 and Figure 4, on the left) with decreasing height above and in the upper part of the canopy, except in the case of 31 Aug 2012 when measurements were taken during the night. Only in the lower part of the canopy does the concentration rapidly increases closer to the ground due to respiration flux. This behaviour is supported by measurements taken on 6th June and 30th August. In contrast, specific concentrations monotonically increase in all cases with decreasing height, because the shapes of the CO_2 profiles are similar to the profiles of volumetric concentration.

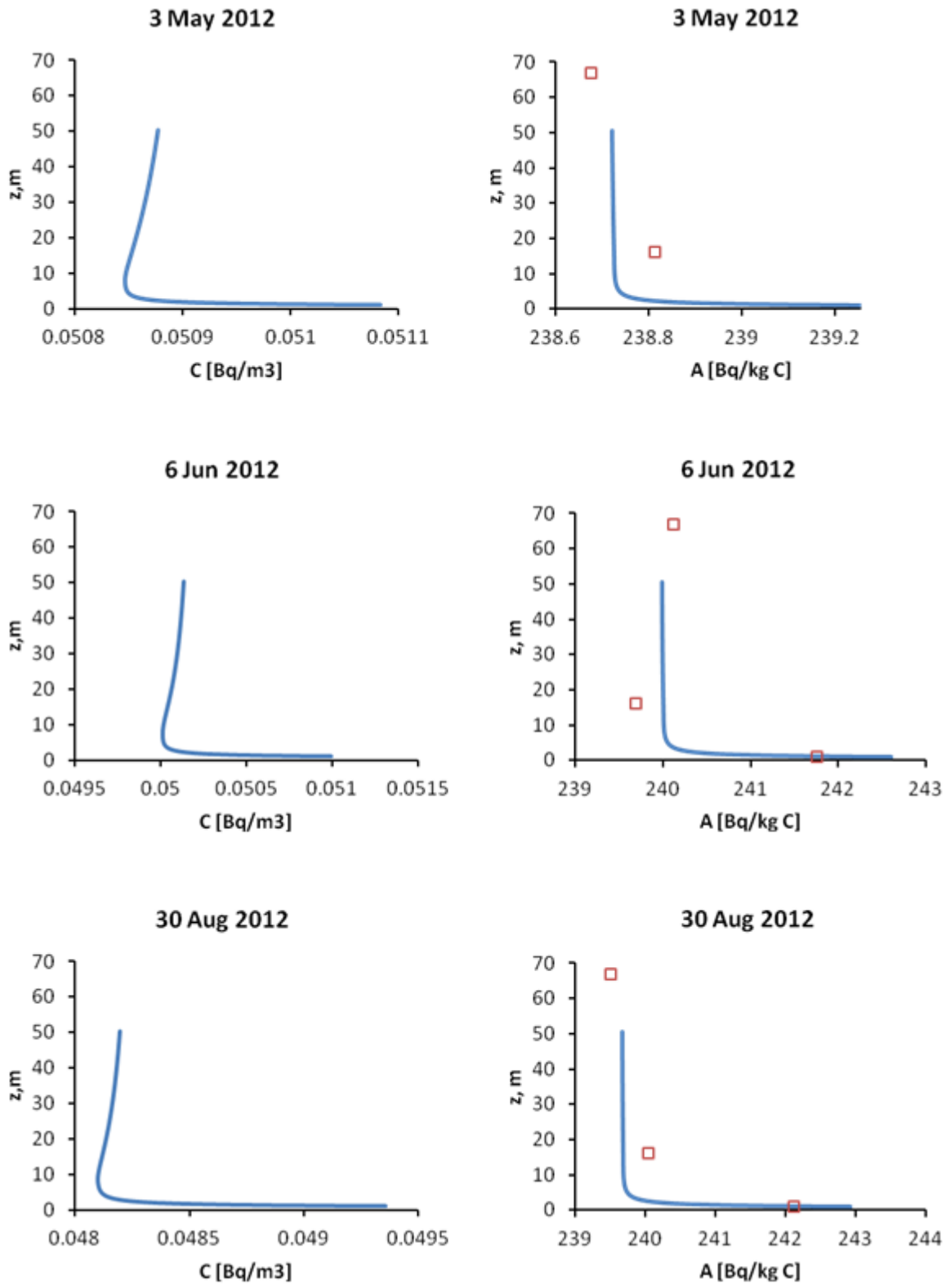

Figure 3: Calculated volumetric and specific C-14 concentrations (blue curves) and measured C-14 specific concentrations (red squares) for the conditions at the SMEAR-II station May to August 2012 (dates are shown at the top of the figures).

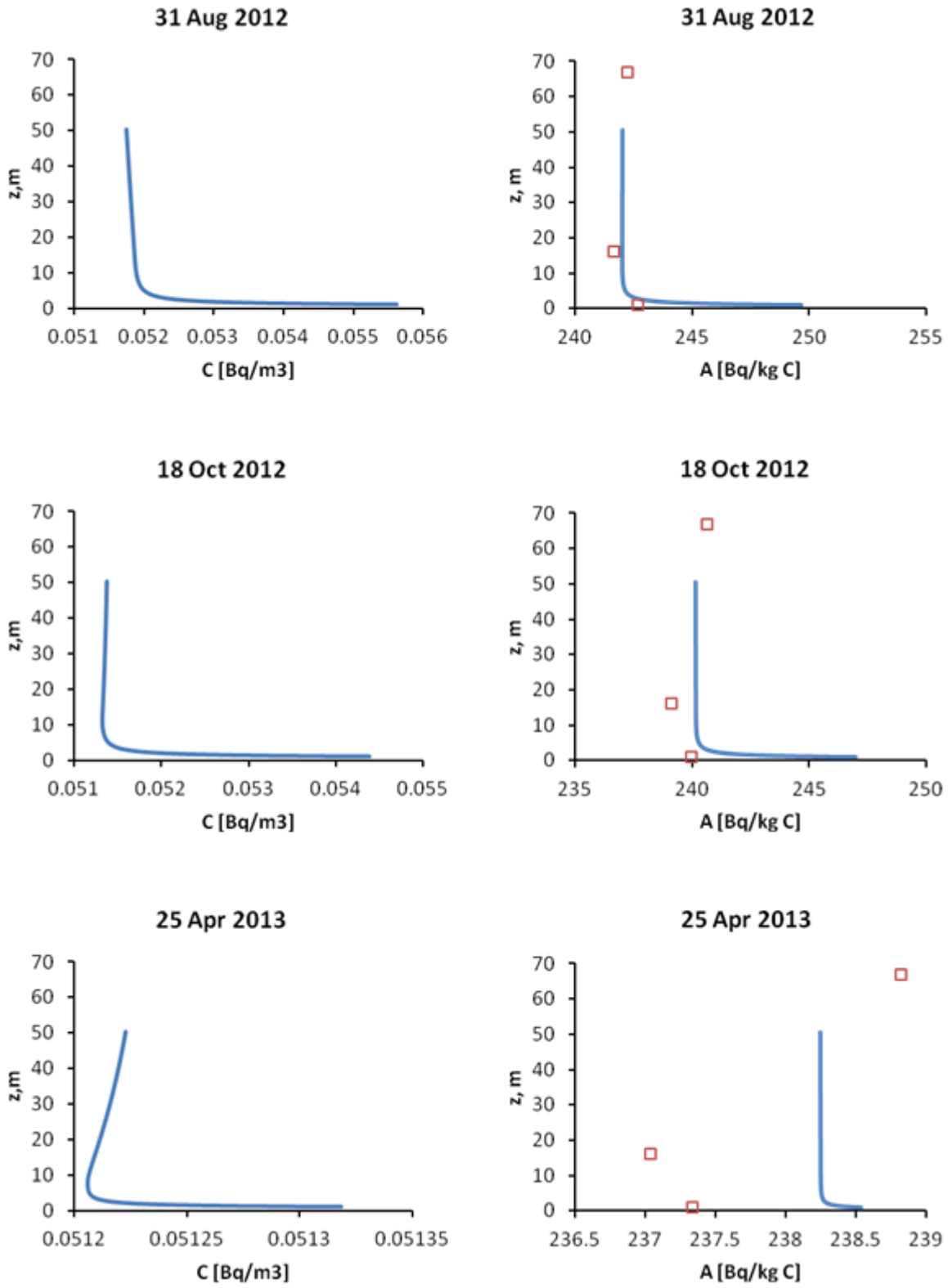

Figure 4: Calculated volumetric and specific C-14 concentrations (blue curves) and measured C-14 specific concentrations (red squares) for the conditions at the SMEAR-II station August 2012 to April 2013 (dates are shown at the top of the figures).

Only in one case (25th April) do the simulated results strongly deviate from measurements. In this case, a strong negative gradient of C-14 volumetric concentration is observed above the canopy. At all other dates with stronger photosynthesis rates than was observed in this case, the observed gradients of C-14 concentration were much smaller. This is probably an indication of non-stationary horizontally non-homogeneous conditions, for which the assumptions of this one-dimensional model are violated.

2.2.4 Conclusions Relating to Posiva Calculations

In most cases, the simulated vertical profiles of C-14 agree reasonably well with measurements, especially considering that the vertical flux of C-14 from the ground surface was parameterised rather than measured. In two cases, a sharp increase in concentration near the ground predicted by the model is confirmed by measurements. In a single case, simulated profiles were significantly different from measurements. The disagreements may be due to dominance by horizontal processes (advection) that are not represented in the model. However, the limited number of profiles that could be fitted and the small number of data points characterizing each profile mean that care must be taken not to overinterpret the significance of the model-data comparisons made above.

2.3 INTERPRETATION UNDERTAKEN BY THE BIOPROTA TECHNICAL SUPPORT TEAM

2.3.1 Initial Interpretation

The SMEAR II results from multiple atmospheric samples collected on the same date are displayed in Figure 5 to Figure 7. Slight upward trends in both $\Delta^{13}C$ and $\Delta^{14}C$ between April and September 2012 are seen in Figure 5 and Figure 6. The similarity of these trends gives rise to the correlation seen between $\Delta^{13}C$ and $\Delta^{14}C$ values in Figure 7.

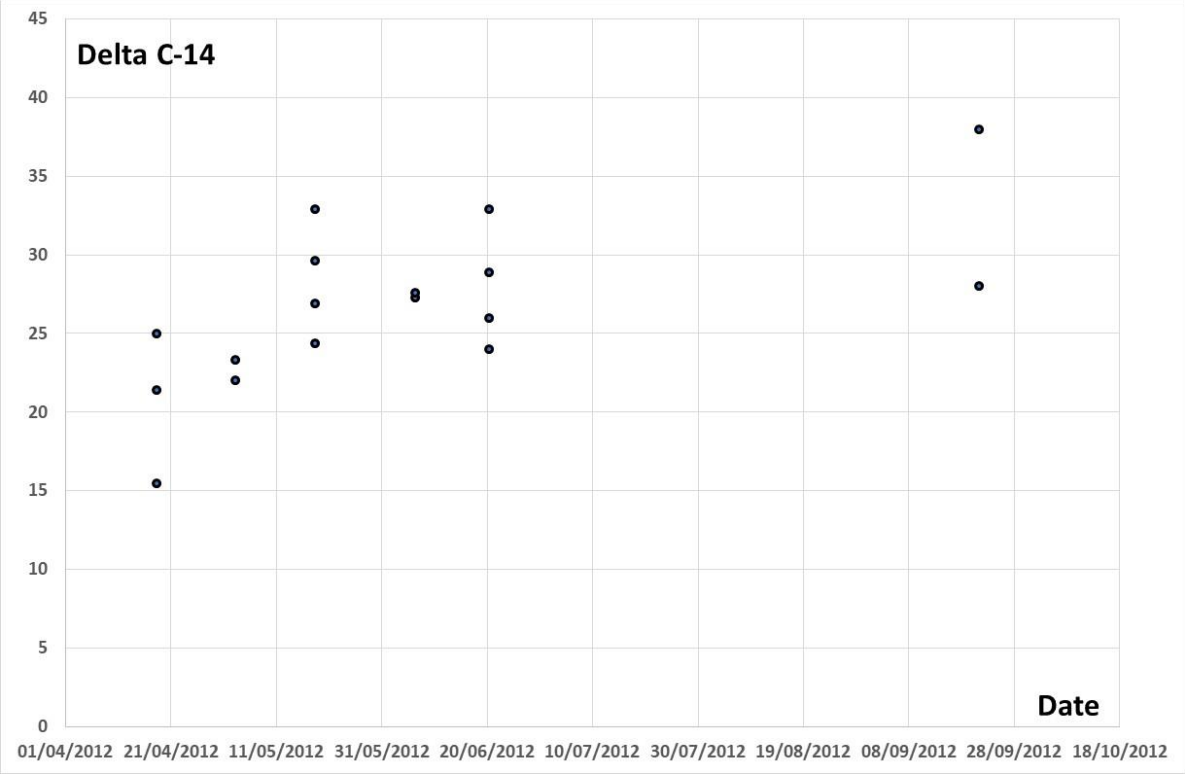

Figure 5: Values of $\Delta^{14}C$ (‰) in above-ground air samples at the SMEAR II station. Heights of sampling not specified.

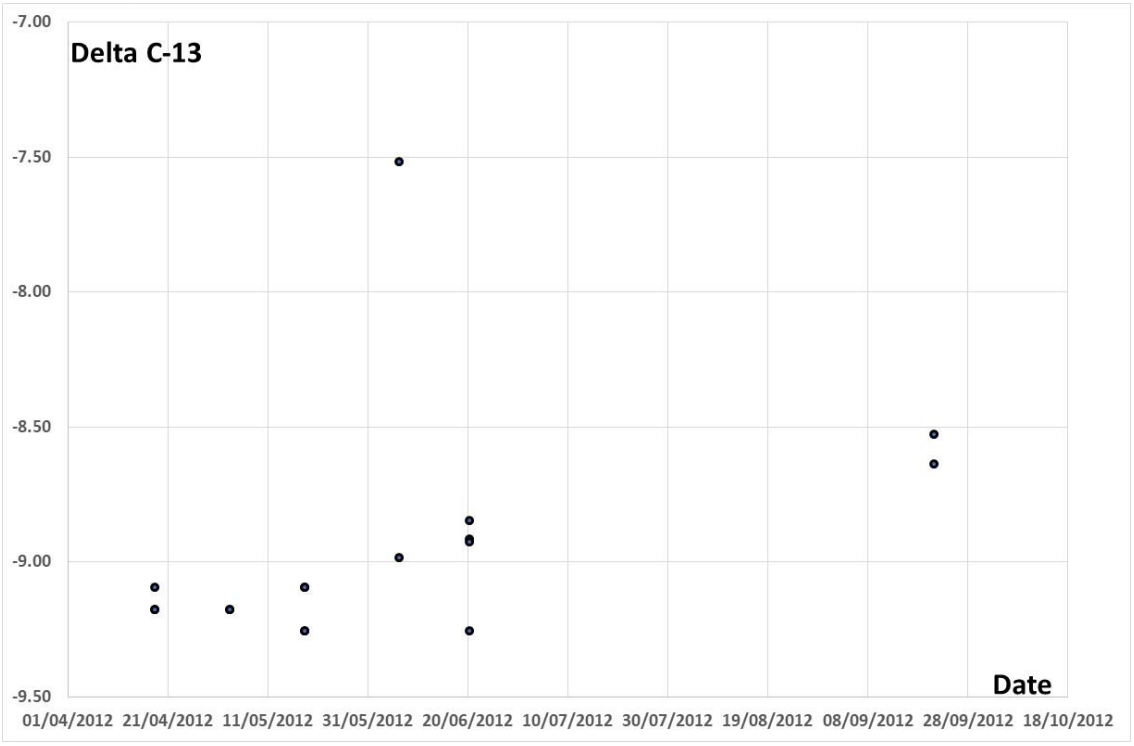

Figure 6: Values of $\Delta^{13}C$ (‰) in above-ground air at the SMEAR II station. Heights of sampling not specified.

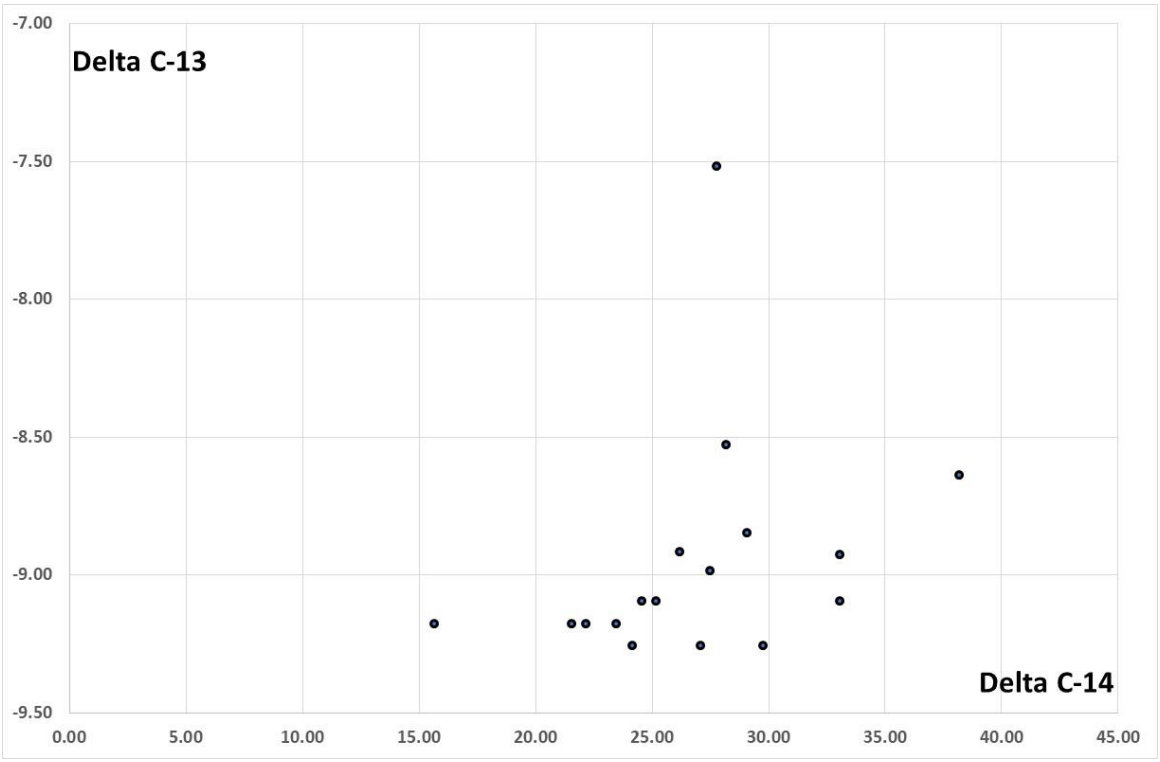

Figure 7: Correlation of $\Delta^{13}C$ and $\Delta^{14}C$ (‰) in above-ground air at the SMEAR II station. Heights of sampling not specified. Data for April to September 2012

Data for individual above-ground air samples, rather than daily averages, are shown in Figure 8 to Figure 12. Figure 8 and Figure 9 show values of $\Delta^{13}C$ and $\Delta^{14}C$ as a function of time (days) into the study, with the start of the study defined as 00:00 on 18 April 2012. These data sets extend for just over one year (372 days), so the trends shown in Figure 5 and Figure 6 are now revealed as part of an approximately sinusoidal annual cycle. The duration of the data set is not sufficient to determine whether longer-term trends exist.

Figure 10 shows that the correlation between $\Delta^{13}C$ and $\Delta^{14}C$ values is maintained for individual samples and over this longer period of study, i.e. the oscillations appear to have the same (annual) period and to be in phase.

Figure 11 and Figure 12 demonstrate that there is no evidence that $\Delta^{13}C$ and $\Delta^{14}C$ values are affected by the height above the ground at which the sample is taken. Specifically, this means that samples from within the canopy (1 m), just above the canopy (16 m) and high above the canopy (67 m and 125 m) cannot be distinguished.

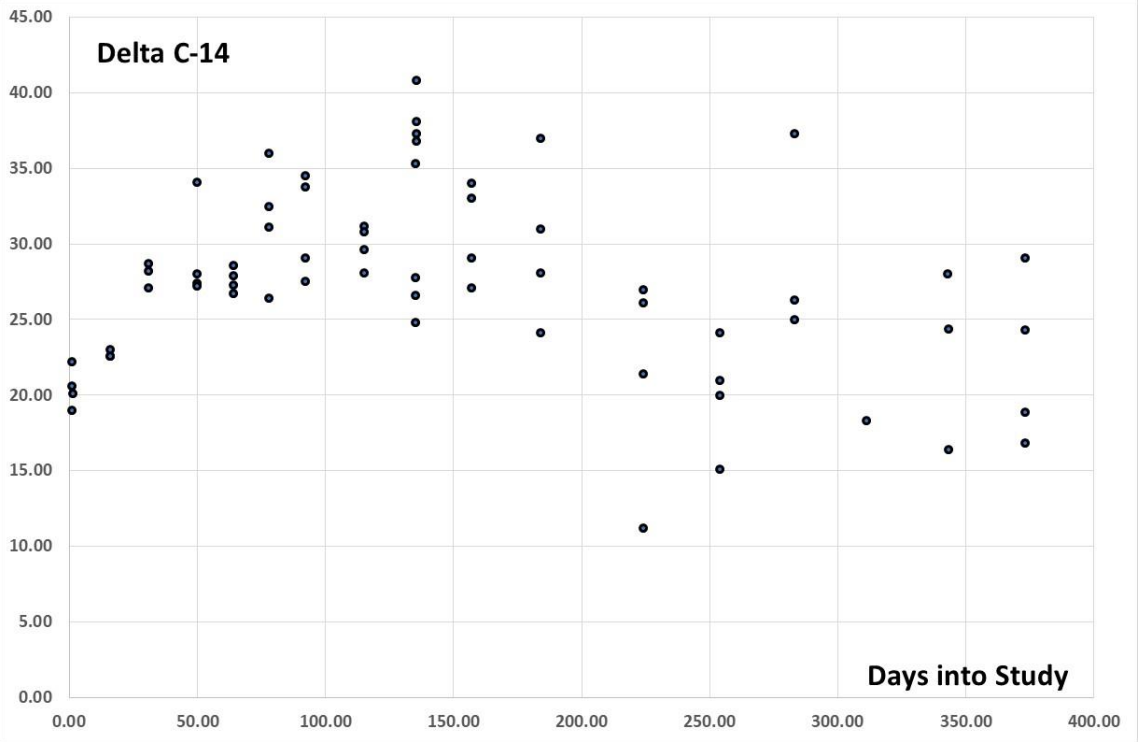

Figure 8: Values of $\Delta^{14}C$ (‰) in above-ground air for individual samples, irrespective of the height of sampling.

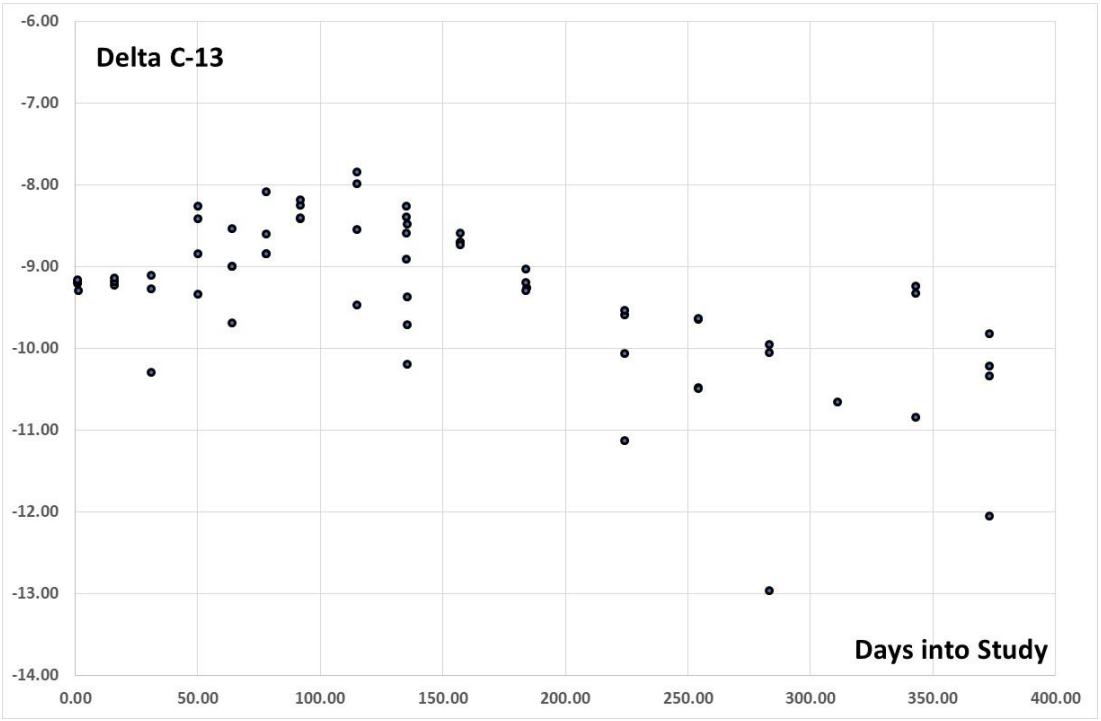

Figure 9: Values of $\Delta^{13}C$ (‰) in above-ground air for individual samples, irrespective of the height of sampling.

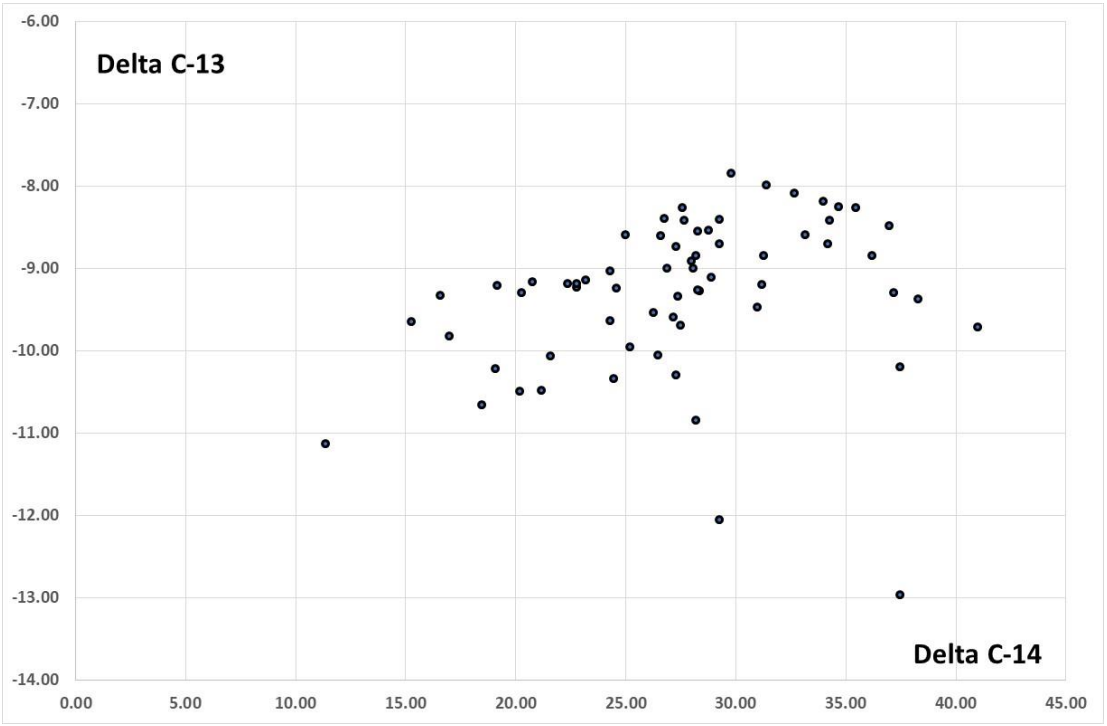

Figure 10: Correlation of $\Delta^{13}C$ and $\Delta^{14}C$ (‰) in above-ground air for individual samples, irrespective of the height of sampling. Data for a 372-day study period.

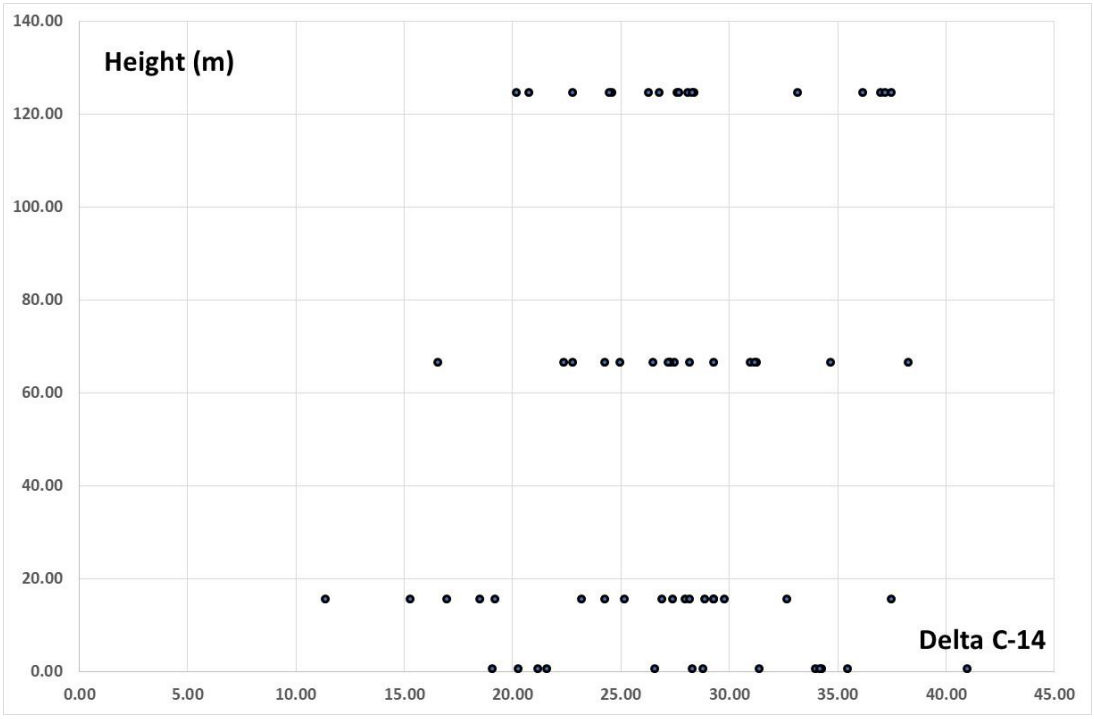

Figure 11: Values of $\Delta^{14}C$ (‰) in above-ground air for individual samples as a function of the height of sampling.

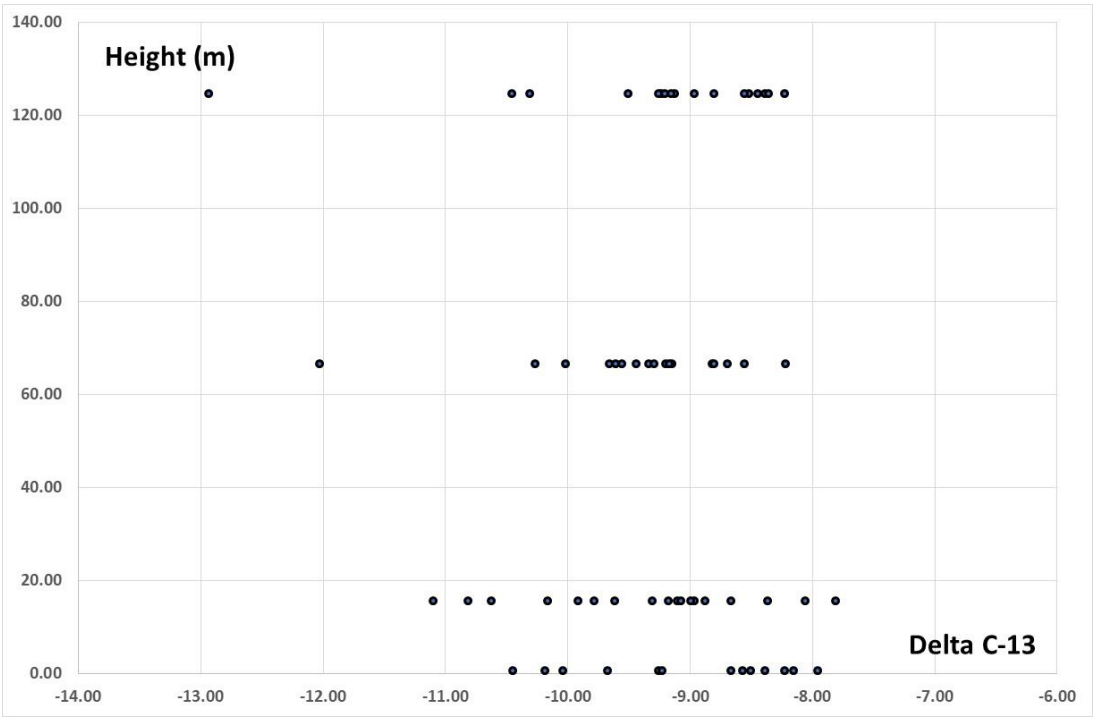

Figure 12: Values of $\Delta^{13}C$ (‰) in above-ground air for individual samples as a function of the height of sampling.

Values of $\Delta^{13}C$ and $\Delta^{14}C$ in the soil atmosphere are shown in Figure 13 to Figure 17. In these figures, the height origin is defined as the boundary between organic and mineral layers in the soil. The height of the soil surface is not defined, but this is not important to the analysis, so it is taken at a notional height of 0.1 m. Also, only data from analyses performed at the VERA laboratory are used, as results from Uppsala and Helsinki are unreliable, incomplete and often physically implausible.

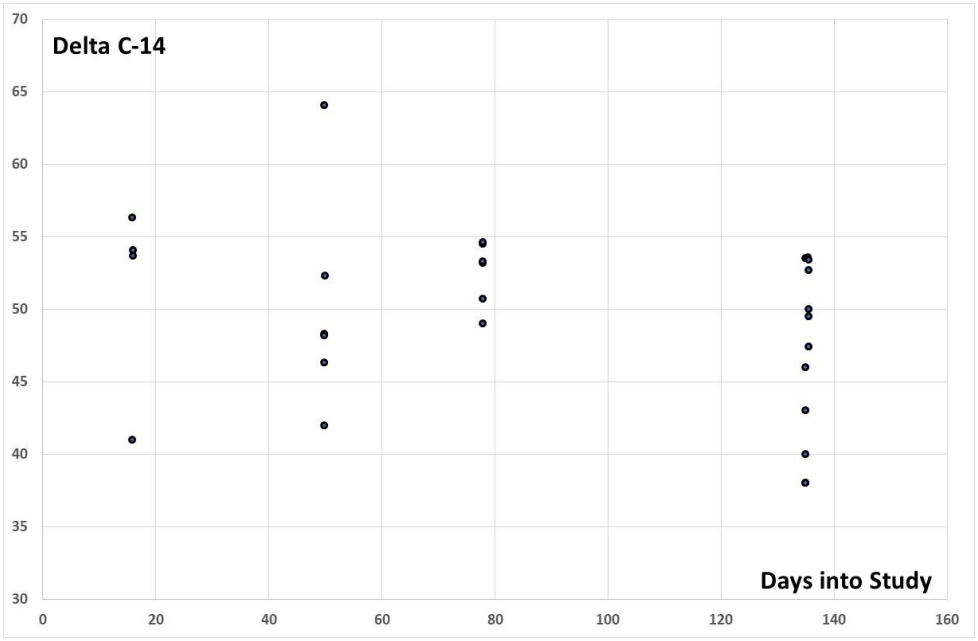

Figure 13: Variations in $\Delta^{14}C$ (‰) in the soil atmosphere as a function of time, neglecting any distinctions with depth.

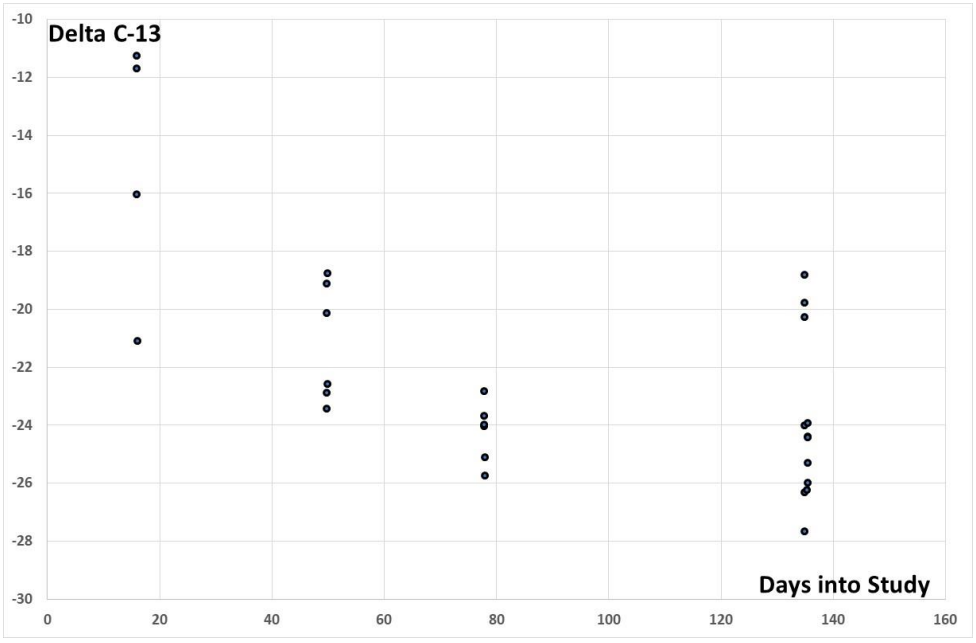

Figure 14: Variations in $\Delta^{13}C$ (‰) in the soil atmosphere as a function of time, neglecting any distinctions with depth.

Figure 13 shows no significant trend with time (a linear regression analysis yielded an R^2 value of 0.09) and although Figure 14 suggests some decrease with time, this is strongly affected by three points at the first time of determination, so cannot be given much weight (a linear regression analysis yielded an R^2 value of 0.39). Figure 15 shows no evidence of any correlation between $\Delta^{13}C$ and $\Delta^{14}C$ values.

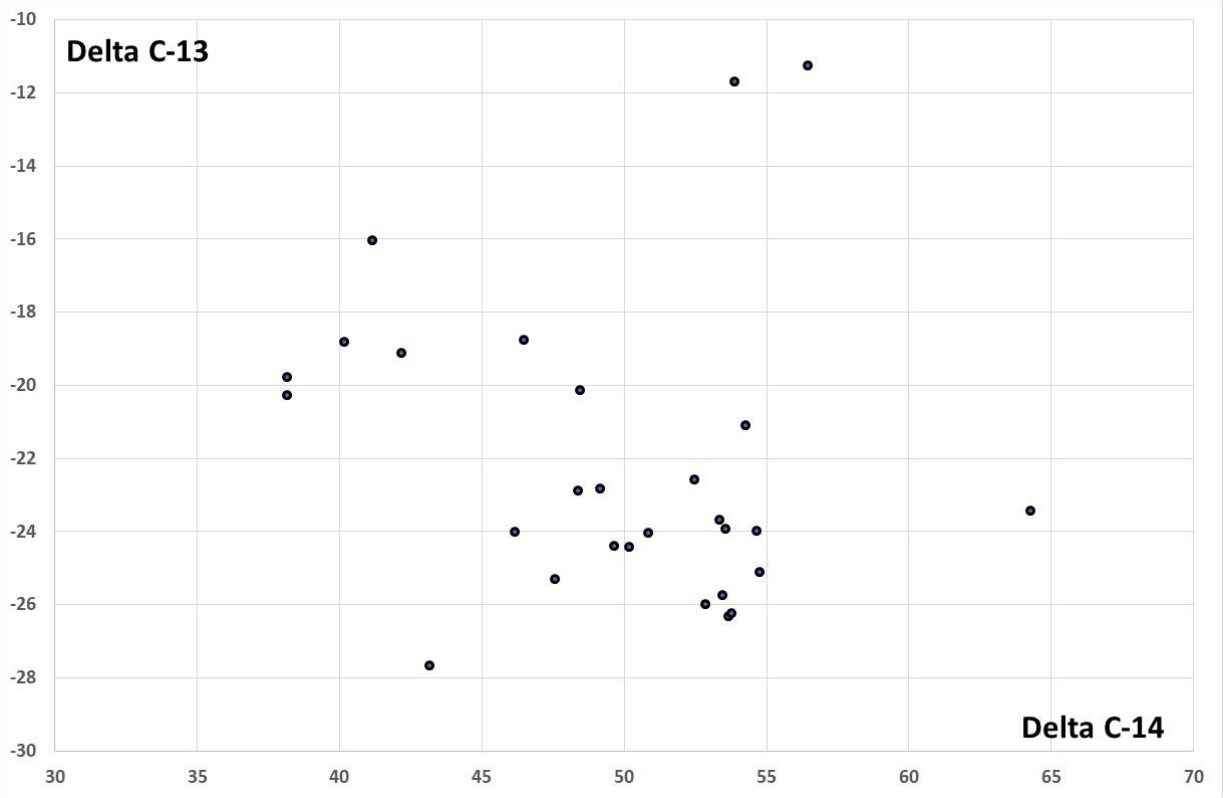

Figure 15: Correlation of $\Delta^{13}C$ and $\Delta^{14}C$ (‰) in the soil atmosphere for individual samples, irrespective of the depth of sampling.

Finally, Figure 16 and Figure 17 show that both $\Delta^{13}C$ and $\Delta^{14}C$ values are not dependent on depth/height in soil.

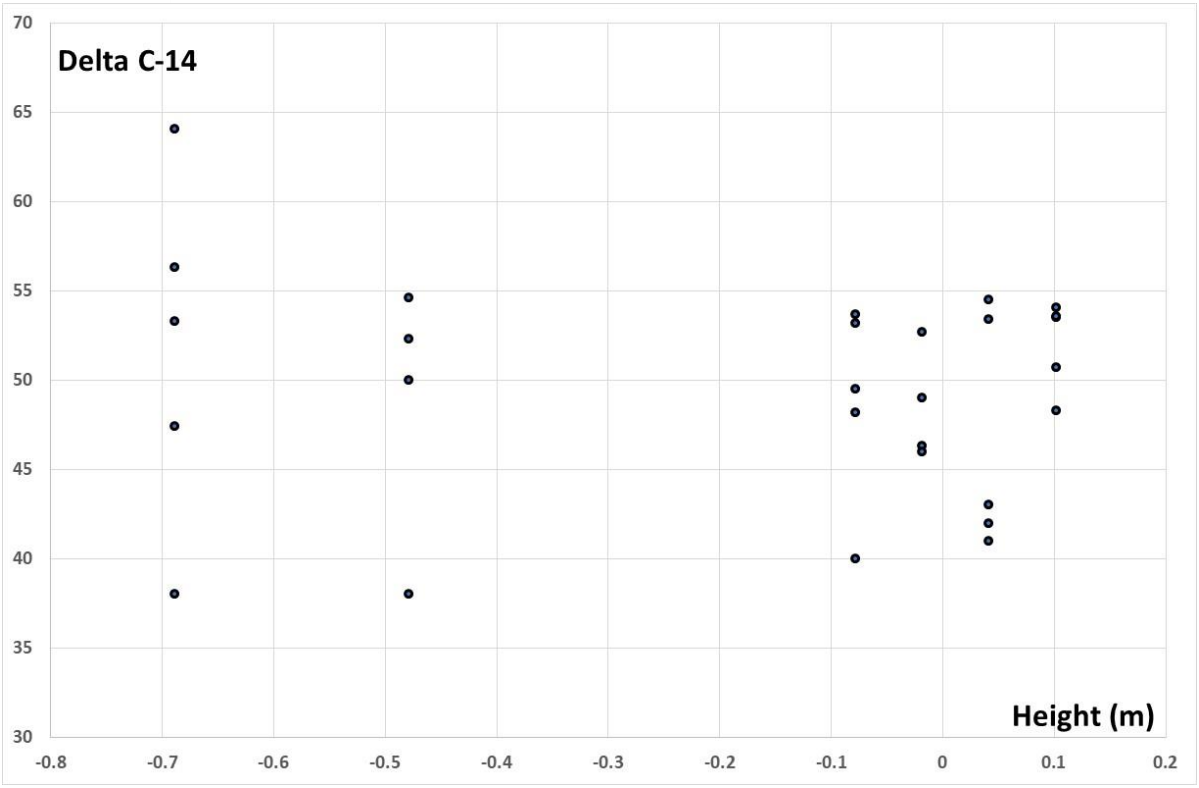

Figure 16: Variation of $\Delta^{14}C$ (‰) values in the soil atmosphere with depth in soil.

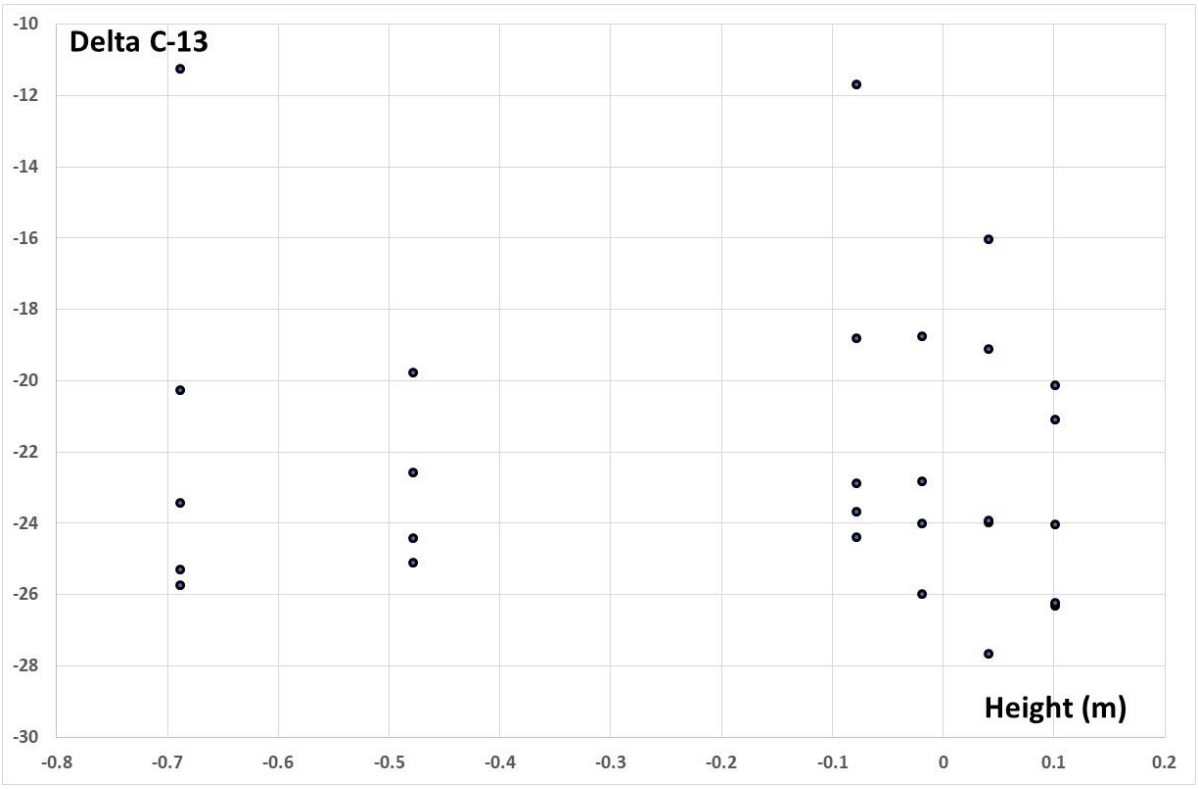

Figure 17: Variation of $\Delta^{14}C$ (‰) values in the soil atmosphere with depth in soil.

The data reviewed above lead to a rather simple description of the system to be modelled. The above-ground atmosphere is characterised by $\Delta^{14}C$ values exhibiting an annual sinusoidal oscillation of between about 15 and 40‰, and with a mean value of about 25 to 30‰. The above-ground atmosphere is also characterised by $\Delta^{13}C$ values exhibiting an annual sinusoidal oscillation of between about -8 and -11‰, and with a mean value of about -9.5‰. Such sinusoidal variations are observed worldwide and the typical atmospheric monitoring value in 2012 was about -8.5‰[a]. No distinctions can be made between $\Delta^{13}C$ and $\Delta^{14}C$ values close to the ground surface (1 m), just above the canopy (16 m) and high above the canopy (67 and 125 m). The soil atmosphere is characterised by a $\Delta^{14}C$ value of about 50‰ and a $\Delta^{13}C$ value of about -22‰, the latter being typical for decaying plant material. Thus, it seems that CO_2 leaving the soil surface is rapidly diluted into the above-ground atmosphere (within the first one metre above the surface). This is thought to arise because the volume of CO_2 leaving the soil surface is small compared with the volume of CO_2 carried through the lower part of the canopy by advection and turbulent diffusion.

Although the annual sinusoidal oscillation in atmospheric $\Delta^{14}C$ values looks quite large, it is appropriate to keep in mind that in absolute terms it corresponds to a variation of about 25‰ of the reference value of about 240 Bq kg(C)$^{-1}$, i.e. 0.025×240 = 6.0 Bq kg(C)$^{-1}$. The positive value partly reflects the consideration that the comparison is with a reference standard defined in 1950, so its specific activity in 2012 was only 99.3% of its original value, giving modern carbon a $\Delta^{14}C$ value of 7.5‰. Residual atmospheric contamination with ^{14}C from atmospheric weapons' testing in the 1950s and early 1960s may explain the remainder of the anomaly, as current ^{14}C concentrations in the atmosphere remain significantly above their 1950 value (see Figure 18), notwithstanding continuing emissions from fossil fuel consumption that dilute the atmospheric carbon reservoir with carbon containing no C-14.

[a] www.esrl.noaa.gov/gmd/dv/iadv/graph.php?code=MLO&program=ccgg&type=sc, accessed 9 March 2018.

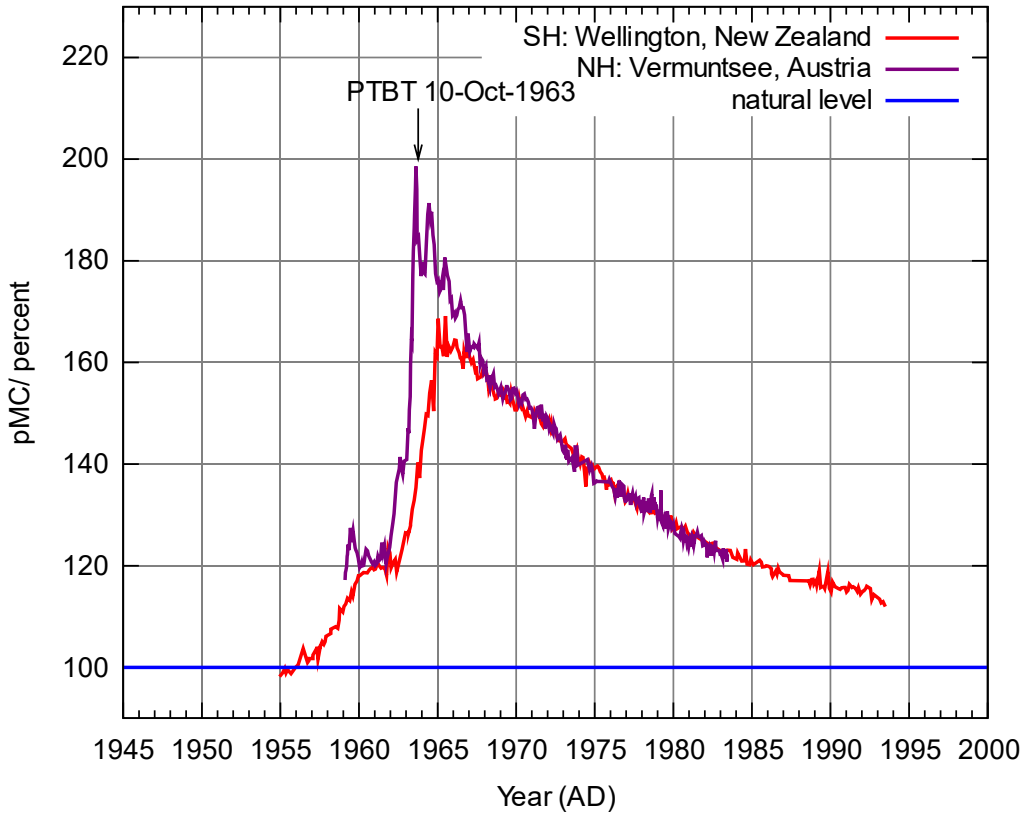

Figure 18: Changes in C-14 Concentrations in the Atmosphere expressed as Percentages of the Reference 1950 Concentration[a] (New Zealand and Austrian sites are representative of the Southern and Northern Hemispheres, respectively).

2.3.2 Simple Analytical Model

Following Kovalets et al. [2018], a 1D diffusion model is adopted. The basic equation for such a model is:

$$-\mathrm{d}(K\{\mathrm{d}C(z)/\mathrm{d}z\})/\mathrm{d}z = S(z) \qquad (5)$$

Where $C(z)$ is the concentration of some substance at height z (m) above the ground surface. The units of $C(z)$ may be Bq m^{-3}, mol m^{-3} or dimensionless etc. depending upon how the substance is defined (e.g. activity concentration, mass concentration or isotopic anomaly). $S(z)$ is the source or sink of the substance at a height of z and has units of Bq m^{-3} s^{-1}, mol m^{-3} s^{-1} or s^{-1} etc. to conform to the units adopted for the concentration. K is a diffusion coefficient with units of m^2 s^{-1}.

It is emphasised that the validity of applying a 1D model relies on the horizontal scale of displacement in the canopy being small compared with its overall spatial extent (200 m by 1200 m). In general, advective wind speeds within a forest canopy are low and a 1D model is typically found to be satisfactory for modelling temperature, momentum and contaminant profiles. However, as noted in Section 2.2, on one measurement occasion, there was a disagreement between the modelled results and the

[a] upload.wikimedia.org/wikipedia/commons/e/e2/Radiocarbon_bomb_spike.svg, accessed 23 March 2018.

observations that could have been due to dominance by horizontal processes (advection) that are not represented in the model. Characteristic timescales for diffusion are discussed further in Section 2.4.

As discussed below, the bottom boundary condition is a flux at the ground surface ($z = 0$). This flux is defined as positive upward in the direction of increasing z and is given by:

$$R = -K\{dC(z)/dz\}\big|_{z=0} \quad (6)$$

For CO_2, the soil is normally a net source to the atmosphere and therefore the upwardly directed flux is positive.

Units of R are Bq m^{-2} s^{-1}, mol m^{-2} s^{-1} or m^{-2} s^{-1} to conform to the units of concentration. In contrast, the top boundary condition, at height Z, is a fixed concentration $C(Z)$ corresponding to the general atmospheric concentration of the substance of interest, in this case CO_2.

For application, Equation 5 is simplified by making $S(z)$ proportional to the concentration of the substance of interest, i.e. $S(z) = -\mu C(z)$. The minus sign is introduced because the substance is assumed to be depleted, e.g. CO_2 by the net effect of photosynthesis less plant respiration. The implication is that the efficiency of photosynthetic uptake is independent of height within the plant canopy. In practice, there will be variations with height due, e.g., to variations in foliage density and light penetration. Thus, assuming that K is independent of height:

$$K\,d(dC(z)/dz)/dz = \mu C(z) \quad (7)$$

The general solution to equation 3 is:

$$C(z) = A_1\exp(kz) + A_2\exp(-kz) \quad (8)$$

Substituting Equation 8 into Equation 7 and equating terms with identical exponents, we obtain:

$$KA_1k^2\exp(kz) = \mu A_1\exp(kz) \text{ and } KA_2k^2\exp(-kz) = \mu A_2\exp(-kz) \quad (9)$$

As Equation 9 must be satisfied at all z in the range $[0, Z]$:

$$KA_1k^2 = \mu A_1 \quad \text{and} \quad KA_2k^2 = \mu A_2 \quad (10)$$

Because k is defined to be positive:

$$k = \{\mu/K\}^{1/2} \quad (11)$$

Also, Equation 6 yields:

$$R = -K\{A_1k - A_2k\} \quad \text{or} \quad A_2 - A_1 = R/Kk \quad (12)$$

It then follows from Equation 8 that:

$$C(Z) = A_1\exp(kZ) + \{A_1 + R/Kk\}\exp(-kZ) \quad (13)$$

Thus:

$$A_1 = [C(Z) - \{R/Kk\}\exp(-kZ)]/[\exp(-kZ) + \exp(kZ)] \quad (14)$$

In summary:

$$C(z) = A_1\exp(kz) + A_2\exp(-kz) \quad (15)$$

$k = \{\mu/K\}^{1/2}$ (16)

$A_1 = [C(Z) - \{R/Kk\}\exp(-kZ)]/[\exp(-kZ) + \exp(kZ)]$ (17)

$A_2 = A_1 + R/Kk$ (18)

An interesting limiting case occurs when depletion in the canopy is very small. This is achieved by letting μ tend to zero. As K is finite, this means that $\{\mu/K\}^{1/2}Z$ becomes small. Thus, using a first-order expansion of the exponential terms in Equation 15, we find that:

$C(z) = A_1 + A_2 + A_1kz - A_2kz \quad = A_1 + A_2 - Rz/K$ (19)

Also:

$A_1 + A_2 = 2A_1 + R/Kk = C(Z) + RZ/K$ (20)

So

$C(z) = C(Z) + \{R/K\}\{Z - z\}$ (21)

This gives the correct bounding concentration at $z = Z$, a linear increase to a maximum at the ground surface and an increment in concentration at the ground surface of RZ/K. Thus, if $R << KC(Z)/Z$ and for little uptake in the canopy, i.e. $\{\mu/K\}^{1/2}Z << 1$, the concentration of the substance at the ground will be very similar to the concentration at the top of the canopy.

It is now possible to apply this to the CO_2 concentration at the SMEAR II station. In this case, the concentration at the top of the canopy is about 400 ppmv, corresponding to 0.0179 mol m^{-3}. The net respiration flux of CO_2 from the soil surface is estimated in Section 2.2 using:

$R = 0.25t_s + 0.27\exp(0.14t_a)$ μmol m^{-2} s^{-1} (22)

Where t_s (C) is the soil temperature and t_a (C) is the air temperature. To maximize R and thus provide a cautious upper estimate of the bound that K must exceed, both t_s and t_a are here taken as 10°C, which is a reasonable maximum for this location. This gives R = 3.6 μmol m^{-2} s^{-1}. The average height of the canopy gives Z = 14 m. Thus, the requirement for a small vertical concentration gradient becomes:

$K >> RZ/C(Z)$ or $K >> 3.6\ 10^{-6} \times 14/0.0179 = 0.0028$ m^2 s^{-1} (23)

Figure 19 to Figure 22 show explicit profile calculations for different values of K and μ, using Equation 15, with $C(Z)$ = 0.0179 mol m^{-3}, Z = 14 m and $R = 3.6\ 10^{-6}$ mol m^{-2} s^{-1}.

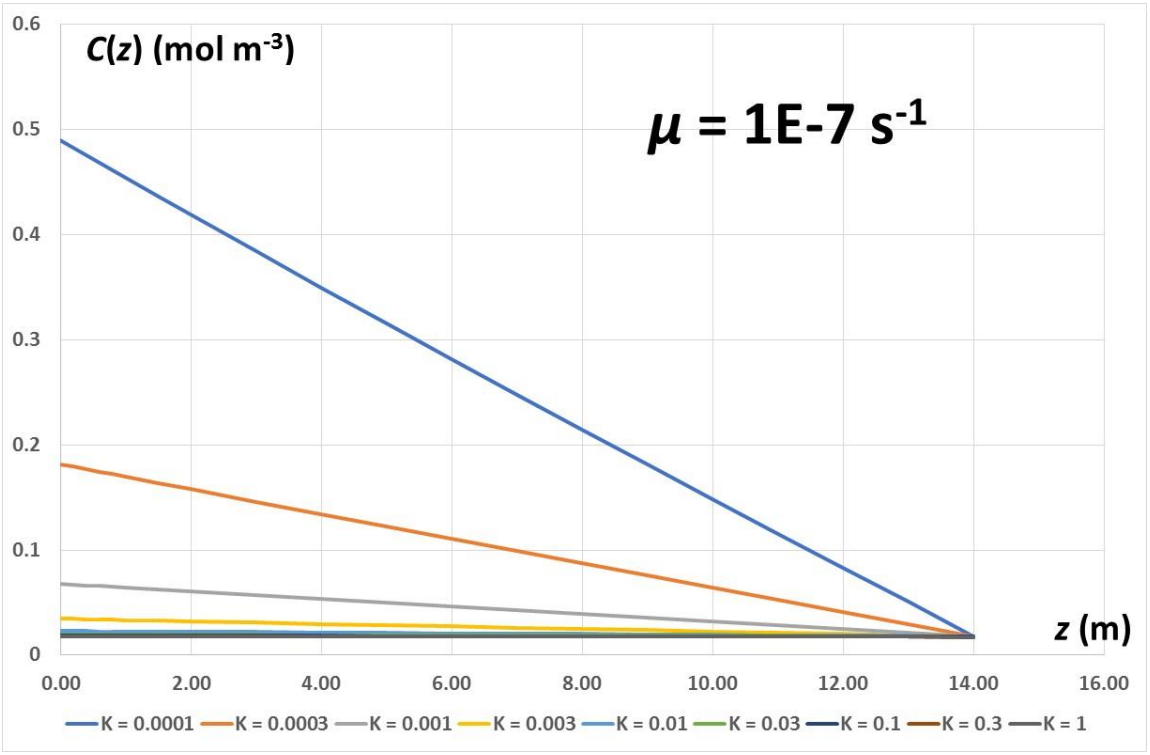

Figure 19: Concentration (C(z)) profiles for different diffusion coefficients (K) and μ of 1E-7 s^{-1}.

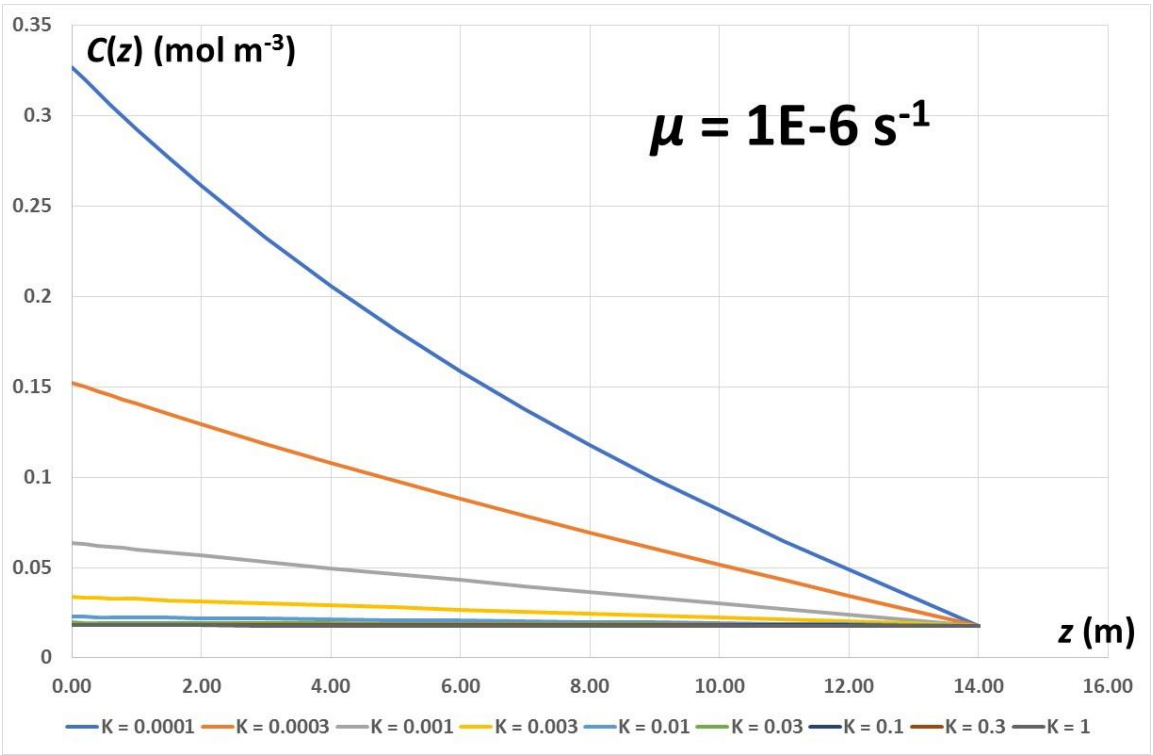

Figure 20: Concentration (C(z)) profiles for different diffusion coefficients (K) and μ of 1E-6 s^{-1}.

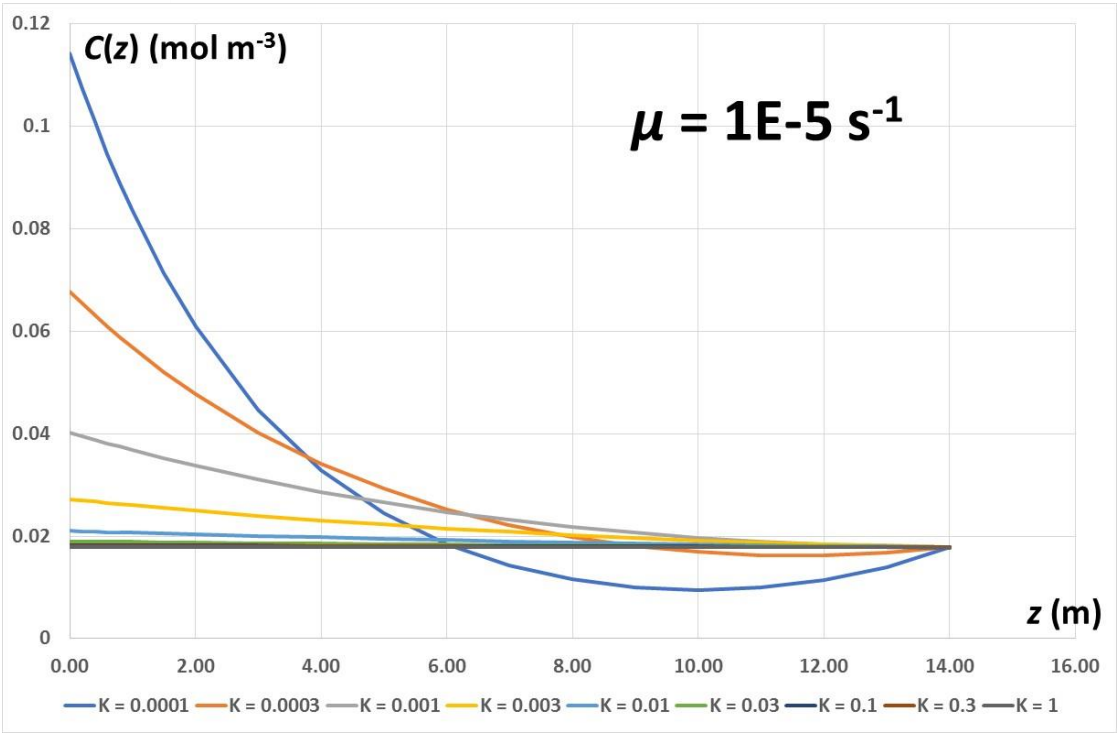

Figure 21: Concentration (C(z)) profiles for different diffusion coefficients (K) and μ of 1E-5 s^{-1}.

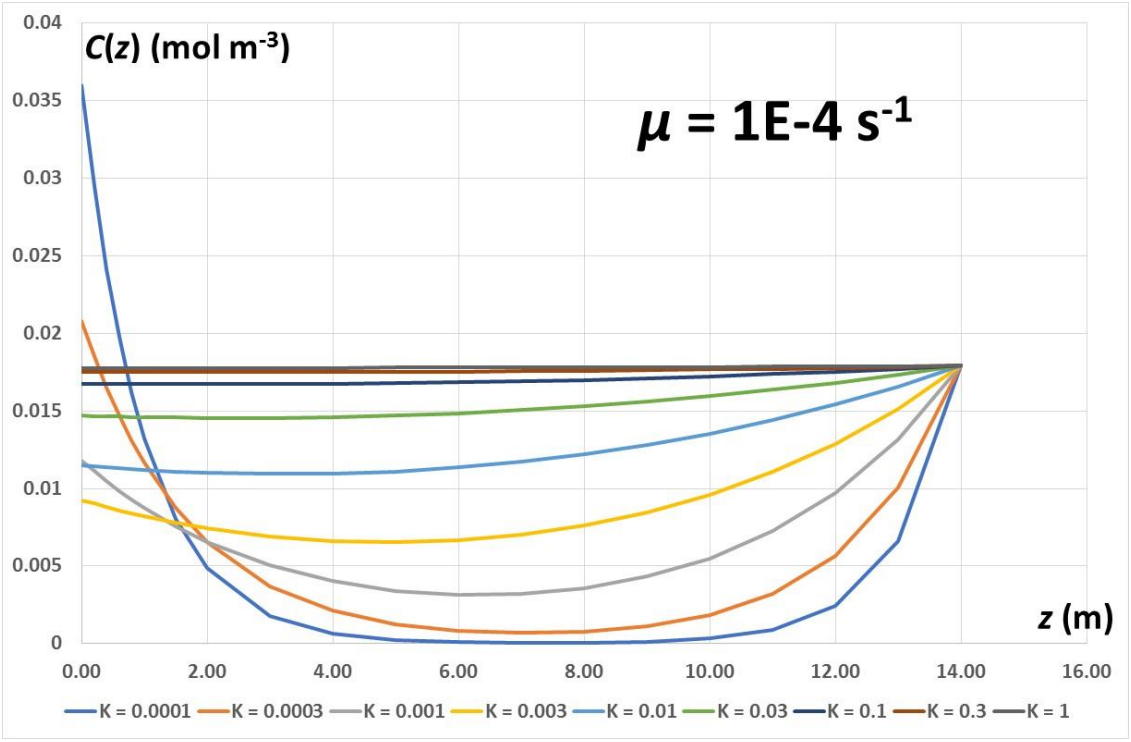

Figure 22: Concentration (C(z)) profiles for different diffusion coefficients (K) and μ of 1E-4 s^{-1}.

This analysis shows the linear response given by Equation 15 at the smallest value of μ that was used ($1\ 10^{-7}$ s^{-1}). Furthermore, the intercepts on the y-axis approach $RZ/K + C(Z)$ as expected, e.g. for $K = 1\ 10^{-4}$ m^2 s^{-1} the intercept is at 0.490 compared with the Equation 20 value of $3.6\ 10^{-6} \times 14/1\ 10^{-4} + 0.0179 = 0.522$. Reducing the value of μ to $1\ 10^{-9}$ s^{-1} gives an intercept of 0.5216, i.e. closely approaching the theoretical limiting value.

As the value of μ increases, canopy uptake causes a reduction in the computed concentration and causes the linear decrease with height to change to an exponential fall-off above the ground surface. At large values of μ and small values of K, complete depletion occurs within the first 1 m above the ground surface. Depletion below the concentration in free air also occurs below the upper limit of the canopy. At a value of μ of $1\ 10^{-4}$ s^{-1} a non-physical situation occurs with small values of K in which the air within the canopy is completely depleted of carbon dioxide due to photosynthetic uptake.

To estimate μ, if the net biomass production is 0.5 kg[C] m^{-2} y^{-1} (value for Duke Swamp from Killey et al. [1998]) this corresponds to 0.5×44/12 = 1.83 kg[CO_2] m^{-2} y^{-1}. To this can be added the CO_2 that is photosynthesised but subsequently used for respiration. Therefore, the total used is about 3.6 kg[CO_2] m^{-2} y^{-1} corresponding to 82 mol y^{-1} or $2.6\ 10^{-6}$ mol s^{-1}. Taking the CO_2 concentration in air to be 0.0179 mol m^{-3} and a canopy height of 14 m, the total CO_2 available for uptake is 0.0179×14 = 0.25 mol m^{-2}. Therefore, based on these calculations, $\mu = 2.6\ 10^{-6}/0.25 = 1.04\ 10^{-5}$ s^{-1}. The case for $\mu = 1.0\ 10^{-5}$ s^{-1} is shown above.

Referring to the above figure, this suggests that uptake for photosynthesis could occur within a few metres of the ground. However, this would depend on the presence of substantial understorey vegetation, as photosynthetic uptake by Scots Pine would be mainly higher in the canopy. Also, the above somewhat overestimates the value of μ because it neglects the consideration that CO_2 produced in respiration will, at least in part, be returned to the sub-canopy atmosphere rather than being lost at the top of the canopy.

Overall, it seems that the lack of isotopic response in the experimental study (see Section 2.3.1) suggests a K value of $3\ 10^{-2}$ m^2 s^{-1} or larger. This ensures that soil CO_2 never contributes more than 6% of total CO_2 in canopy air (for an extreme case of $K = 3\ 10^{-2}$ m^2 s^{-1} and $\mu = 1.0\ 10^{-5}$ s^{-1}, the ground-level concentration of CO_2 is 0.0190 mol m^{-3} compared with an above-canopy value of 0.0179 mol m^{-3}). As the concentration at the base of the canopy increases with decreasing value of K and μ, a cautious basis for assessment calculations is $K = 3\ 10^{-2}$ m^2 s^{-1} and μ of $1.0\ 10^{-5}$ s^{-1}. Applying this to a flux of C-14 from soil surface of 1 Bq m^{-2} s^{-1} gives an air concentration of 457 Bq m^{-3} at the soil surface, decreasing to 424 Bq m^{-3} at 1 m, 292 Bq m^{-3} at 5 m, and 129 Bq m^{-3} at 10 m. Note that these concentrations are for an upper boundary concentration of 0 Bq m^{-3}, i.e. they exclude the ambient concentration of 240 Bq m^{-3}.

In the extreme case adopted for assessment purposes, the ground-level concentration of CO_2 is 0.0190 mol m^{-3} compared with an above-canopy value of 0.0179 mol m^{-3}. Thus, 0.0190 - 0.0179 = 0.0011 mol m^{-3} is contributed from the soil. As the $\Delta^{13}C$ value for the soil atmosphere is about -22‰ and the $\Delta^{13}C$ for the above-ground atmosphere is about -9.5‰, the $\Delta^{13}C$ value at the ground surface would be expected to be about (0.0011×-22‰ + 0.0179×-9.5‰)/0.0190 = -10.2‰, i.e. within the observed above-ground range (Section 2.3.1). Similarly, as the $\Delta^{14}C$ value for the soil atmosphere is about 50‰ and the $\Delta^{14}C$ for the above-ground atmosphere is about 25‰, the $\Delta^{14}C$ value at the ground surface would be expected to be about (0.0011×50‰ + 0.0179×25‰)/0.0190 = 26.4‰, i.e. again within the observed above-ground range (Section 2.3.1).

2.4 CONCLUSIONS RELATING TO THE FINNISH FOREST SCENARIO

Overall it is clear that the profile of C-14 within a forest canopy is determined by the flux from the ground surface and the concentration in air above the canopy. However, the other key controls are the rate of biological utilisation within the forest canopy and the effects of diffusive/dispersive mixing within the canopy. These effects can be represented in a detailed physically based model that takes account of details of the vertical structure of the canopy. However, useful insights can also be gained from sensitivity studies with a simplified model that treats the properties of the canopy to be independent of height. Both types of model show that enhanced concentrations of C-14 arising due to a flux from the forest floor are likely to be rapidly attenuated with height within the canopy atmosphere. This further emphasises that a 1D model is likely to be adequate, as horizontal displacements of emitted C-14 will be small in the limited time available for C-14 to diffuse upward over about one metre and be removed from the atmosphere by biomass uptake. However, more refined modelling would take account of diurnal variations, with CO_2 released from the soil at night diffusing upward through the canopy and being lost from the system without being taken up by plants for use in photosynthesis. For $K = 10^{-2}$ m^2 s^{-1} and a canopy depth of 14 m, the characteristic diffusion time for loss is about $14^2/3\ 10^{-2} = 6530$ s, so timescales for diffusion are comparable with timescales for diurnal variation in photosynthetic intensity. In contrast, during the day, the characteristic length for depletion is about one metre, so the characteristic diffusion timescale is about $1^2/3\ 10^{-2} = 33$ s. Thus, horizontal variability in conditions and wind-driven advection are much less likely to be of significance during the day than at night. However, the situation at night is of limited interest in an assessment context, because incorporation of C-14 in biomass by photosynthesis will not occur.

3. DUKE SWAMP SCENARIO

In a previous BIOPROTA study, a model was proposed for transport of C-14 from Waste Management Area C (WMA-C) to Duke Swamp [Limer at al., 2017]. However, little work was done on quantifying the source term from WMA-C or on modelling the spatial distribution of C-14 in Duke Swamp. Thus, in this phase of the work, a request was issued for participants to simulate the detailed spatial distribution of C-14 in Duke Swamp. In practice, to date, the only detailed analysis that has been undertaken is that by the Technical Support Team. This is reported below. It is hoped that this analysis will provide a stimulus to the application of other approaches and to a discussion of the key processes that appear to be operating at Duke Swamp.

3.1 DUKE SWAMP: BACKGROUND

Duke Swamp is a wetland ecosystem on Atomic Energy of Canada Limited (AECL)'s Chalk River Laboratories (CRL) site that receives C-14 through releases from the up-gradient Waste Management Area (WMA) "C", primarily through groundwater influx (Figure 23). Groundwater flow is from 'Lake 233' on one side of WMA-C towards the Duke Swamp, below WMA-C; a cross-section of the stratigraphy is given in Figure 24. WMA-C consists of a series of unlined sand trenches that were constructed in 1963 and which received about 100,000 m^3 of low-level radioactive waste through to 2006. The facility is located on a large dune ridge above the highest recorded water table. The area is predominantly compacted sandy glacial till underlain by granitic gneiss bedrock [Donders et al., 1996]. Waste was initially covered with 1.5 m uncontaminated sand backfill from 1983 and subsequently provided with an engineered cover c. 2013-14 [CNSC, 2015]; also, in 1983 a polyethylene cover was placed over about 1/6 of the southern end of the disposal area.

The uptake of C-14 in vegetation in Duke Swamp itself has been studied for over 20 years (e.g. Milton et al. [1998]; King-Sharp et al. [2005]), as has the quantification of C-14 levels in a wider range of environmental media, including air, groundwater, surface water, sediments and invertebrates (e.g. Sheppard et al. [1994]; Evenden et al. [1998]; Hardwick [1999]).

Historical focus was limited to the area within the swamp where the highest radionuclide concentrations were expected to occur. In 2001, a sampling survey was carried out across a broader area within Duke Swamp, to quantify C-14 levels in surface vegetation and, to a lesser extent, in soils. A subset of the sites sampled was then selected for more detailed study to assess whether C-14 levels measured in sedentary species (e.g., plants and fungi) reflected those measured in mobile organisms (e.g., animals). There followed a series of reports that were not readily available (e.g. King-Sharp et al. [2005]), though an analysis of those findings with regards C-14 concentrations in environmental media and uptake into biota was later published in the Journal of Environmental Radioactivity [Yankovich et al., 2013]. Subsequent to that publication, a study into the spatial distribution of C-14 concentrations in sphagnum moss (Figure 25) and the underlying sediment has been published [Yankovich et al., 2014]. It is possible that the 15 sites where C-14 activity in sediment was measured by Hardwick [1999] (see Figure 26) are co-located with some of 46 locations considered in the Yankovich et al. [2014] study. However, some further investigation would be required to confirm their status as the ID numbers are not the same. All of this work has focussed on the Duke Swamp area itself.

Independent of the work described above, in recent years a PhD student from Oregon State University has undertaken two sampling campaigns (2013 and 2014) looking at the area between the discharge point, WMA-C, and Duke Swamp [Napier, 2015]. Groundwater, soil gas, and plant samples were collected to observe vertical profiles of stable and radioactive carbon at 22 sampling locations between the release point and Duke Swamp (Figure 27). A small subset of those locations, four along the Duke Swamp boundary, are co-located with locations where C-14 in groundwater was measured and reported in Killey et al. [1998].

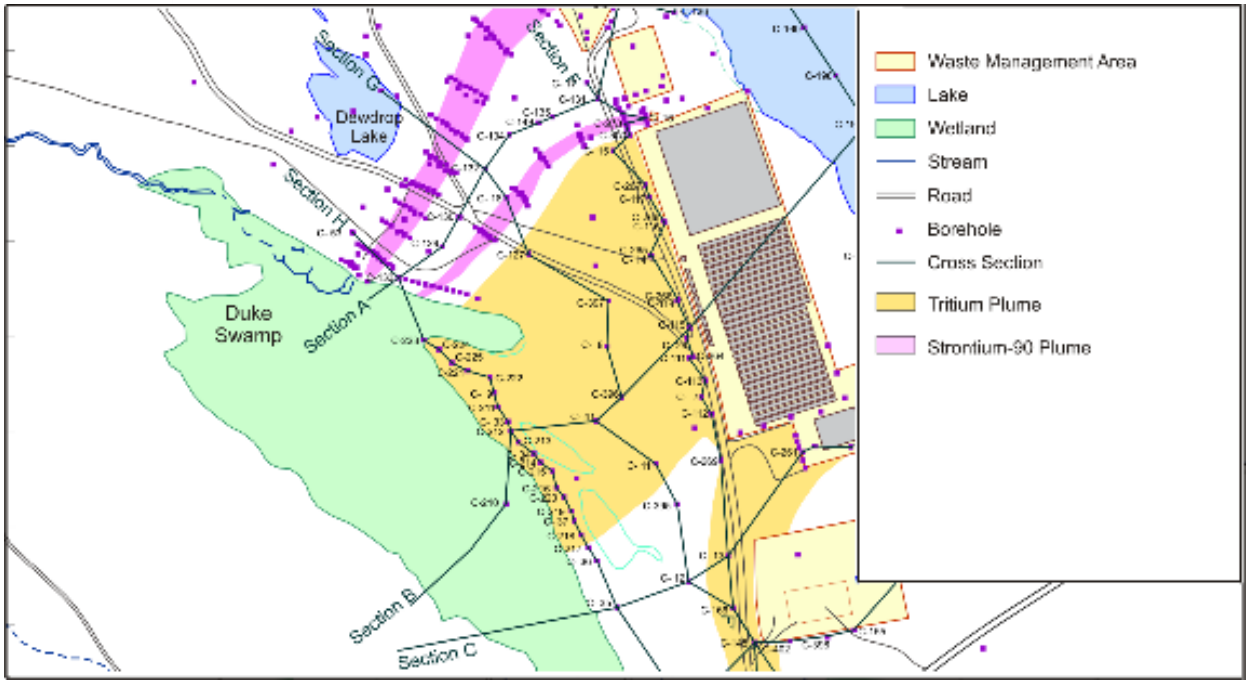

Figure 23: Well map near Waste Management Area C, located at Chalk River Laboratories. The C-14 plume is expected to be similar to the tritium plume highlighted in the figure; best available copy taken from presentation given by J. Napier in 2015.

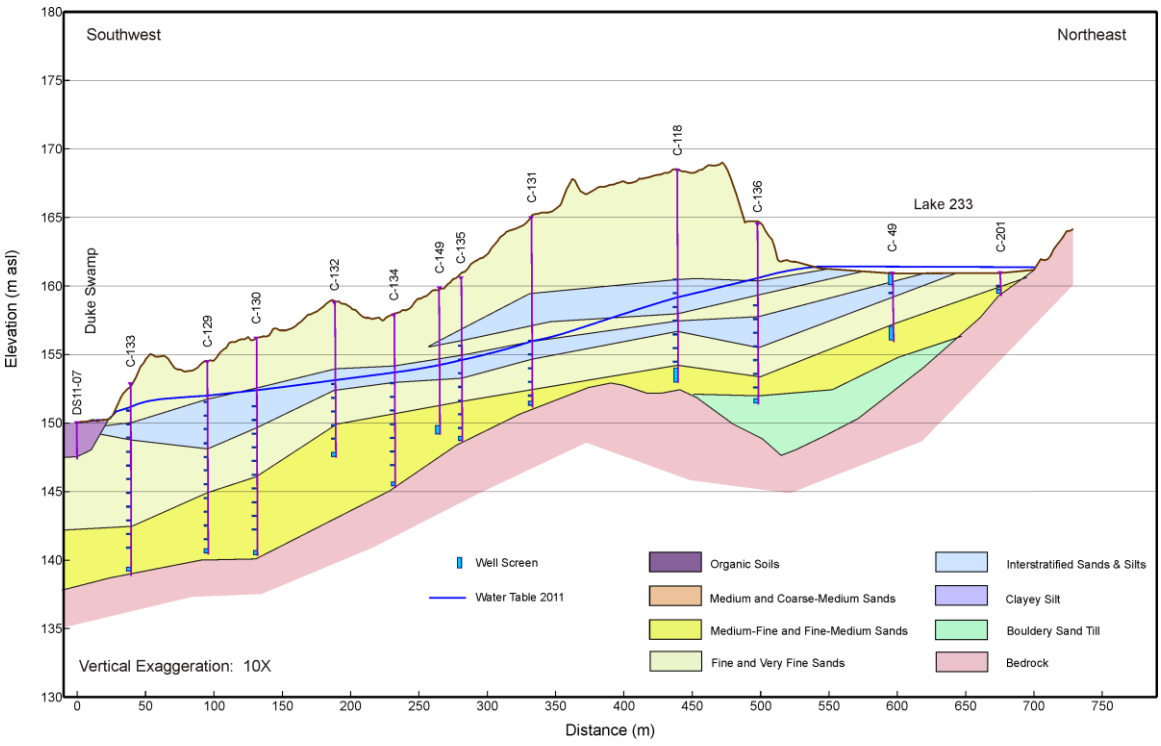

Figure 24: Cross-section of the stratigraphy between Waste Management Area C, located at Chalk River Laboratories and Duke Swamp (Section A from Figure 23); taken from presentation given by J. Napier in 2015.

Statistical analysis and linear regression applied to the data collected have shown different significant variables between subsets close to the release point, WMA-C, and the surface emission point, Duke Swamp. In particular, the data collected indicates the likelihood of two different contamination pathways for the vegetation downstream of WMA-C. Close to the facility, plant C-14 specific activity was best explained through incorporation of contaminated soil gas emitted by WMA-C. However, close to the swamp, plant C-14 activity was best explained by the distance to the surface of the contaminated groundwater. Both are linked to the physical movement of carbon through the vadose zone due to diffusion and dispersion.

Further description of Duke Swamp site is provided in Appendix A, together with the data set considered for potential model-data comparisons.

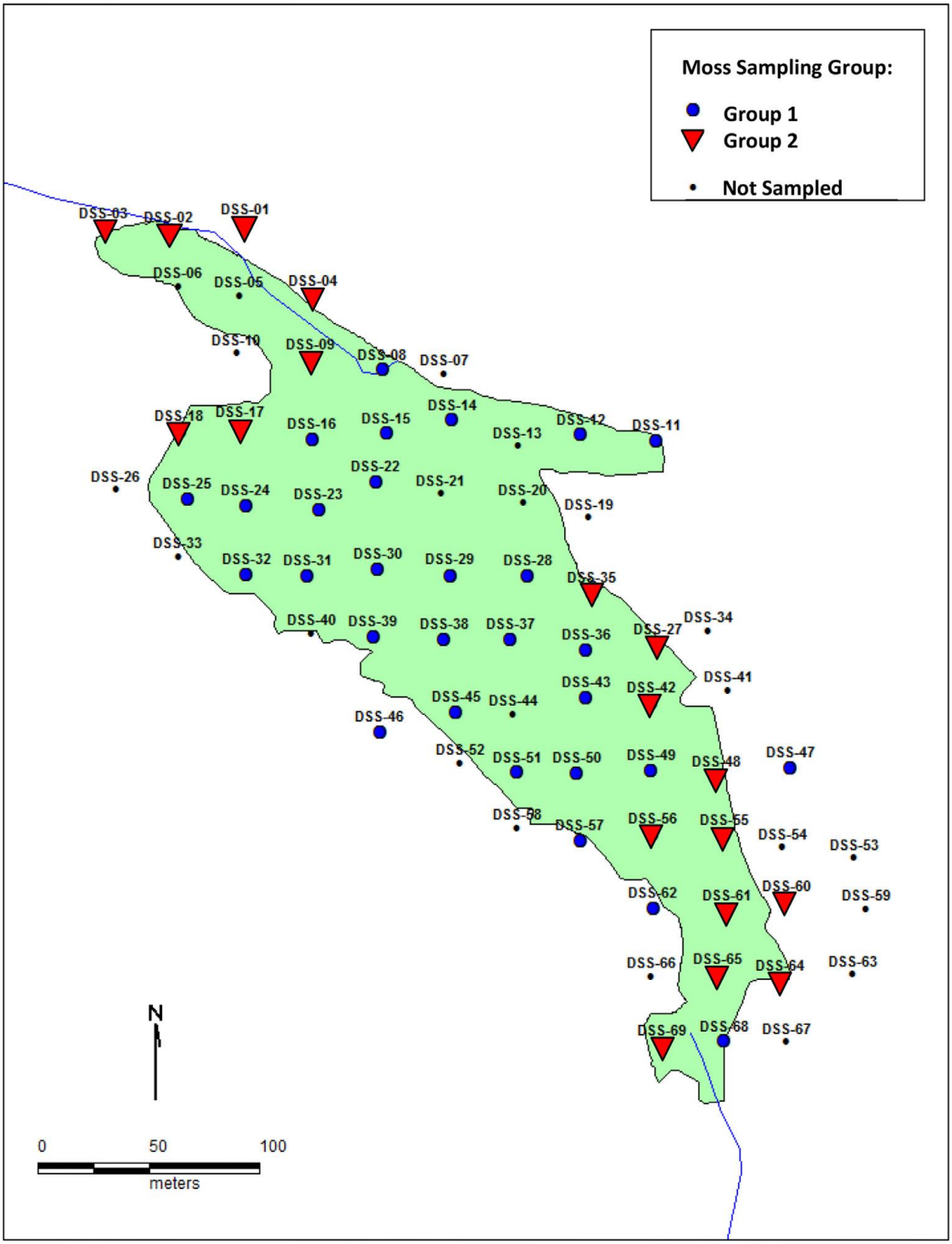

Figure 25: Sphagnum moss sampling locations from Yankovich et al. [2014]. Sediment samples were also obtained from some of these locations.

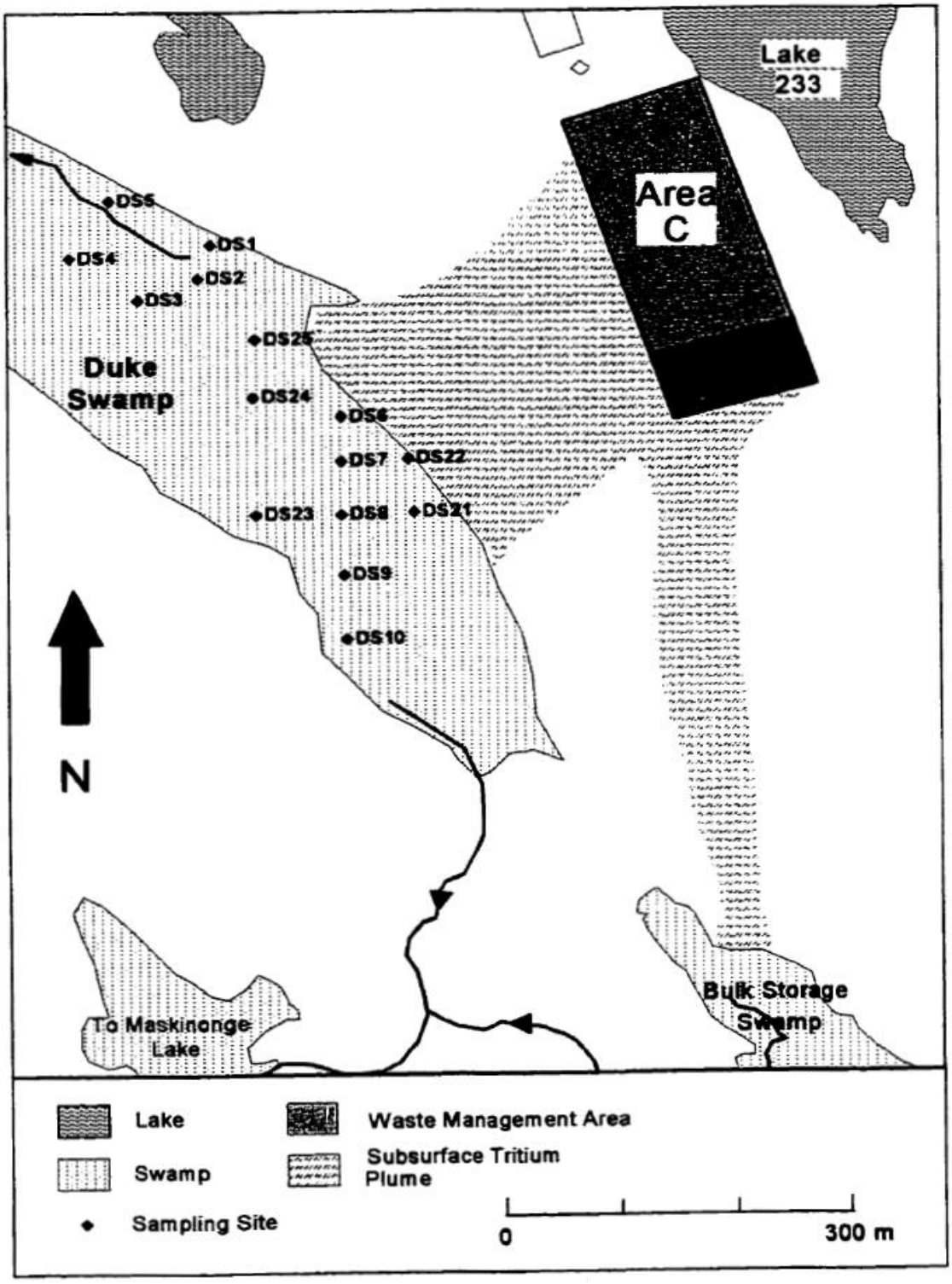

Figure 26: Sampling locations considered in Hardwick [1999].

Figure 27: Aerial photograph with sampling locations from Napier [2015].

3.2 OBJECTIVES

In a previous study [Limer et al., 2017], detailed consideration was given to modelling the transport of C-14 between Waste Management Area C (WMA-C) and Duke Swamp, but much less attention was given to establishing the magnitude of the source term from WMA-C or to modelling the detailed spatial distribution of C-14 within Duke Swamp. Therefore, the BIOPROTA Technical Support Team has focussed on these issues in its most recent programme of work. In Section 3.3, an analysis is provided of the source term from WMA-C, considering both the total inventory of C-14 present and the flux of C-14 being released. Taken together, these two estimates of inventory and flux permit calculation of the potential period over which the current flux could be sustained.

The flux of C-14 projected to enter Duke Swamp constitutes the starting point of an analysis of how C-14 is likely to become distributed in the swamp over time. This analysis is reported in Section 3.4. It shows the likely importance of volatilisation, uptake into biomass and transport in groundwater in the lower part of the swamp. A 1D model with two vertical layers that was implemented in the compartment modelling code AMBER [Quintessa, 2017] is shown to give a good representation of the experimental observations.

3.3 SOURCE-TERM ESTIMATION

3.3.1 Estimation of the Flux of C-14 Entering Duke Swamp based on Analyses of Groundwater

The source term to the groundwater system originates from WMA-C. For a transect between WMA-C and Duke Swamp, Killey et al. [1998] determined linear groundwater velocities in the range 0.09 to 2.1 m d^{-1}, with a mean value of 0.42 m d^{-1}. As the distance between WMA-C and Duke Swamp is about 200 m (from the near edge of WMA-C) to 300 m (from the centre of WMA-C), the unretarded groundwater transit time is about 250/0.42 = 600 d. This indicates that there is likely to be a delay of no more than a few years between C-14 being released from WMA-C and entering Duke Swamp. Killey et

al. [1998] further estimated that the total groundwater input to Duke Swamp from the WMA-C area is 103,000 m^3 y^{-1}.

Groundwater samples from multiple boreholes at multiple depths were analysed for C-14. The concentrations found ranged from 50 Bq L^{-1} to 490 Bq L^{-1}. The spatial distribution of concentrations is shown in Figure 5 of Killey et al. [1998]. As both C-14 concentrations and groundwater fluxes were available at most borehole intervals, it was possible to compute the total C-14 flux entering Duke Swamp in groundwater during 1991 to be 6.5 GBq, i.e. a rate of 6.5 GBq y^{-1}.

However, Killey et al. [1998] pointed out that streamflow through the weir on Duke Stream for 1 December 1990 to 30 November 1991 was 77,100 m^3. This is based on weekly measurements, but Killey et al. [1998] used data from Lower Bass Creek to determine that this value is probably in error by no more than ±10% due to selective monitoring of the effects of short-term fluctuations. This streamflow includes runoff of 10,400 m^3 from precipitation falling on the rocky southwestern boundary of Duke Swamp as well as on Duke Swamp itself. Therefore, the groundwater contribution to this outflow is 66,700 m^3 y^{-1} rather less than the estimated groundwater inflow of 103,000 m^3 y^{-1}. As this approach to determining groundwater flux is probably more accurate than the method of combining flux measurements from borehole sections, the annual flux of C-14 entering Duke Swamp in 1991 is estimated as 66,700×6.5/103,000 = 4.2 GBq. This is slightly more than the value of 3.6 GBq y^{-1} given by Killey et al. [1998] and no explanation has been found for the difference.

Killey et al. [1998] also calculated a second mass balance using H-3 fluxes. A total of 14.6 TBq was discharged in the Duke Stream during the study year of 1991. Applying a potential evapotranspiration rate of 630 mm y^{-1} to Duke Swamp and assuming that the actual evapotranspiration rate is equal to the potential evapotranspiration rate for this wetland area, Killey et al. [1998] used an area of 60,000 m^2 to estimate an evapotranspiration rate of 37,800 m^3 y^{-1}. With an average H-3 concentration in water of 1.96 10^8 Bq m^{-3}, this gives losses in evapotranspiration of 7.4 TBq. Thus, the total loss of H-3 from the system is 22 TBq y^{-1}. For comparison, based on groundwater flow data, Killey et al. [1998] estimated the H-3 input to Duke Swamp as 43.7 TBq y^{-1}. Using the same scaling approach as for C-14, this decreases to 66,700×43.7/103,000 = 28 TBq y^{-1}, which is in better agreement with the total estimated loss. Again, Killey et al. [1998] give a somewhat smaller value of 24.0 TBq y^{-1}.

Overall, it seems that the C-14 flux into Duke Swamp in 1991 was probably in the range 3.6 to 6.5 GBq y^{-1}, and there is no reason to assume that the flux was very different in immediately preceding years. However, the flux entering the groundwater system from WMA-C must have been somewhat larger, as losses in the gas phase from the vadose zone are expected to have occurred. Nevertheless, the flux from WMA-C is likely to have been of a similar order of magnitude and a reasonable basis for calculation would be to assume a reference value of 6.5 GBq y^{-1}, as the principal aim of the calculations is to simulate the groundwater concentrations given in Figure 5 of Killey et al. [1998], as a basis for the detailed studies of C-14 transport in Duke Swamp described in Section 3.4.

3.3.2 Storage of C-14 in the Aquifer

Taking an input to the groundwater system of 6.5 GBq y^{-1} and a transit time of 600 d (1.643 y) (based on the assumption that C-14 is not retarded in the sandy materials comprising the aquifer), the total C-14 inventory stored in groundwater at any time is 10.7 GBq. From Figures 3 and 4 of Killey et al. [1998], a reasonable estimate of the volume of interest can be based on a 200 m width and 250 m length of the transect and a 10 m depth. This gives a volume of 500,000 m^3. With a porosity of 0.38 [Killey et al., 1998], this gives a water volume of 190,000 m^3 and an average concentration of 1.07 10^{10}/1.90 10^8 = 56 Bq L^{-1}. This is in good agreement with the range of concentrations shown in Figure 5 of Killey et al. [1998]. This shows about 5% of the volume with concentrations of 300 – 1000 Bq L^{-1}, about 10% with 100 – 300 Bq L^{-1} and about 30% with 30 to 100 Bq L^{-1}, giving an average concentration of about

60 Bq L^{-1}. Thus, the concentrations of C-14 in the aquifer are in good agreement with the source-term estimates given in Section 3.3.1. However, this is not an independent confirmation, as the measured groundwater calculations were used in obtaining the flux estimates given in Section 3.3.1.

3.3.3 Uptake of C-14 in Duke Swamp and Losses by Volatilisation

Killey et al. [1998] also estimated the C-14 uptake by the vegetation and peat of Duke Swamp. For the vegetation, their analysis was based on the C-14 specific activity of 25 samples of *Picea glauca* (white spruce). This information was combined with an estimate of the primary productivity of the wetland as 500 g[C] m^{-2} y^{-1}, based on literature data. This gave an accumulation of 330 MBq of C-14 during 1991 within the area defined by the 10 Bq g^{-1} contour. Killey et al. [1998] noted that there is a fourfold variability in C-14 concentrations measured in different plant species from a given location in the wetland. Although this suggests a similar degree of uncertainty in the annual uptake, Killey et al. [1998] also point out that white spruce is a substantial contributor to primary productivity, so reducing the uncertainty in the inventory.

For the peats, C-14 concentrations were obtained from peat cores, with analyses of the surface, middle and base of the cores. Again, the 10 Bq g^{-1} contour was assumed to represent the areal extent of contamination of the peat. Within this contour, each peat column was divided into layers 0.3 m thick and the average specific activity of each layer was determined. The total C-14 content of the peat was determined assuming an average porosity of 0.6, a dry bulk density of 0.4 g cm^{-3} and a 50% carbon content of the peat. This gave a total waste-derived C-14 inventory in the peat of 7.6 GBq. As there was no means of identifying when this C-14 was added to the peat, it was assumed to have been delivered at a uniform rate over the 20-year period for which C-14 from WMA-C had been arriving at Duke Swamp. Thus, the accumulation rate was estimated to be 0.29 GBq y^{-1} (this seems to be a typographical error for 0.38 GBq y^{-1})

From the discussion in Section 3.3.1, the C-14 input into Duke Swamp in 1991 was probably in the range 3.6 to 6.5 GBq. Of this, about 0.33 GBq was accumulated in the vegetation and 0.29 GBq (or 0.38 GBq) was accumulated in the peat. Killey et al. [1998] determined that the loss of C-14 from Duke Swamp in surface waters was only about 1.5 to 2.0% of the input, i.e. about 0.05 to 0.13 GBq. Thus, 2.9 to 5.8 GBq of the input remains unaccounted for, leading to the estimate by Killey et al. [1998] that 79 to 84% of the C-14 input to the swamp in 1991 was lost to the atmosphere.

3.3.4 Relation of the New Source-term Data to Previous Modelling Studies

In Limer et al. [2017], calculations were made using a multi-compartment model for a source term of 1 TBq released over a 150-year period, i.e. a release rate of 6.67 GBq y^{-1}. This is slightly larger than the upper limit of the rate of C-14 delivery to Duke Swamp in groundwater estimated above. Detailed examination of the model shows that equilibrium is achieved on a timescale of about 10 years. Therefore, the results presented in Limer et al. (2017) at 30 years represent the equilibrium situation. Concentrations in groundwater at 30 years are shown in Figure 44 of Limer et al. [2017]. For a degree of saturation of the vadose zone, *S*, of 0.5, aquifer concentrations ranged from 105 Bq L^{-1} close to WMA-C down to 34 Bq L^{-1} close to Duke Swamp. This is in good agreement with the average value for the aquifer of 60 Bq L^{-1} calculated in Section 3.3.2 based on the information in Killey et al. [1998]. For S = 0.7, the aquifer concentrations are somewhat higher ranging from 170 Bq L^{-1} down to 140 Bq L^{-1}.

A cautious estimate of the concentrations anticipated in the aquifer, as modelled by Limer et al. [2017] can be obtained by neglecting transport by diffusion and considering the system as an advective flow regime. The overall flow regime is illustrated in Figure 28.

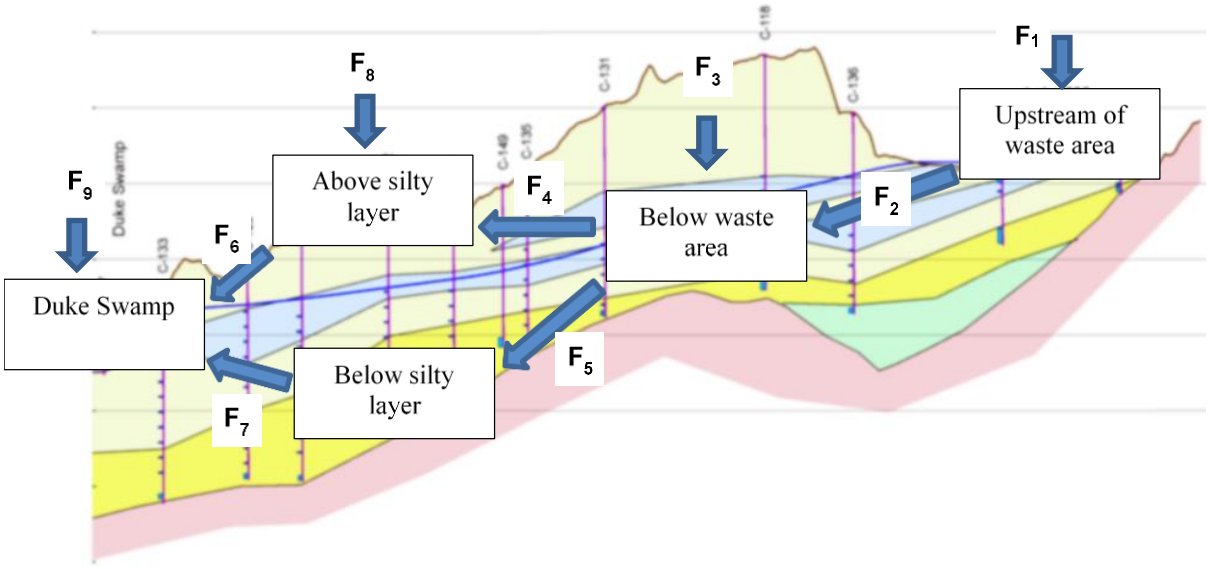

Figure 28: Conceptualisation of the overall flow regime.

Values of the various flows F_1 to F_9 are given in Appendix A.

For an input rate of 6.67 GBq y^{-1}, the groundwater concentration of C-14 below and immediately downstream of WMA-C calculated neglecting losses through the vadose zone is 6.67 10^9/2.31 10^7 = 289 Bq L^{-1}. As expected, this is somewhat larger than the model estimates of 105 Bq L^{-1} (S = 0.5) and 170 Bq L^{-1} (S = 0.7). Note that the trend is to approach the limiting value as S increases, so decreasing diffusive volatilisation losses.

Similarly, for an input rate of 6.67 GBq y^{-1}, the groundwater concentration of C-14 immediately upstream of Duke Swamp calculated neglecting losses through the vadose zone is given by 6.67 $10^9/F_7$ = 6.67 $10^9/\{(1 – \alpha)(F_4 + F_5)\}$ = 6.67 $10^9/\{(1 – \alpha)3.78\ 10^7\}$ = 176/(1 – α) Bq L^{-1}. The model estimates of 34 Bq L^{-1} (S = 0.5) and 140 Bq L^{-1} (S = 0.7) are consistent with α = 0, i.e. all the water being routed below the silty layer. Mixing with meteoric water delivered to above the silty layer (F_8) would give a concentration of 6.67 10^9/6.84 10^7 = 98 Bq L^{-1}. This is below the concentration modelled for S = 0.7.

3.3.5 Relation of the C-14 Inventory Estimate for Duke Swamp to More Recent Modelling studies

Finally, it is of interest to compare the inventories of C-14 in Duke Swamp vegetation and peat estimated by Killey et al. [1998] with data from Yankovich et al. [2014], relating to sampling in 2001, as summarised in Appendix A. The sampling locations are arranged on an approximately square grid with a side length of about 50 m[a]. There are 46 sampling points that lie within Duke Swamp, so the associated area is about 46×50×50 = 115,000 m^2. Taking the measured concentrations to apply to the top 0.3 m of the swamp, the total volume is 34,500 m^3. Following Killey et al. [1998], a dry bulk density of 0.4 g cm^{-3} (400 kg m^{-3}) and a 50% carbon content of the peat are assumed. Thus, the total mass of carbon is

[a] In Figure 2 of Yankovich et al. [2014], which is reproduced in Appendix A, the scale bar implies that the sampling points are separated by about 30 m. However, the text of the paper refers to them being arranged on a 50 m grid. Based on a 50 m grid, the area of Duke Swamp is estimated to be 115,000 m^2. This is in good accord with the statement by Yankovich et al. [2014] that the swamp covers an area of approximately 0.1 km^2.

34,500×400×0.5 = 6.90 10^6 kg[C]. The average specific activity of the Sphagnum moss from Table 16 in Appendix A is 3840 Bq kg[C]$^{-1}$ (including only sample points within the swamp). However, this includes a contribution from background of about 250 Bq kg[C]$^{-1}$, so a rounded average is about 3600 Bq kg[C]$^{-1}$. Thus, the total C-14 content of Duke Swamp originating from WMA-C is estimated to be 6.90 10^6 × 3600 = 2.48 10^{10} Bq (24.8 GBq). This is somewhat larger than the estimate of a total waste-derived C-14 inventory in the peat of 7.6 GBq given by Killey et al. [1998] for 1991. This is consistent with continuing accumulation of C-14 at a similar rate over the years after 1991 (see also Section 3.4.1).

3.3.6 Potential Duration of the Source Term from Waste Management Area C

Very little information is available on the total inventory of C-14 in WMA-C. However, Donders et al. [1996] gave data for dissolved C-14 concentrations in five soil cores beneath WMA-C and for DIC and DOC concentrations in these same cores. The concentrations and associated specific activity values are given in Table 2.

Table 2: Concentration Data for C-14 in Five Cores from WMA-C.

Core	DIC (mg L^{-1})	DOC (mg L^{-1})	Activity (Bq L^{-1})	Specific Activity (Bq kg[C]$^{-1}$)
CT-1	4.6	4.8	<45	<4.79E+06
CT-2	16.8	0.7	67	3.83E+06
CT-3	9.3	0.8	<45	<4.46E+06
CT-4	24.4	8.1	112	3.45E+06
CT-5	34	9.8	720	1.64E+07

In Table 2, the specific activity is defined relative to the total carbon in solution, i.e. DIC plus DOC.

Donders et al. [1996] estimated that WMA-C contained about 1 10^5 m^3 of waste in a series of trenches covering an area of about 5 10^4 m^2 (5 ha). Thus, the average depth of waste was then about 2 m. The weight percent moisture content of the soils was 1.4 to 18.7%, where 15 to 18% represents fully saturated soil [Donders et al., 1996]. Assuming 10% water content by volume, the total water content of the wastes was 1 10^4 m^3. Taking the activity concentration of in solution to be about 190 Bq L^{-1} (based on Table 2), the total activity in solution is estimated to be about 1.9 GBq. Also, if about 1.47 10^4 m^3 y^{-1} of water infiltrates through the waste (flow F_3 in Figure 1), the total flux of C-14 from the wastes is estimated as 1.47 10^7 × 190 = 2.79 10^9 Bq y^{-1} (2.79 GBq y^{-1}). This is close to the value of 6.5 GBq y^{-1} estimated in Section 3.3.1.

3.3.7 Timescale for Depletion of the C-14 Inventory of Waste Management Area C

Donders et al. [1996] described the wastes as comprising caps from scintillation vials, plastic, chunks of translucent rubbery material, Styrofoam balls, fibrous material in green dye and flakes of metal, in a sand-fill matrix. It seems likely that the dry bulk density of this material is around 1000 kg m^{-3} and that its carbon content is in the range 1 to 10% by mass. Adopting 10% as a cautious estimate, the total mass of carbon present is estimated as 1 10^5 m^3 × 1000 kg m^{-3} × 0.1 = 1 10^7 kg. Assuming this to have a specific activity equal to that in solution, i.e. about 4 10^6 Bq kg[C]$^{-1}$, the total C-14 inventory is about 4 10^{13} Bq (4000 GBq). This is a cautious over-estimate. If used with the estimated output flux of 6.5 GBq y^{-1}, it implies that the characteristic time for depletion of the inventory would be no longer than 4000/6.5 = 615 years. Taking radioactive decay into account would reduce the upper bound from 615 years to 555 years.

3.4 MODELLING C-14 TRANSPORT IN DUKE SWAMP

In Sections 3.4.1 and 3.4.2, what is known of the inventory and distribution of C-14 in Duke Swamp is summarised. Subsequent sections then describe modelling studies designed to account for both the inventory and distribution data.

3.4.1 The Inventory of C-14 in Duke Swamp and Losses by Volatilisation

As discussed in Section 3.3 and based on Killey et al. [1998], the total C-14 inventory in the peat of Duke Swamp in 1991 was estimated as 7.6 GBq. Based on Yankovich et al. [2014], the inventory in 2001 was 24.8 GBq.

In 1991, C-14 had accumulated in Duke Swamp for about 20 years. Thus, the accumulation rate was 7.6/20 = 0.38 GBq y^{-1}. By 2001, accumulation had occurred for 30 years, giving an accumulation rate of 24.8/30 = 0.83 GBq y^{-1}. Assuming an influx of 3.6 to 6.5 GBq y^{-1} (see Section 3.3), this implies that 0.83/6.5 = 0.13 to 0.83/3.6 = 0.23 of C-14 entering Duke Swamp is subject to long-term retention there, with the remainder (0.77 to 0.87) largely lost through volatilisation (see also Section 3.3). Killey et al. [1998] estimated losses of 0.79 to 0.84 by volatilisation and 0.015 to 0.02 by surface-water drainage.

An alternative calculation relating to volatilisation is based on measured air concentrations above the swamp. Yankovich et al. [2014] reported C-14 specific activity values in air that were similar to those in Sphagnum moss. Taking a typical value to be 3600 Bq kg[C]$^{-1}$ (excluding the background contribution), and assuming a typical wind speed of 2 m s^{-1} over a height of 2 m and a lateral extent of 100 m, the volumetric flow rate of air across the swamp is 1.26 10^{10} m^3 y^{-1}. This air is about 400 ppm CO_2 by volume or 2.1 10^{-4} kg[C] m^{-3}. Therefore, the rate of loss of ^{14}C is 1.26 10^{10} × 2.1 10^{-4} × 3600 = 9.7 10^9 Bq y^{-1} (9.7 GBq y^{-1}). This demonstrates that the measured air concentrations are large enough to account for the losses by volatilisation that have been inferred by other methods.

3.4.2 The Distribution of C-14 in Duke Swamp

Based on the discussion provided above, a reasonable basis for modelling is that about 6.5 GBq y^{-1} of C-14 enters Duke Swamp in groundwater. The distribution of C-14 in Duke Swamp is given in Yankovich et al. [2014]. The locations of the samples are shown in Figure 25. These are arranged on an approximately square grid, as shown on Figure 29. The measured concentrations are shown on a corresponding square grid at Figure 30. Note that C-14 concentrations were not returned for some locations (shown as blank) and values were less than the limit of detection at some other locations (shown as zero). The same information is shown graphically in Figure 31.

From Figure 30 and Figure 31, the C-14 plume is seen to impinge upon Duke Swamp from the North or North-east along a front approximately 200 m wide. Along this front, the concentration of C-14 averaged over a penetration into the swamp of about 50 m is in the range 8200 to 47,000 Bq kg[C]$^{-1}$, being highest in the centre of the impinging plume and falling off towards its edges. From 50 to 100 m into the swamp, concentrations of 2,000 to 6,000 Bq kg[C]$^{-1}$ are representative and further in concentrations drop to around 1,000 Bq kg[C]$^{-1}$ or less.

DSS-01									
DSS-05	DSS-04								
DSS-10	DSS-09	DSS-08	DSS-07						
DSS-17	DSS-16	DSS-15	DSS-14	DSS-13	DSS-12	DSS-11			
DSS-24	DSS-23	DSS-22	DSS-21	DSS-20	DSS-19				
DSS-32	DSS-31	DSS-30	DSS-29	DSS-28	DSS-35				
	DSS-40	DSS-39	DSS-38	DSS-37	DSS-36	DSS-27	DSS-34		
		DSS-46	DSS-45	DSS-44	DSS-43	DSS-42	DSS-41		
			DSS-52	DSS-51	DSS-50	DSS-49	DSS-48	DSS-47	
				DSS-58	DSS-57	DSS-56	DSS-55	DSS-54	DSS-53
						DSS-62	DSS-61	DSS-60	DSS-59
						DSS-66	DSS-65	DSS-64	DSS-63
						DSS-69	DSS-68	DSS-67	

Figure 29: Sampling locations at Duke Swamp arranged on a square grid.

270									
	930								
	1600	960							
980	630	1100	2000		960	1200			
0	290	380							
420	720	290	3500	8200	47000				
		0	1800	0	6500	17000			
		550	1000		3600	15000			
				1900	2300	1800	9200	370	
					760	2800	5700		
						580	1400	3500	
							1200	1100	
						690	0		

Figure 30: Concentrations of C-14 in Sphagnum at the various sampling locations (Bq kg[C]$^{-1}$).

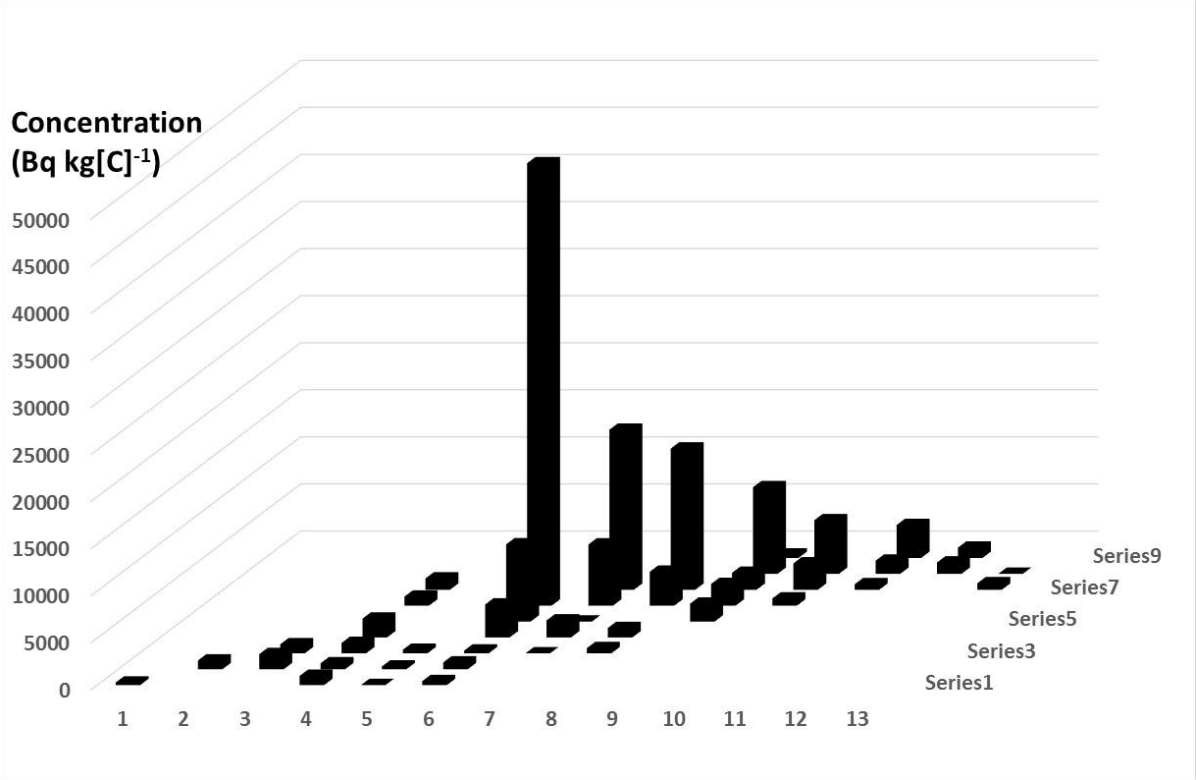

Figure 31: Concentration of C-14 by grid square. Numbers 1 to 13 run from North to South and Series 1 to 9 run from West to East.

3.4.3 Initial Single-layer Model

The data illustrated in Section 3.4.2 initially suggested that a 1D single-layer model of C-14 transport in Duke Swamp could be used. That model is illustrated in Figure 32.

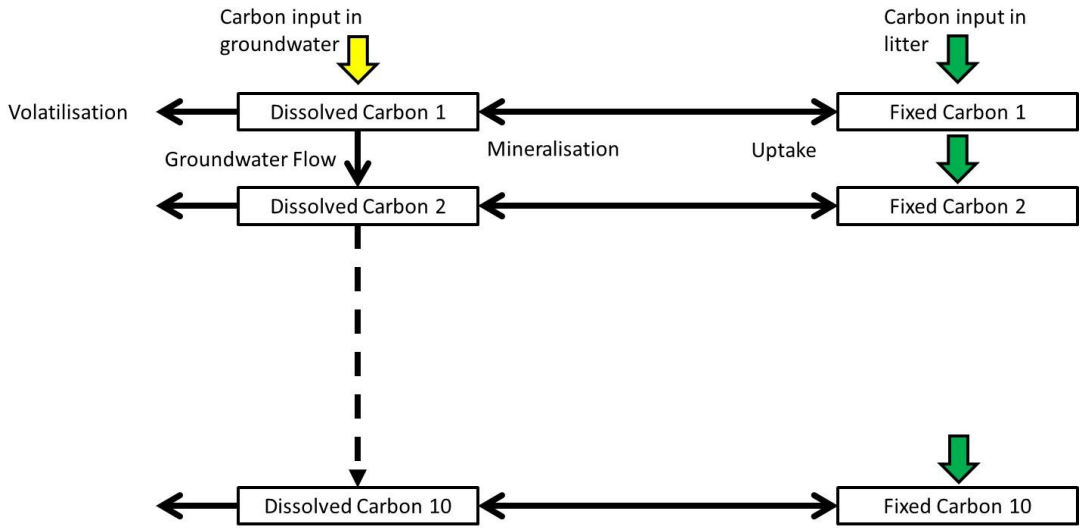

Figure 32: Initial 1D model for C-14 transport in Duke Swamp.

In this model, compartments 1 lie at the upstream boundary of the swamp, i.e. closest to WMA-C, and compartments 10 lie at the downstream boundary of the swamp. Dissolved carbon includes both DIC and DOC. Fixed carbon (i.e. fixed into biomass by photosynthesis) comprises solid organic matter that can either be living or dead and decaying. Thus, uptake is mainly into the living component. This is through photosynthesis and may be of carbon taken up by the roots or of carbon in carbon dioxide released to the air. Mineralisation occurs from the dead component. The primary production each season defines the carbon flux from the living to the dead component and the rate of loss of carbon from the fixed carbon pool by mineralisation. In the following, the sizes of the compartments are first addressed and then consideration is given to the carbon fluxes into, out of, and between them. It is emphasised that treatment of fixed carbon as a single compartment is a simplification. In practice, there are a wide variety of types of chemically and physically stabilised organic matter in soils and these are subject to mineralisation at different rates. However, the data available for Duke Swamp are not sufficient to allow these different types to be distinguished in the model. Also, the model does not allow for flow channelling in the swamp. Heterogeneities in the flow regime could result in variations in the penetration of C-14 into the swamp. This issue has not been addressed in the current study.

The volume of each dissolved carbon compartment, V, is 500 m × 50 m × 0.3 m = 7,500 m^3 multiplied by the total porosity. This assumes that CO_2 dominates in the gas phase and that DIC dominates in the liquid phase. The two will have similar volumetric concentrations. For Duke Swamp, the total porosity is 0.6 (see Section 3.3), so V = 4,500 m^3. In general, the concentration of CO_2 in the soil atmosphere is about a factor of ten larger than in the above-ground atmosphere. Here, a value of 4,000 ppmv is adopted. This corresponds to 0.00214 kg[C] m^{-3}. Thus, the carbon content of each dissolved carbon compartment is 9.64 kg[C].

The mass of each fixed carbon compartment is the volume of 7,500 m^3 multiplied by the dry bulk density (400 kg m^{-3}) and the fraction of dry matter that is carbon (0.5). As calculated previously, this is 1.5 10^6 kg[C].

The flux of contaminated groundwater into Duke Swamp has been estimated as 6.84 10^4 m^3 y^{-1} (see Section 3.3). Taking this groundwater to have a carbon content of 0.00214 kg[C] m^{-3}, the influx of carbon in groundwater is estimated to be 146.6 kg[C] y^{-1}. The total flux of precipitation directly into Duke Swamp is 3.46 10^4 m^3 y^{-1} (see Appendix A). Assuming a CO_2 concentration in groundwater of 4,000 ppmv throughout the swamp, water and carbon flows between the various compartments are as listed in Table 3.

Carbon fluxes due to mineralisation can be determined from the rate of primary production. This has been estimated as 0.5 kg[C] m^{-2} y^{-1} [Killey et al., 1998]. As each compartment is 500 m × 50 m = 25,000 m^2, the carbon flux due to mineralisation is 12,500 kg[C] y^{-1}.

Uptake into vegetation either through the roots or by release from soil to the sub-canopy atmosphere and uptake by the foliage is usually anticipated to contribute only a small fraction of plant carbon. In agricultural systems, this fraction is typically 0.01 to 0.05. However, in an organic soil the situation is likely to be different. By observation (see Section 3.4.1), about 20% of C-14 entering the swamp in groundwater seems to be retained in the long term. Here, the fraction is taken to be 0.2 for all inorganic carbon entering soil solution, either in influx from outside the system or as a result of mineralisation within the system. Thus, the carbon flux due to uptake is estimated as 0.2×12,500 = 2,500 kg[C] y^{-1}.

For each dissolved carbon compartment, there is a net loss of carbon in groundwater of 7.4 kg[C] y^{-1}. Therefore, by mass balance, the loss of carbon by volatilisation is 12,500 – 2,500 – 7.4 = 9,992.6 kg[C] y^{-1}.

Based on the above, it is possible to calculate rate constants for all relevant transfers of carbon in the model. For convenience, the compartments are designated DC1 to DC10 and FC1 to FC10 using an obvious nomenclature.

This model was implemented in AMBER. Illustrative results are shown in Figure 33 for an input flux of 1 GBq y^{-1}.

For an input rate of 1 GBq y^{-1}, the total activity retained in the swamp at 1 year is 0.2 GBq, at 10 years it is 1.93 GBq and at 30 years it is 5.40 GBq. Thus, for 6.5 GBq y^{-1}, the retention in the swamp at 30 years is 35.1 GBq, which is slightly larger than the experimental estimate.

Table 3: Groundwater and carbon fluxes between the dissolved carbon compartments.

Compartments	Groundwater Flux (m^3 y^{-1})	Carbon Flux (kg[C] y^{-1})
Into 1	68,400	146.6
From 1 to 2	71,860	154.0
From 2 to 3	75,320	161.4
From 3 to 4	78,780	168.8
From 4 to 5	82,240	176.2
From 5 to 6	85,700	183.6
From 6 to 7	89,160	191.1
From 7 to 8	92,620	198.5
From 8 to 9	96,080	205.9
From 9 to 10	99,540	213.3
Out of 10	103,000	220.7

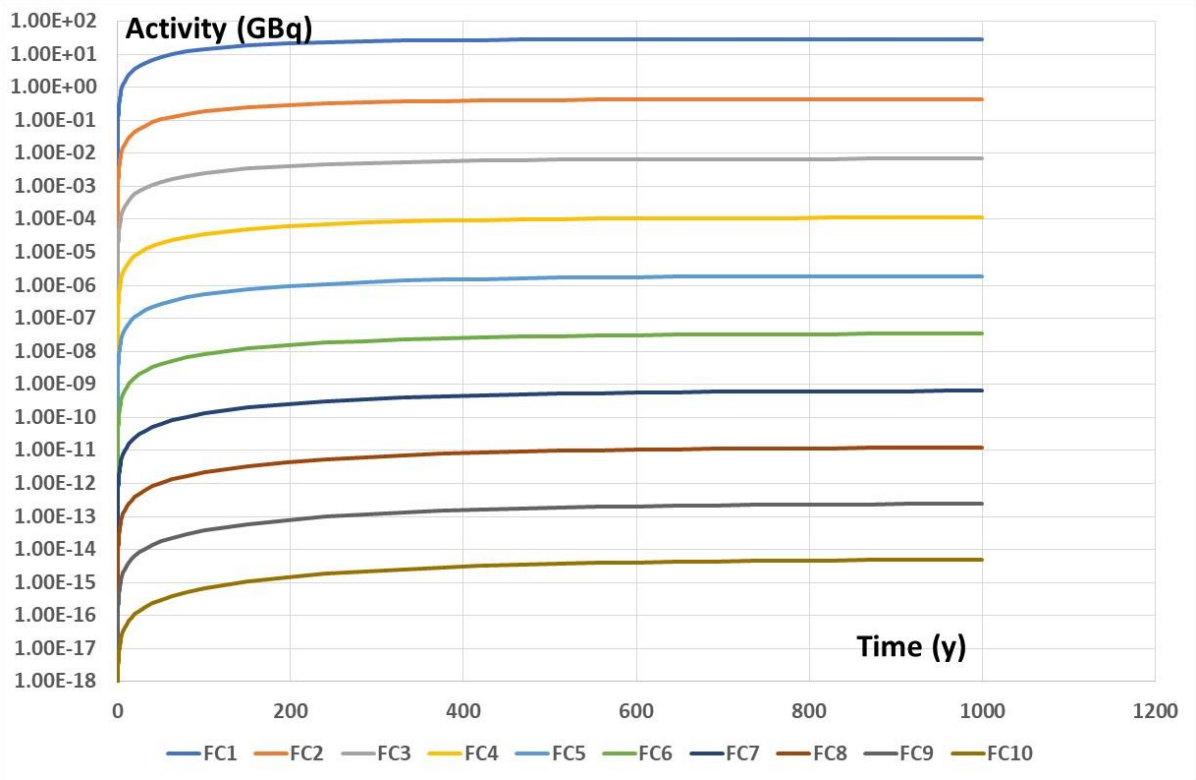

Figure 33: Activity of C-14 in the fixed carbon compartments of the single-layer model for the initial reference case.

3.4.4 Limitations of the Initial Model and its Modification

Some limitations of the 1D model of C-14 transport in Duke Swamp described in Subsection 3.4.3 can be illustrated by considering an approximate analytic solution of this model at equilibrium. This solution is set out below. It shows that the spatial resolution of 50 m used initially is not sufficiently fine and that numerical dispersion dominates at that scale.

The governing equations for the model are:

$$\partial C(x,t)/\partial t = -v(x)\,\partial C(x,t)/\partial x - (k_1 + k_2 + k_R)C(x,t) + k_3 S(x,t) \quad (24)$$

$$\partial S(x,t)/\partial t = k_2 C(x,t) - (k_3 + k_R)S(x,t) \quad (25)$$

where $C(x,t)$ (Bq m^{-3}) is the concentration of C-14 in groundwater in the swamp;

$S(x,t)$ (Bq m^{-3}) is the concentration of C-14 in Sphagnum;

$v(x)$ (m y^{-1}) is the groundwater velocity;

x (m) is the distance into the swamp;

t (y) is the time in years;

k_1 (y^{-1}) is the loss rate from groundwater by volatilisation;

k_2 (y^{-1}) is the loss rate from groundwater by uptake by Sphagnum;

k_3 (y^{-1}) is the loss rate from Sphagnum to groundwater by mineralisation;

k_R (y^{-1}) is the radioactive decay constant of C-14.

At equilibrium:

$$v(x)dC(x)/dx = k_3S(x) - (k_1 + k_2 + k_R)C(x) \quad (26)$$

$$k_2C(x) = (k_3 + k_R)S(x) \quad (27)$$

Leading to:

$$dC(x)/dx = \{[k_2k_3/(k_3 + k_R) - (k_1 + k_2 + k_R)]/v(x)\}C(x) \quad (28)$$

For $v(x)$ independent of x (which is not precisely the case at Duke Swamp, but is a good approximation over the spatial scale being modelled), this has the solution:

$$C(x) = C(0)\exp(-\lambda x) \quad (29)$$

Where:

$$\lambda = [-k_2k_3/(k_3 + k_R) + (k_1 + k_2 + k_R)]/v \quad (30)$$

The interest of this approximate solution is that the characteristic length of penetration into the swamp ($L = 1/\lambda$) is given by:

$$L = v/[-k_2k_3/(k_3 + k_R) + (k_1 + k_2 + k_R)] \quad (31)$$

In the initial model:

$$k_1 = 1040\ y^{-1} \qquad k_2 = 260\ y^{-1} \qquad k_3 = 0.00833\ y^{-1} \quad (32)$$

Also:

$$v = 68{,}400/(500\times0.3\times0.6) = 760\ m\ y^{-1} \quad (33)$$

where 68,400 $m^3\ y^{-1}$ of groundwater flows into a cross-sectional area of 500 m by 0.3 m high with a porosity of 0.6.

Finally, $k_R = \ln(2)/5730 = 0.000121\ y^{-1}$. Thus:

$$L = 760/[-260\times0.00833/(0.00833+0.000121) + (1040 + 260 + 0.000121)] \quad (34)$$

Or

$$L = 760/[-256.28 + 1300] = 0.73\ m \quad (35)$$

Note from Equation 31 that if radioactive decay is neglected:

$$L = v/k_1 = 760/1040 = 0.73\ m \quad (36)$$

Thus, assuming a uniform groundwater velocity, the degree of penetration into the swamp is simply governed by the ratio between the groundwater velocity ($m\ y^{-1}$) and the rate constant for volatilisation (y^{-1}).

Based on the above analysis, the initial model was reimplemented, but with a compartmental width of 0.2 m, i.e. less than the characteristic transport distance. Illustrative results are shown in Figure 34 for

an input flux of 1 GBq y^{-1}. The only difference between this analysis and that shown in Figure 33 is that the compartment widths have been reduced from 50 m to 0.2 m.

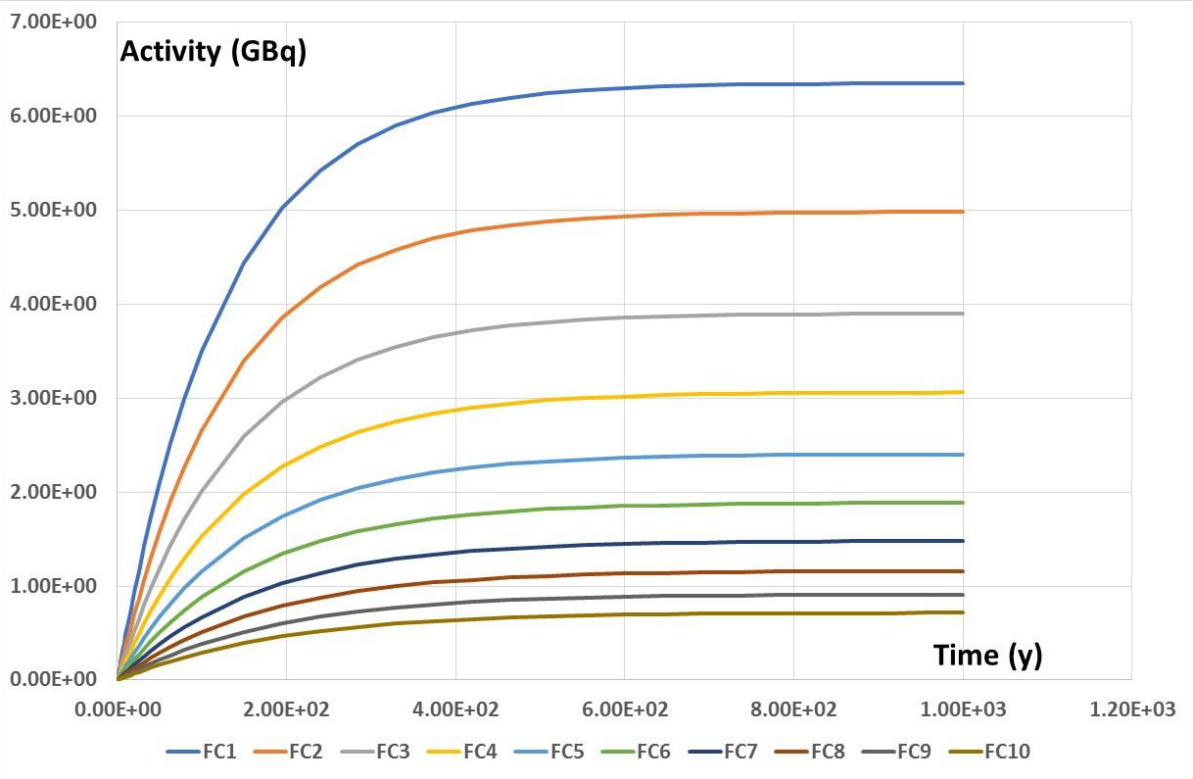

Figure 34: Activity of C-14 in the ten fixed carbon (FC) compartments for a C-14 input rate of 1 GBq y^{-1}.

The equilibration time is a few hundred years, determined by the mineralisation rate of 8.33 10^{-3} y^{-1}, i.e. a half time of 83 years. The spatial distribution in the system at various times is illustrated in Figure 35. If a more complex model of mineralisation had been used, equilibration would have exhibited several saturating exponential components rather than the single component form illustrated in Figure 34.

Recall that each compartment is 0.2 m wide. At 100 years, there is 3.5 GBq in FC1, 2.7 GBq in FC2, 2.0 GBq in FC3 and 1.5 GBq in FC4. Thus, the half depth of penetration is about 0.5 m (from the mid-point of FC1 to the boundary between FC3 and FC4), corresponding to an attenuation length of 0.5/ln(2) = 0.72 m, in line with the analysis presented above.

This analysis demonstrates that such a 1D model cannot be an adequate representation of Duke Swamp, as it permits C-14 to penetrate less than 1 m into the swamp. This issue can be overcome using a 2-layer model, as described in Subsection 3.5.

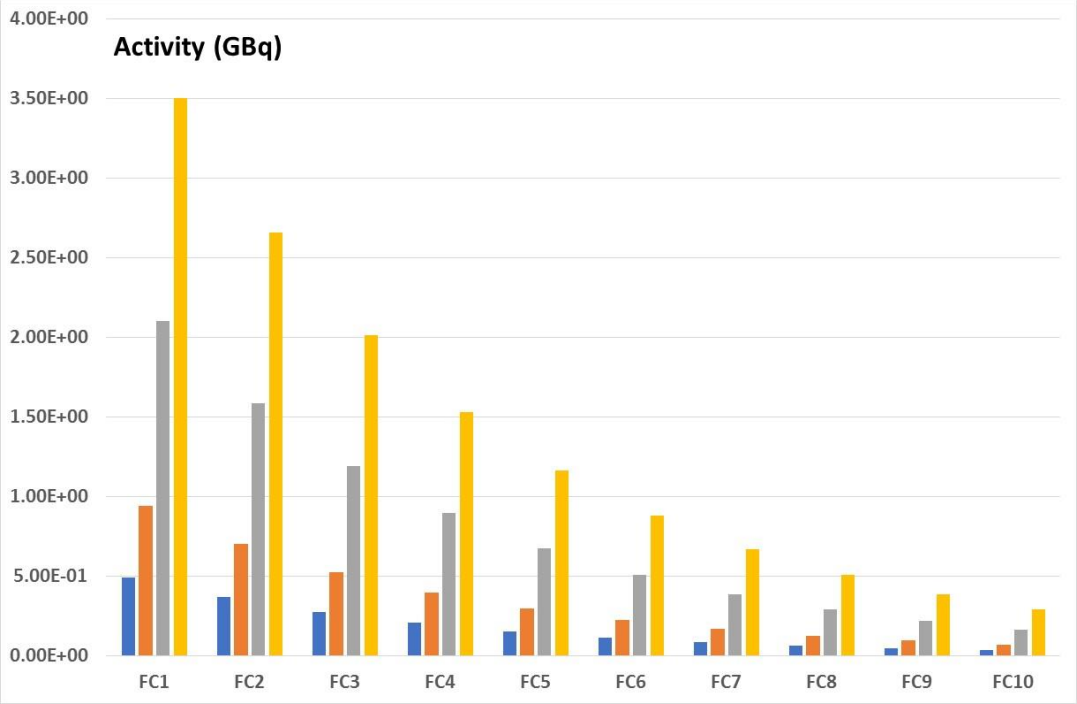

Figure 35: Activity of C-14 in the fixed carbon compartments for an entry rate of 1 GBq y^{-1} and for times of 10, 20, 50 and 100 years.

3.4.5 A Two-layer Model for C-14 Transport in Duke Swamp

In Section 3.4.4, it has been shown that using physically realistic parameter values in a single layer model of Duke Swamp leads to a characteristic penetration distance for C-14 of 0.73 m, which is less than the amount of penetration observed. This contradiction is readily resolved using a two-layer model in which groundwater transport with little volatilisation dominates in the lower layer, whereas volatilisation and plant uptake dominate in the upper layer. Dispersive exchanges are postulated to occur between the lower layer and the upper layer. In this section, the structure of the model is described, initial estimates of parameter values are given, and results of various model simulations are illustrated. The model has been implemented in AMBER.

Conceptual Structure of the Model

The general conceptual structure of the model is shown in Figure 36. Duke Swamp is conceptualised in terms of a 1D transect of width L m. This transect is distinguished into two layers. The lower layer has a thickness of H_1 m and the upper layer has a thickness of H_2 m. Thus, the total depth of the model is $H_1 + H_2$ m. Along the transect, the model is distinguished into 20 strips of varying width, W_i (for i = 1, 20) m. The first five strips are of width 1 m, the next five of width 2 m, the next five of width 5 m and the final five of width 10 m. Thus, the overall model extends 90 m into the swamp, which is greater than the observed distance to which C-14 has penetrated the swamp. It is also convenient to define a cumulative width, WC_i as the total width of all strips from 1 to i. Thus, values of WC_i are 1, 2, 3, 4, 5, 7, 9, 11, 13, 15, 20, 25, 30, 35, 40, 50, 60, 70, 80 and 90 m.

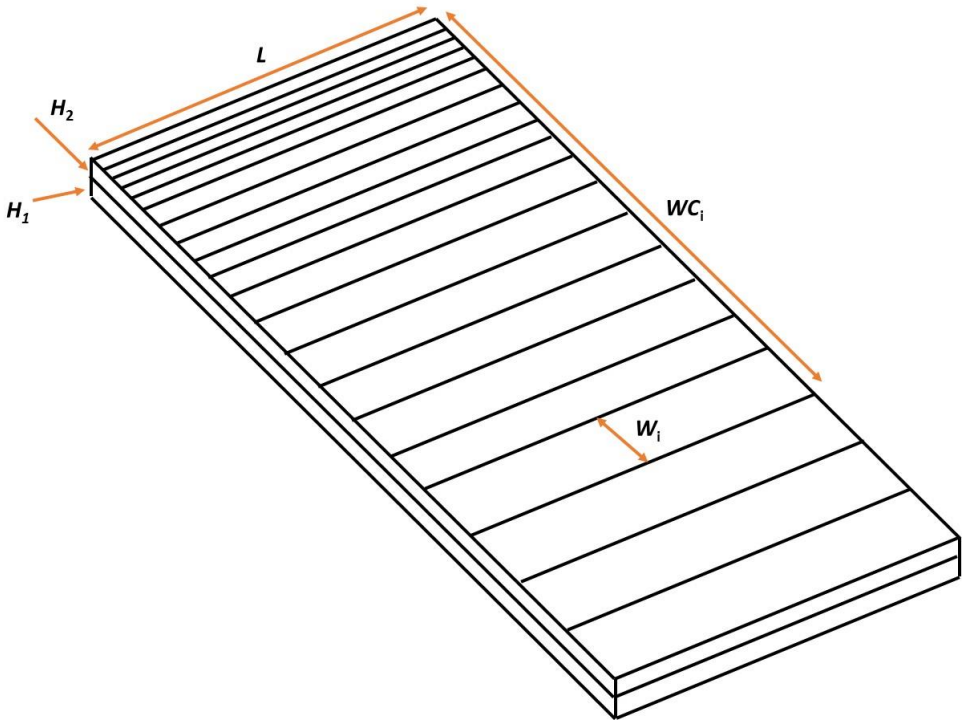

Figure 36: Geometry of the 1D transect model of Duke Swamp.

The volume of any component of the model is given by $V_{ij} = L \times W_i \times H_j$, where i is in the range 1 to 20 and j is in the range 1 to 2. The horizontal area of any compartment, $A\text{-}h_{ij} = L \times W_i$. This is independent of the index j. The vertical area of any compartment, perpendicular to the direction of groundwater flow, $A\text{-}v_{ij} = L \times H_j$. This is independent of the index i.

Each component of the model is distinguished into two elements: organic solids and water. Mineral solids and air may be present, but these do not need to be explicitly represented. The water content of each component is designated by the porosity, φ, and is a dimensionless fraction. The dry bulk density of organic matter in each component is ρ and has dimensions of kg m^{-3}. The stable carbon concentration in soil water is defined as C_{water} and has units of kg m^{-3}. The stable carbon concentration in organic matter is defined as $C_{organic}$ and is dimensionless (kg[C] per kg dry mass). Thus, the amounts of carbon in solution and in organic matter in any compartment, $C_{mass\text{-}s}$ and $C_{mass\text{-}o}$ kg are given by:

$$C_{mass\text{-}s} = V \times \varphi \times C_{water} \qquad C_{mass\text{-}o} = V \times \rho \times C_{organic} \tag{37}$$

Here the subscripts i and j are implied.

In total, the model has 80 compartments (1 wide, 20 long, 2 deep, each distinguished into soil water and organic soil solids). Transfers between the compartments are illustrated in Figure 37. Note that the model treats the swamp as being of constant depth, i.e. any vertical growth or erosion is neglected. This is consistent with adopting a mass-balance approach to the estimation of carbon fluxes between the model compartments.

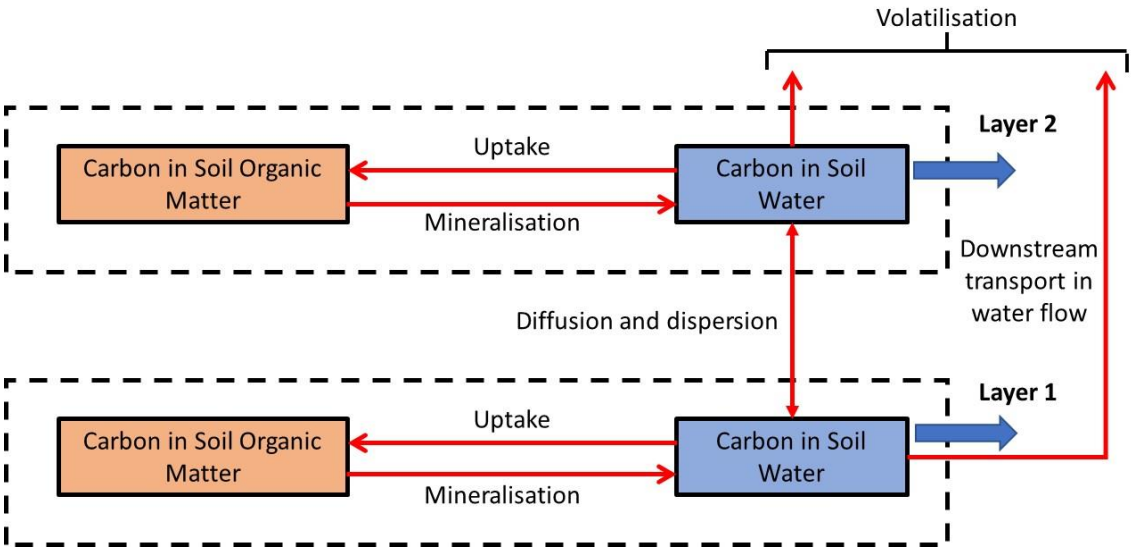

Figure 37: Transport processes in four compartments associated with downstream index i.

As the carbon contents of these various compartments have already been defined, the rate coefficients for transfers between the compartments can be defined by calculating the associated mass fluxes of carbon and then dividing by the mass of carbon in the donor compartment. The following describes estimation of those fluxes.

Mineralisation is taken to balance the production of biomass. Thus, if the biomass production is B kg[C] m^{-2} y^{-1}, the total flux of carbon from mineralisation is AB kg[C] y^{-1}, which is distinguished into AB_1 from layer 1 and AB_2 from layer 2, such that $B_1 + B_2 = B$. In practice, most mineralisation is likely to occur in the upper layer, with the deeply buried organic matter being less susceptible. Thus, $B_2 >> B_1$.

Carbon entering the soil water after mineralisation will be in dissolved form and will rapidly equilibrate with the soil atmosphere. This carbon may be lost at the surface through volatilisation, taken up by plants or transported downstream in soil water.

The downstream loss of carbon in soil water is estimated by multiplying the groundwater flow rate through the downstream vertical side of the compartment (F, m^3 y^{-1}) by the carbon content of the water (C_{water}, kg m^{-3}). The flow rates in the upper and lower layers are calculated as:

$$F_{in\text{-}u} + Infiltration \times L \times WC \times f_1 \qquad F_{in\text{-}l} + Infiltration \times L \times WC \times (1\text{-}f_1) \qquad (38)$$

Where *Infiltration* (m y^{-1}) is the infiltration rate, i.e. precipitation less actual evapotranspiration and f_1 (dimensionless) is the fraction of the infiltration that is routed to the upper layer. Note that $L \times WC$ m^2 is the cumulative upstream area that must be considered in defining the total infiltration into the swamp upstream of the compartment of interest (including that compartment).

The flow of water out through the vertical downstream side of a compartment is slightly larger than the flow of water in through the vertical upstream side. This is because there is an increment from the infiltration into the compartment. As the water in the compartment is taken to have a fixed concentration of carbon, this means that the flow out carries slightly more carbon than the flow in. The difference is FC (kg[C] y^{-1}) and is given by:

$$FC = L \times W \times Infiltration \times C_{water} \qquad (39)$$

Thus, the mass fluxes of carbon available for uptake in biomass and for volatilisation, M (kg[C] y^{-1}), are given by:

$$M_1 = AB_1 - FC\times(1-f_1) \qquad M_2 = AB_2 - FC\times f_1 \qquad (40)$$

for the lower and upper layers, respectively.

These fluxes are partitioned using:

$$M_{1\text{-vol}} = M_1 * v_1 \qquad M_{1\text{-bio}} = M_1(1-v_1) \qquad (41)$$

$$M_{2\text{-vol}} = M_2 * v_2 \qquad M_{2\text{-bio}} = M_2(1-v_2) \qquad (42)$$

where v_1 and v_2 are the fractions of carbon from the lower and upper layers that go to volatilisation as a proportion of the total that goes either to volatilisation or to biomass production. The subscripts 'vol' and 'bio' indicate volatilisation and biomass production, respectively.

Vertical dispersion is calculated with a vertical diffusion/dispersion coefficient, V_{diff} (m^2 y^{-1}). The rate coefficient for diffusion/dispersion from the upper to the lower layer is calculated as $2\times V_{diff}/\{(H_1 + H_2)H_2\}$. Similarly, the rate coefficient for diffusion/dispersion from the lower to the upper layer is calculated as $2\times V_{diff}/\{(H_1 + H_2)H_1\}$.

Horizontal dispersion is neglected in this version of the model, but the model structure has been designed to facilitate its inclusion, as required. Because of the competition with volatilisation and biomass uptake in the upper layer, such dispersion is likely to be mainly of significance in the lower layer.

The parameters of the model, their units, and their specified values in the initial test case, are listed in Table 4. The sink compartments are not included in this description, as they can be of arbitrary size.

Table 4: Parameter values used in the Reference Case for the two-layer model.

Parameter	Units	Specified Value	Comment
Area_h	m^2	L*W	Horizontal area of each compartment.
Area_v	m^2	W*H1 or W*H2	Vertical area of each compartment.
B	kg m^{-3}	B1 or B2	Dry bulk density of each compartment.
B1	kg m^{-3}	400	Dry bulk density of the lower layer.
B2	kg m^{-3}	400	Dry bulk density of the upper layer.
Cflux	kg y^{-1}	Calculated	Flux of carbon out of each compartment in flowing groundwater.
Cinflux	kg y^{-1}	Calculated	Net carbon loss from each compartment due to infiltrating rainwater.
Cmass	kg	Calculated	Content of carbon in each compartment.
Conc_C14	mol kg[C]$^{-1}$	Calculated	Concentration of C-14 in each compartment (Amount divided by the mass of carbon in the compartment).
Corganic	-	0.4	Fraction of carbon in dry organic matter.
Cwater	kg[C] m^{-3}	0.00214	Concentration of carbon in soil water.
Flux_Lower	mol y^{-1}	0.73	Flux of C-14 into the lower layer. Total flux of 1.0 mol y^{-1} partitioned by the thickness of the layer as a fraction of the total.
Flux_Upper	mol y^{-1}	0.27	Flux of C-14 into the upper layer. Total flux of 1.0 mol y^{-1} partitioned by the thickness of the layer as a fraction of the total.
Fraction_Infilt	-	0.5	Fraction of infiltration routed to the upper layer.
H1	m	2.3	Thickness of the lower layer of the swamp.
H2	m	0.7	Thickness of the upper layer of the swamp.
InC_lower	kg[C] y^{-1}	Calculated	Inflow of carbon in groundwater into the lower layer. Calculated as the inflow of water multiplied by the carbon concentration in that water.
InC_upper	kg[C] y^{-1}	Calculated	Inflow of carbon in groundwater into the upper layer. Calculated as the inflow of water multiplied by the carbon concentration in that water.
Infiltration	m y^{-1}	0.346	Infiltration rate.
Inflow_Lower	m^3 y^{-1}	52440	Inflow of water into the lower layer.
Inflow_Upper	m^3 y^{-1}	15960	Inflow of water into the upper layer.
L	m	Length	Length of each compartment.
Length	m	200	Width of the section.
Mflux	kg y^{-1}	Calculated	Carbon flux due to mineralisation.
P1	-	0.5	Porosity of the lower layer.
P2	-	0.5	Porosity of the upper layer.
PPL	kg[C] m^{-2} y^{-1}	0.01	Primary production of the lower layer.
PPU	kg[C] m^{-2} y^{-1}	0.49	Primary production of the upper layer.
V	m^3	H*L*W	Volume of each compartment.
Vdiff	m^2 y^{-1}	30	Vertical dispersion coefficient between soil water in the upper and lower layers.

Parameter	Units	Specified Value	Comment
Vl	-	0.4	Fractional volatilisation from the lower, inactive layer of the swamp.
Vu	-	0.8	Fractional volatilisation from the upper, active layer of the swamp.
W	m	Varies from 1 to 10	Width of each compartment.
WC	m	Varies	Cumulative width to the far boundary of each compartment.

Results for the Reference Case are illustrated in the following figures. Figure 38 shows the distribution of C-14 concentrations in Duke Swamp at 30, 100, 300 and 1000 years. Note the gradual progression of the plume into the swamp. This shows penetration throughout much of the model, due to transport in the lower layer and dispersive exchange with the upper layer.

The build-up of C-14 in Duke Swamp is illustrated in plots of the time-course of activity build-up in the system. The amounts of activity in the water compartments are very small, so Figure 39 and Figure 40 illustrate build-up in the organic components of the lower and upper layers, respectively. The results have been normalised to an input rate of 1 GBq y^{-1}.

Figure 39 shows a steady penetration deeper into the model throughout the simulation, as would be expected for advective flow in a single layer. Figure 40 shows activity entering the layer from upstream being mainly accumulated in the first two compartments (S112 and S122). Build-up further into the model domain arises largely from transport in the lower layer and subsequent dispersive exchange with the upper layer. This explains the different shapes of the curves in these more downstream compartments.

It is also instructive to look at the activity profiles at 40 years and 100 years. These are shown for the lower layer in Figure 41 and the upper layer in Figure 42.

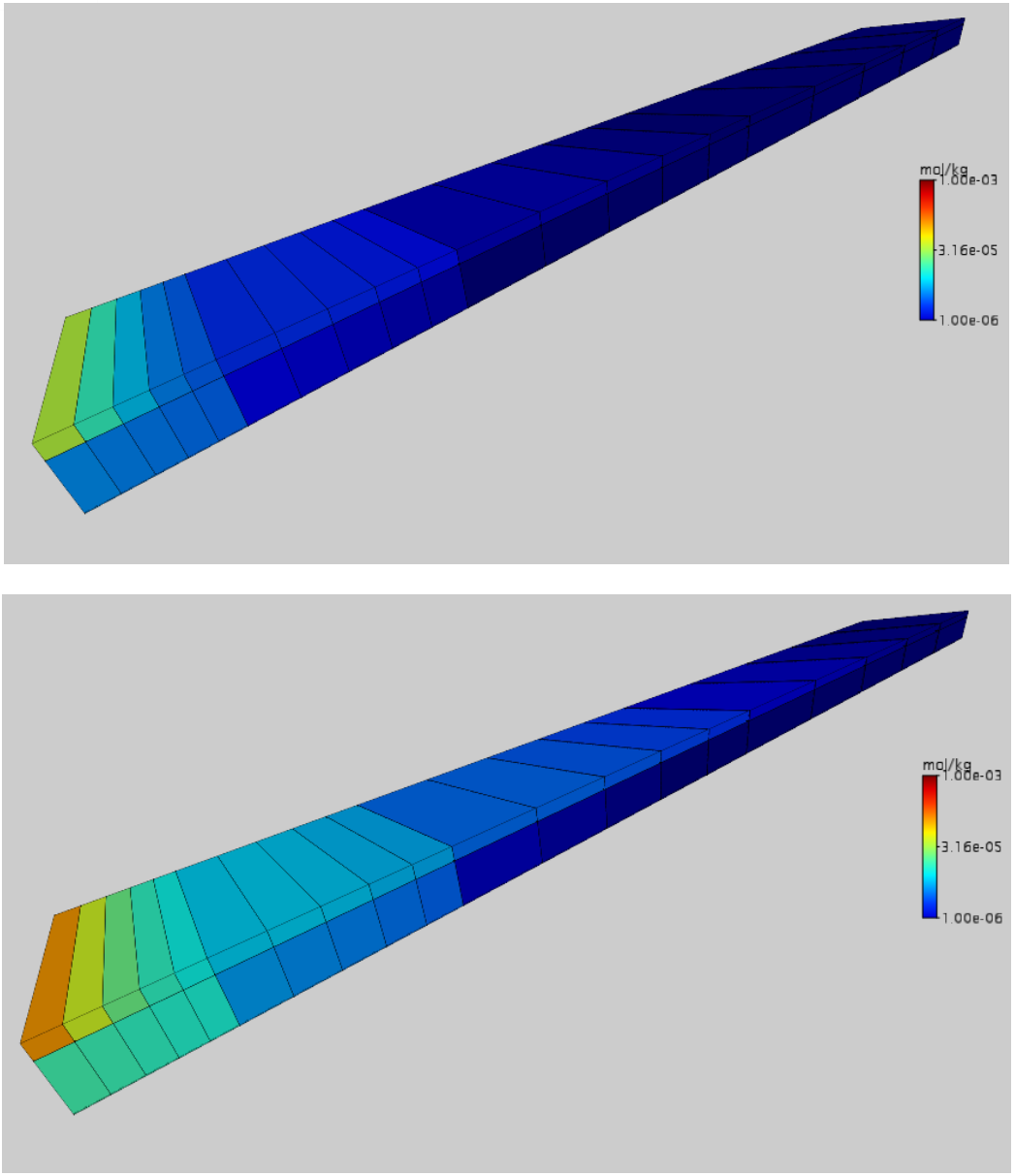

Figure 38: Penetration of C-14 into Duke Swamp at 30 (top) and 100 years (bottom).

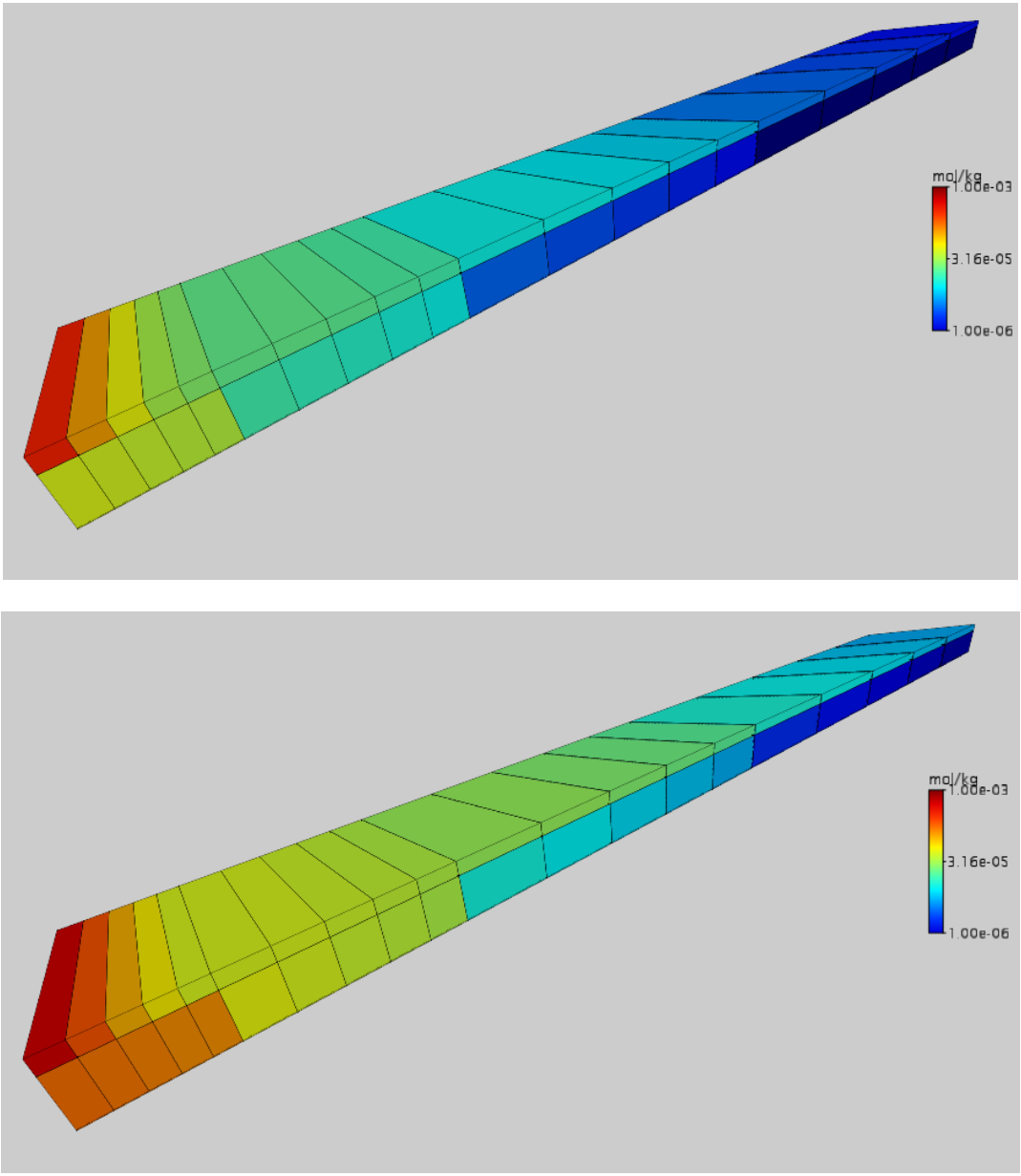

Figure 38 continued: Penetration of C-14 into Duke Swamp at 300 (top) and 1000 (bottom) years.

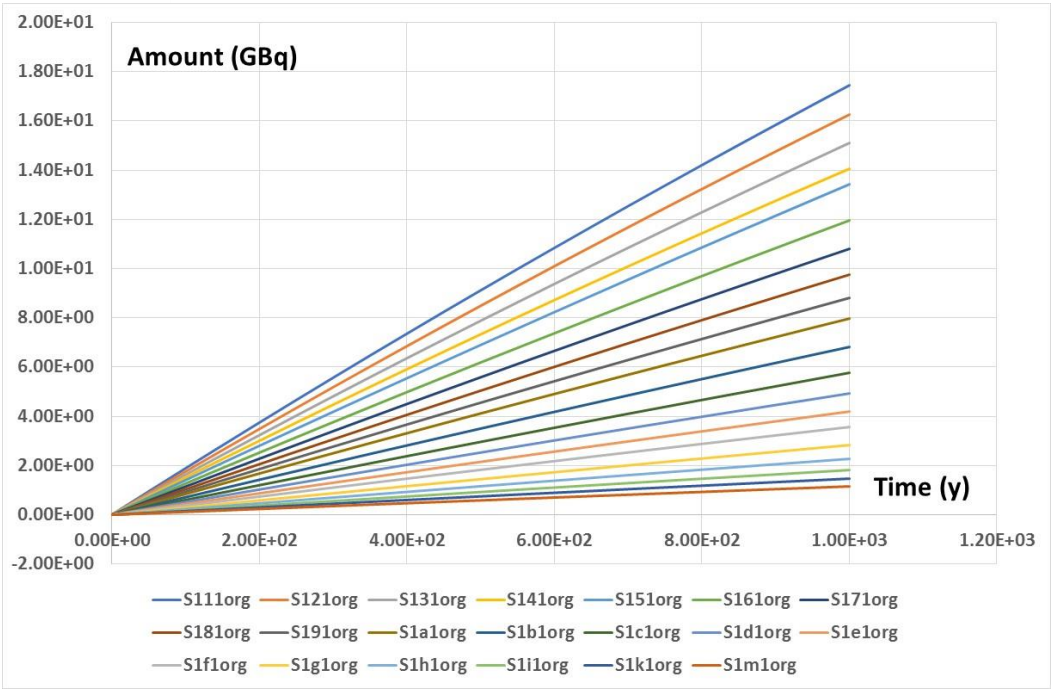

Figure 39: Build-up of C-14 activity in the organic compartments of the lower layer of the model for an input rate of 1 GBq y^{-1}.

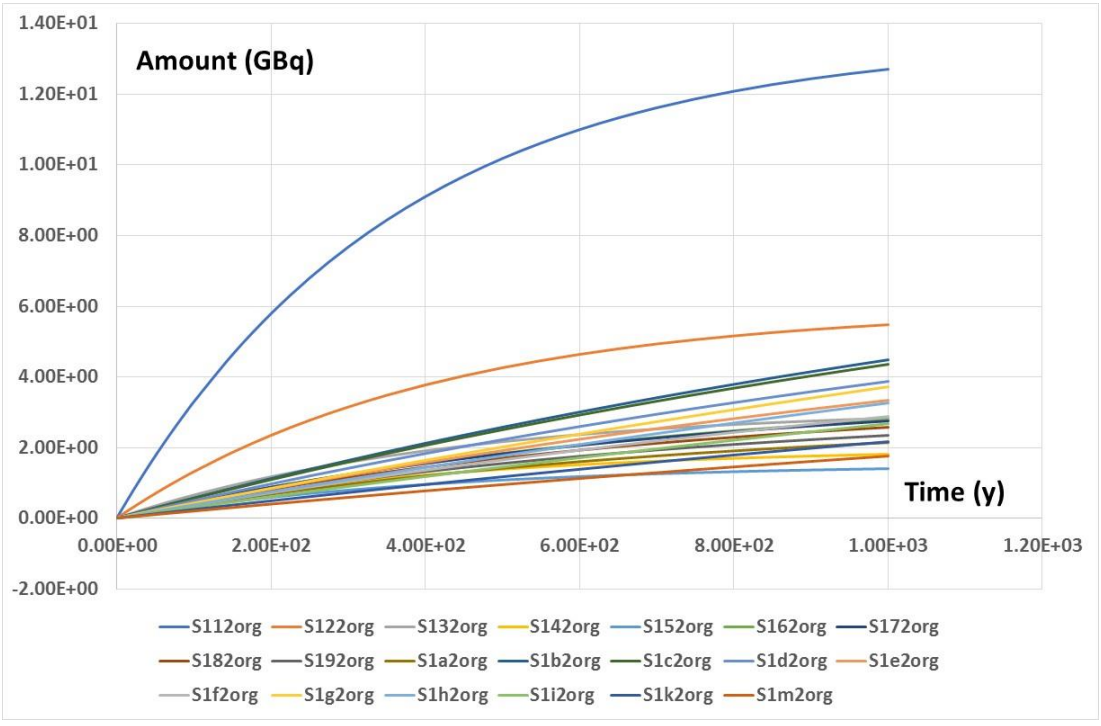

Figure 40: Build-up of activity in the organic compartments of the upper layer of the model for an input rate of 1 GBq y^{-1}.

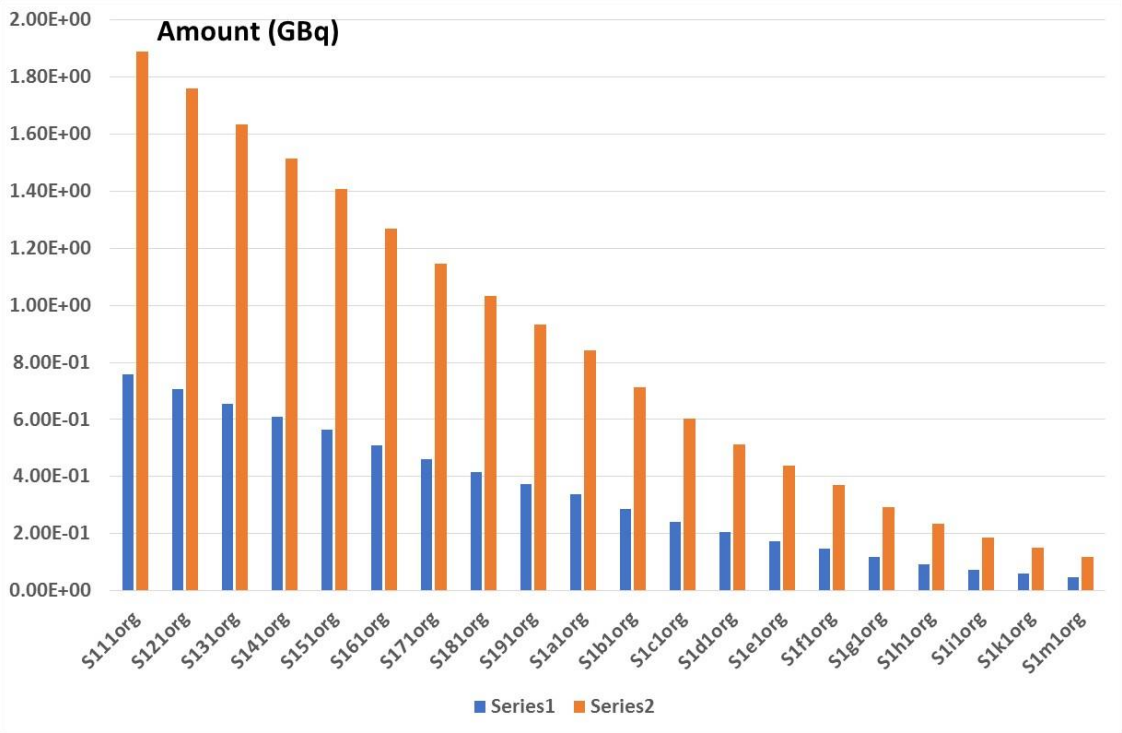

Figure 41: Profiles of activity in the organic compartments of the lower layer at 40 years (Series 1) and 100 years (Series 2).

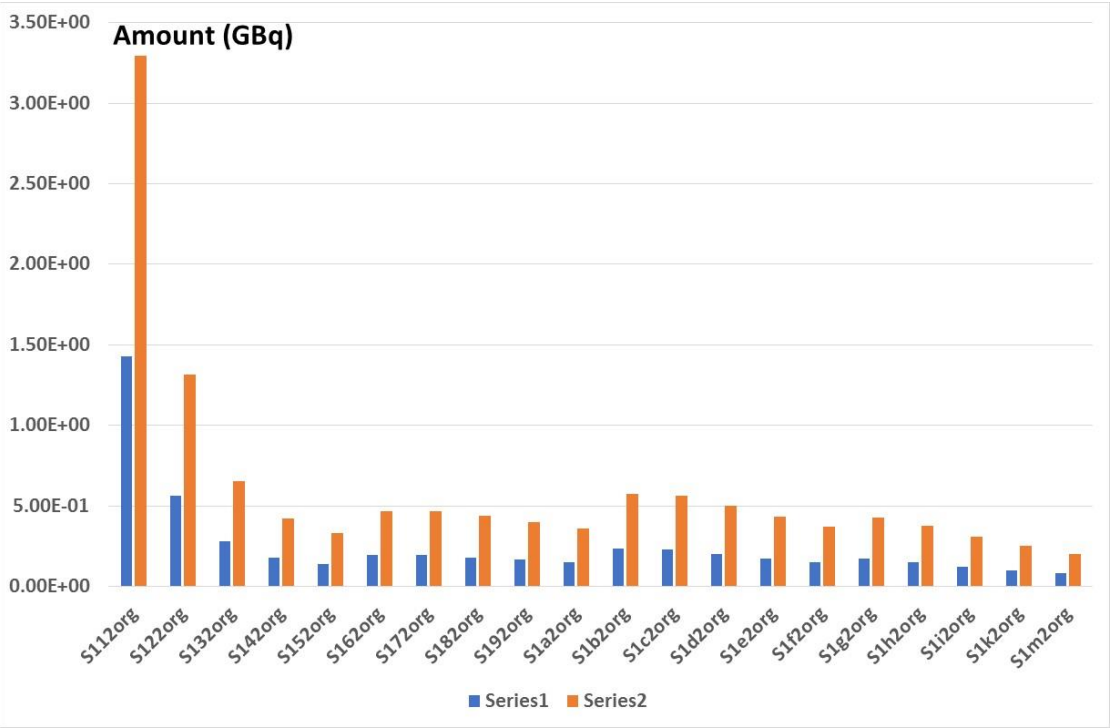

Figure 42: Profiles of activity in the organic compartments of the upper layer at 40 years (Series 1) and 100 years (Series 2).

The lower layer exhibits a steady decline in amount, with most of the activity in the first ten layers (i.e. the first 15 m). In the upper layer, much of the activity is located within the first two metres of the edge of the swamp, but the lower layer then generates a rather flat profile throughout much of the depth of the profile (the increases at S162 relative to S152, Sib2 relative to S1a2, and S1g2 relative to S1f2 reflect increases in compartment width from 1 m to 2 m, 2 m to 5 m, and 5 m to 10 m, respectively. This general pattern of C-14 penetration into the swamp is in accord with the observational data described previously.

After 40 years of input at 1 GBq per year, the activity content of Duke Swamp is 6.84 GB in the lower layer and 5.11 GBq in the upper layer. Thus, the total is 11.95 GBq or 30% of the input. At 100 years, there is 17.1 GBq in the lower layer and 12.2 GBq in the upper layer. Thus, overall retention is 29.3 GBq or 29% of the input. Experimentally, about 20% of the input has been estimated as being retained, but this was based on sampling from the upper layer only.

Overall, the simulated spatial distribution and total amount of C-14 present in Duke Swamp is in reasonable agreement with observations. This is illustrated further in the next subsection.

Detailed Comparison of Results from the Reference Case with a 1D Profile constructed from the Experimental Observations

Data from Yankovich et al [2014] that are used in the following comparison are listed in Table 5. These data have been augmented by calculations of the distances of the individual sampling points from the upstream edge of Duke Swamp, where the location of that edge was estimated from Figure 3, using the exact locations of the sampling points as a guide and approximating the edge as a set of linear segments. The data listed in Table 5 are illustrated in Figure 43.

Note: The three zero concentrations listed in Table 5 signify measurements of samples that gave results below the limits of detection.

The Reference Case was run for an input of 1 mol y^{-1} of C-14, with results reported as mol $kg[C]^{-1}$ in the organic matter of the upper and lower layers of Duke Swamp. However, the model responds linearly to changes in the input flux, so the results are numerically identical for an input flux of 1 GBq y^{-1} but must be interpreted as having units of GBq $kg[C]^{-1}$.

With this interpretation, concentrations as a function of time are shown for the lower and upper layers of Duke Swamp in Figure 44 and Figure 45, respectively.

In Figure 44, the results fall into four distinct groups. This reflects the width of the compartments, which changes from 1 m for the first five compartments to 2 m for the next five, 5 m for the next five, and 10 m for the final five. This increases numerical dispersion and hence results in a decrease in concentration as the compartment size increases. In Figure 45, the first two compartments rapidly accumulate C-14 to higher concentrations than the other compartments. This is because a fraction of the input of C-14 is routed to the upper layer, where it is efficiently taken up in biomass production (or lost in volatilisation) and cannot penetrate further into the swamp.

For comparison with the experimental data, profiles of penetration into Duke Swamp are shown for 40 and 100 years of continuous uniform input in Figure 46 and Figure 47, for the lower and upper layers, respectively.

Numerical values of the results given in Figure 46 and Figure 47 are provided in Table 6. The results scale approximately with the duration of the input over this period. Therefore, the comparisons given below are based on the 40-year input period, which is comparable with the period for which releases of C-14 from WMA-C had occurred prior to the experimental measurements of Yankovich et al. [2014].

Table 5: Distances of measurement locations from the upstream boundary of Duke Swamp and associated C-14 concentrations.

Location	Easting	Northing	Distance (m)	Concentration (Bq/kg[C])
DSS-01	241.867	754.864	16.37	270
DSS-02	186.582	749.011	33.43	1100
DSS-03	138.916	751.777	81.1	0
DSS-04	291.725	703.114	4.52	930
DSS-08	341.957	648.836	17.17	960
DSS-09	290.031	655.927	39.49	1600
DSS-11	542.482	596.76	4.08	1200
DSS-12	487.32	601.012	20.73	960
DSS-14	393.272	611.732	30.24	2000
DSS-15	345.18	602.486	53.61	1100
DSS-16	290.821	597.766	87.39	630
DSS-17	238.786	606.701	108.93	980
DSS-18	193.999	603.663	136.29	690
DSS-22	337.169	566.817	89.43	380
DSS-23	295.655	546.383	127.53	290
DSS-24	242.412	549.295	154.61	0
DSS-25	199.423	554.272	174.27	160
DSS-27	543.602	447.291	8.13	17000
DSS-28	448.272	497.105	38.93	8200
DSS-29	391.944	497.892	88.69	3500
DSS-30	338.891	502.308	134.15	290
DSS-31	287.506	497.412	173.46	720
DSS-32	242.832	498.831	196.36	420
DSS-35	495.59	484.508	5.52	47000
DSS-36	491.527	443.466	32.33	6500
DSS-37	435.91	451.151	70.28	0
DSS-38	387.441	451.332	113.52	1800
DSS-39	335.172	452.907	159.61	0
DSS-42	538.53	404.433	26.52	15000
DSS-43	490.998	408.265	57.12	3600
DSS-45	396.21	397.33	132.69	1000
DSS-46	340.113	383.304	186.85	550
DSS-47	640.359	356.576	45.49	370
DSS-48	586.431	349.739	8.57	9200
DSS-49	539.11	354.89	52.13	1800
DSS-50	484.4	352.923	101.07	2300
DSS-51	440.684	353.36	131.59	1900
DSS-55	592.285	307.476	14.93	5700
DSS-56	539.965	308.047	64.86	2800
DSS-57	486.936	303.609	116.87	760
DSS-60	637.246	259.165	15.27	3500
DSS-61	593.95	252.406	29.06	1400
DSS-62	540.298	253.864	80.09	580
DSS-64	633.152	200.669	6.88	1100
DSS-65	587.651	205.439	37.35	1200
DSS-68	591.773	156.593	3.84	0
DSS-69	547.049	153.199	43.49	690

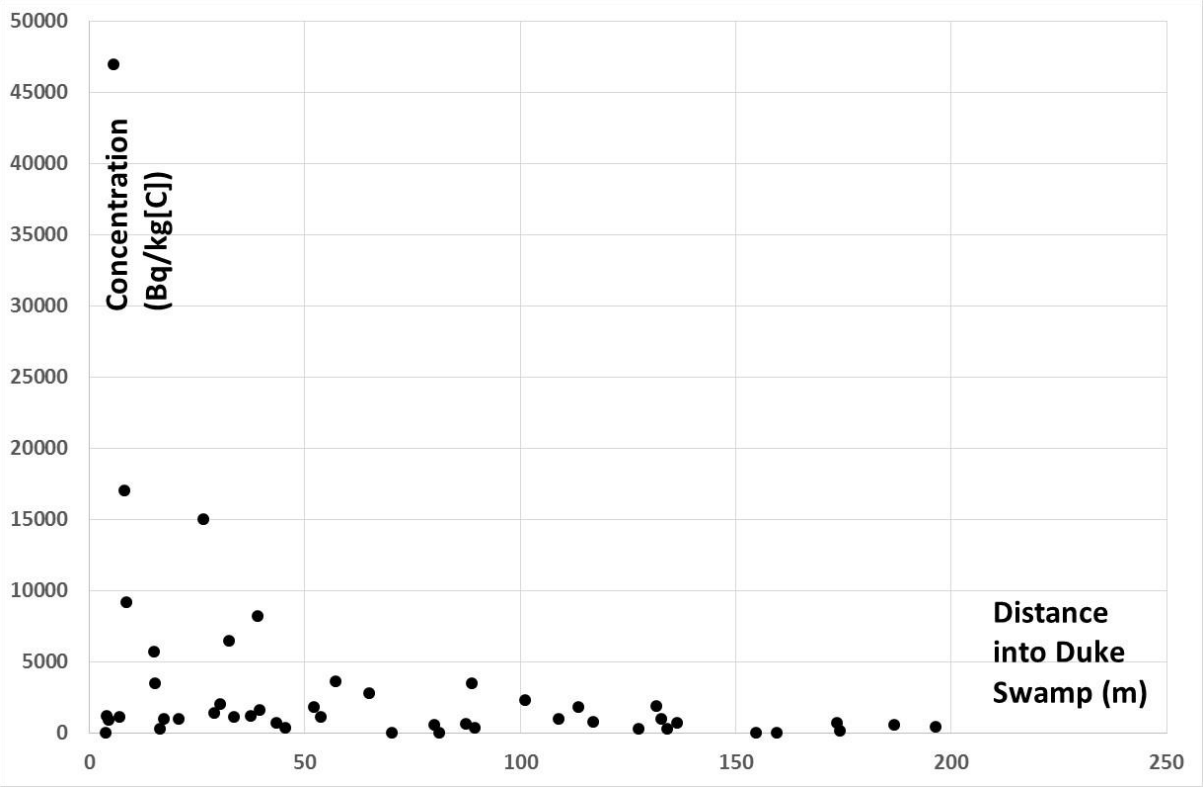

Figure 43: Measured concentrations of C-14 as a function of distance into Duke Swamp.

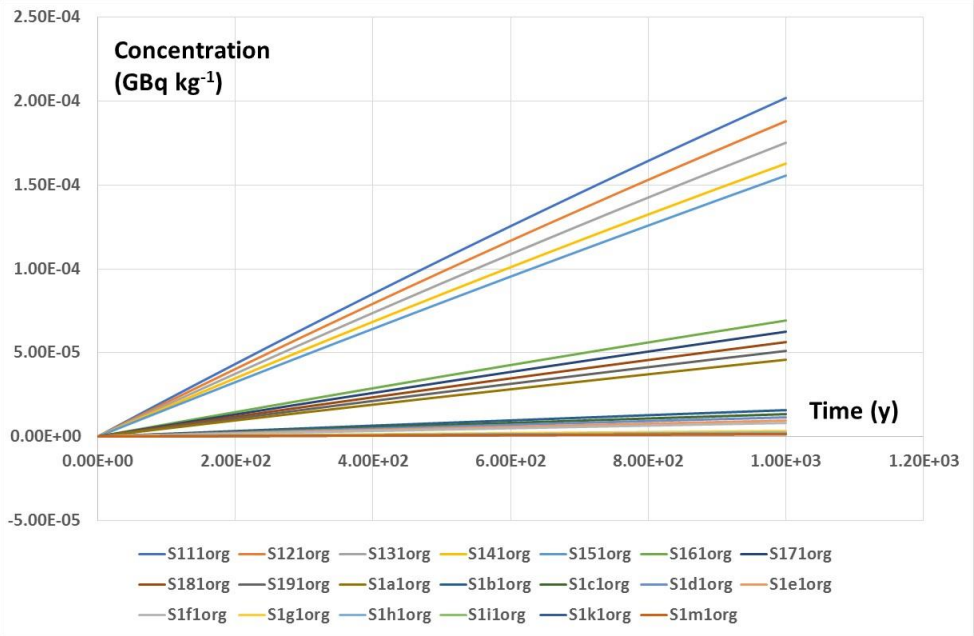

Figure 44: Simulated concentrations of C-14 in the organic matter of the lower layer of Duke Swamp for the Reference Case and an input flux of 1 GBq y^{-1}.

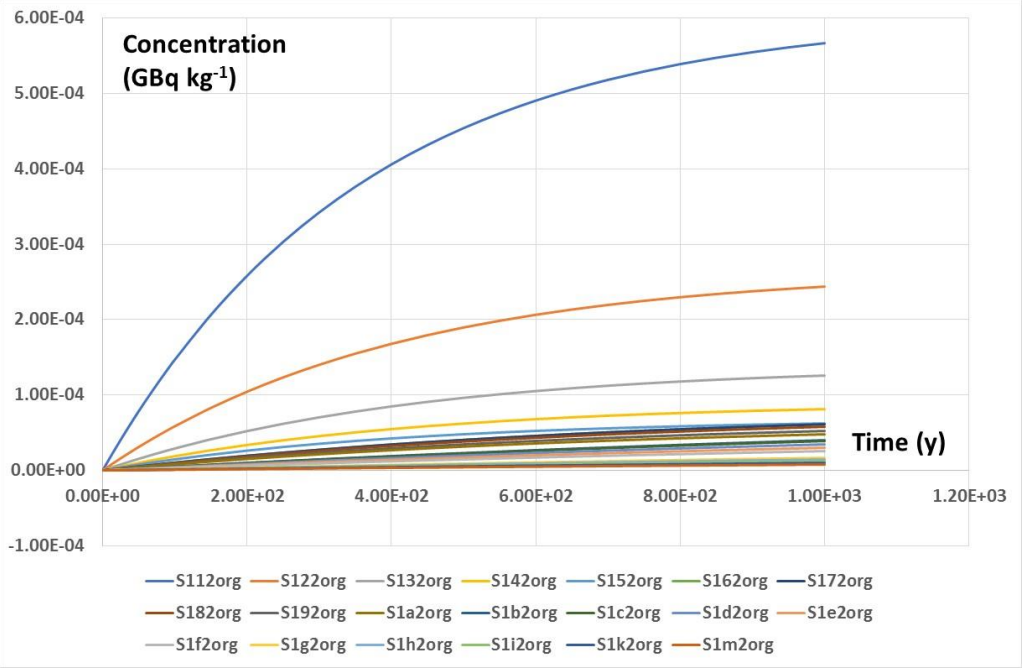

Figure 45: Simulated concentrations of C-14 in the organic matter of the upper layer of Duke Swamp for the Reference Case and an input flux of 1 GBq y^{-1}.

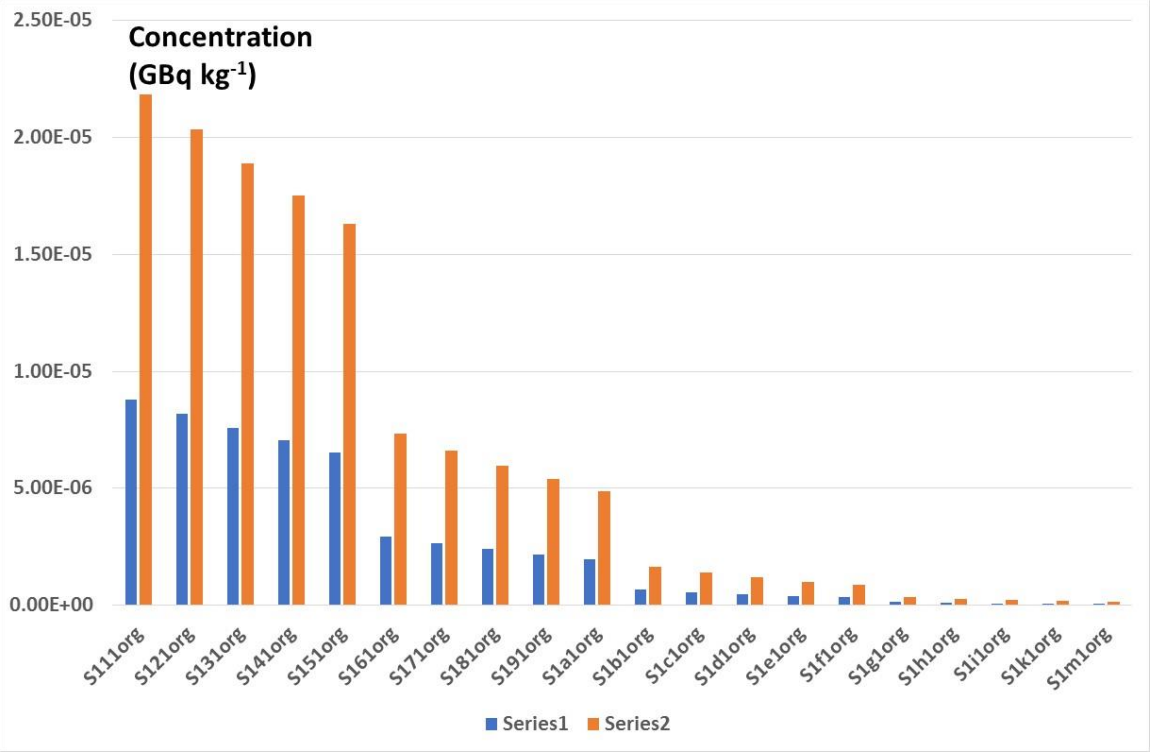

Figure 46: Simulated concentrations of C-14 in organic matter in the lower layer of Duke Swamp for the Reference Case at 40 years (Series 1) and 100 years (Series 2).

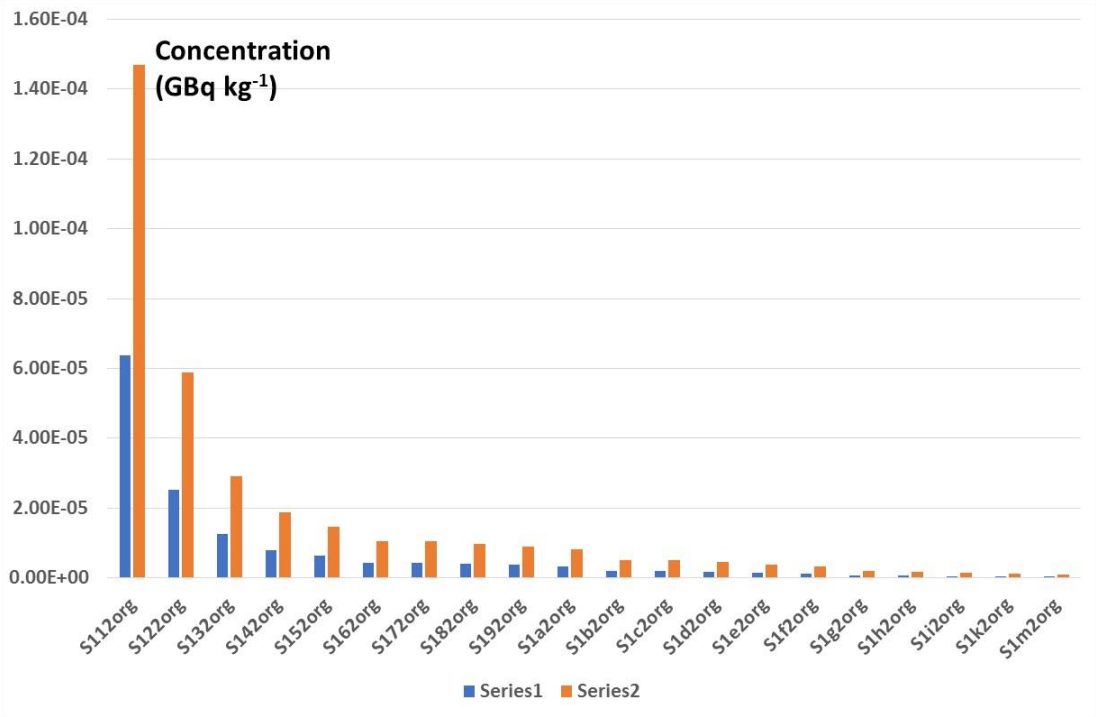

Figure 47: Simulated concentrations of C-14 in organic matter in the upper layer of Duke Swamp for the Reference Case at 40 years (Series 1) and 100 years (Series 2).

Table 6: Concentrations of C-14 (GBq kg[C]$^{-1}$) for the Reference Case with an input rate of 1 GBq y^{-1} over two periods (40 and 100 years).

Compartment	Input Period		Compartment	Input Period	
	40 years	100 years		40 years	100 years
S111org	8.79E-06	2.19E-05	**S112org**	6.37E-05	1.47E-04
S121org	8.18E-06	2.03E-05	**S122org**	2.53E-05	5.88E-05
S131org	7.59E-06	1.89E-05	**S132org**	1.25E-05	2.92E-05
S141org	7.04E-06	1.75E-05	**S142org**	8.07E-06	1.88E-05
S151org	6.54E-06	1.63E-05	**S152org**	6.34E-06	1.48E-05
S161org	2.95E-06	7.34E-06	**S162org**	4.34E-06	1.04E-05
S171org	2.66E-06	6.63E-06	**S172org**	4.35E-06	1.05E-05
S181org	2.40E-06	5.98E-06	**S182org**	4.06E-06	9.78E-06
S191org	2.17E-06	5.41E-06	**S192org**	3.71E-06	8.93E-06
S1a1org	1.96E-06	4.88E-06	**S1a2org**	3.37E-06	8.10E-06
S1b1org	6.61E-07	1.65E-06	**S1b2org**	2.09E-06	5.15E-06
S1c1org	5.61E-07	1.40E-06	**S1c2org**	2.04E-06	5.03E-06
S1d1org	4.76E-07	1.19E-06	**S1d2org**	1.81E-06	4.46E-06
S1e1org	4.05E-07	1.01E-06	**S1e2org**	1.56E-06	3.85E-06
S1f1org	3.44E-07	8.61E-07	**S1f2org**	1.34E-06	3.29E-06
S1g1org	1.36E-07	3.39E-07	**S1g2org**	7.72E-07	1.92E-06
S1h1org	1.08E-07	2.70E-07	**S1h2org**	6.75E-07	1.68E-06
S1i1org	8.62E-08	2.16E-07	**S1i2org**	5.56E-07	1.38E-06
S1k1org	6.90E-08	1.73E-07	**S1k2org**	4.49E-07	1.12E-06
S1m1org	5.53E-08	1.39E-07	**S1m2org**	3.62E-07	9.01E-07

From Table 6, it is seen that the concentration in layer 2 decreases by about one order of magnitude between S112org and S152org. Thus, most of the C-14 entering the upper layer of Duke Swamp is retained within 5 m of the boundary. However, thereafter, the concentration decreases by a further order of magnitude by S1i2org. This gives a penetration into the swamp of 65 m to the centre of S1i2org. The long tail of penetration arises from transport in the lower layer, followed by exchange and local retention in the upper layer. This is in broad agreement with Figure 43, which shows high concentrations only in the first few metres, but with a long tail of above-background concentrations penetrating 100 m or more into the swamp.

Quantitatively, Table 7 shows the observed concentrations and the predicted concentrations for an input rate of 1 GBq y^{-1} in the Reference Case. The predicted concentrations are the values for the compartment within which the estimated distance lies.

'Not calculated' is for sampling points located more than 90 m from the boundary of the swamp. These points are listed in Table 8, together with the mean concentrations associated with them.

The data in Table 8 indicate that the local background concentration of C-14 is a few hundred Bq per kg[C]. This is not of great significance in comparison with the much higher concentrations associated with C-14 entering the swamp from WMA-C.

In Figure 48, the observed and calculated concentrations of C-14 at the various sample points are plotted. It should be kept in mind that the calculations are for an input C-14 flux to Duke Swamp of 1 GBq y^{-1}. This point is discussed further below.

Table 7: Observed concentrations and predictions for an input rate of 1 GBq y^{-1}.

Distance (m)	Concentration (Bq/kg[C])	Corresponding Compartment	Predicted Compartment Concentration (Bq/kg[C])
16.37	270	S1b2org	2095
33.43	1100	S1e2org	1564
81.1	0	S1m2org	362
4.52	930	S152org	6336
17.17	960	S1b2org	2095
39.49	1600	S1f2org	1337
4.08	1200	S152org	6336
20.73	960	S1c2org	2043
30.24	2000	S1e2org	1564
53.61	1100	S1h2org	675
87.39	630	S1m2org	362
108.93	980	Not calculated	
136.29	690	Not calculated	
89.43	380	S1m2org	362
127.53	290	Not calculated	
154.61	0	Not calculated	
174.27	160	Not calculated	
8.13	17000	S172org	4351
38.93	8200	S1f2org	1337
88.69	3500	S1m2org	362
134.15	290	Not calculated	
173.46	720	Not calculated	
196.36	420	Not calculated	
5.52	47000	S162org	4338
32.33	6500	S1e2org	1564
70.28	0	S1k2org	449
113.52	1800	Not calculated	
159.61	0	Not calculated	
26.52	15000	S1d2org	1813
57.12	3600	S1h2org	675
132.69	1000	Not calculated	
186.85	550	Not calculated	
45.49	370	S1g2org	772
8.57	9200	S172org	4351
52.13	1800	S1h2org	675
101.07	2300	Not calculated	
131.59	1900	Not calculated	
14.93	5700	S1a2org	3368
64.86	2800	S1i2org	556
116.87	760	Not calculated	
15.27	3500	S1b2org	2095
29.06	1400	S1d2org	1813
80.09	580	S1m2org	362
6.88	1100	S162org	4338
37.35	1200	S1f2org	1337
3.84	0	S142org	8068
43.49	690	S1g2org	772

Table 8: Concentrations of C-14 at locations more than 90 m from the boundary of Duke Swamp.

Distance (m)	Concentration (Bq/kg[C])
108.93	980
136.29	690
127.53	290
154.61	0
174.27	160
134.15	290
173.46	720
196.36	420
113.52	1800
159.61	0
132.69	1000
186.85	550
101.07	2300
131.59	1900
116.87	760
Mean	**791**

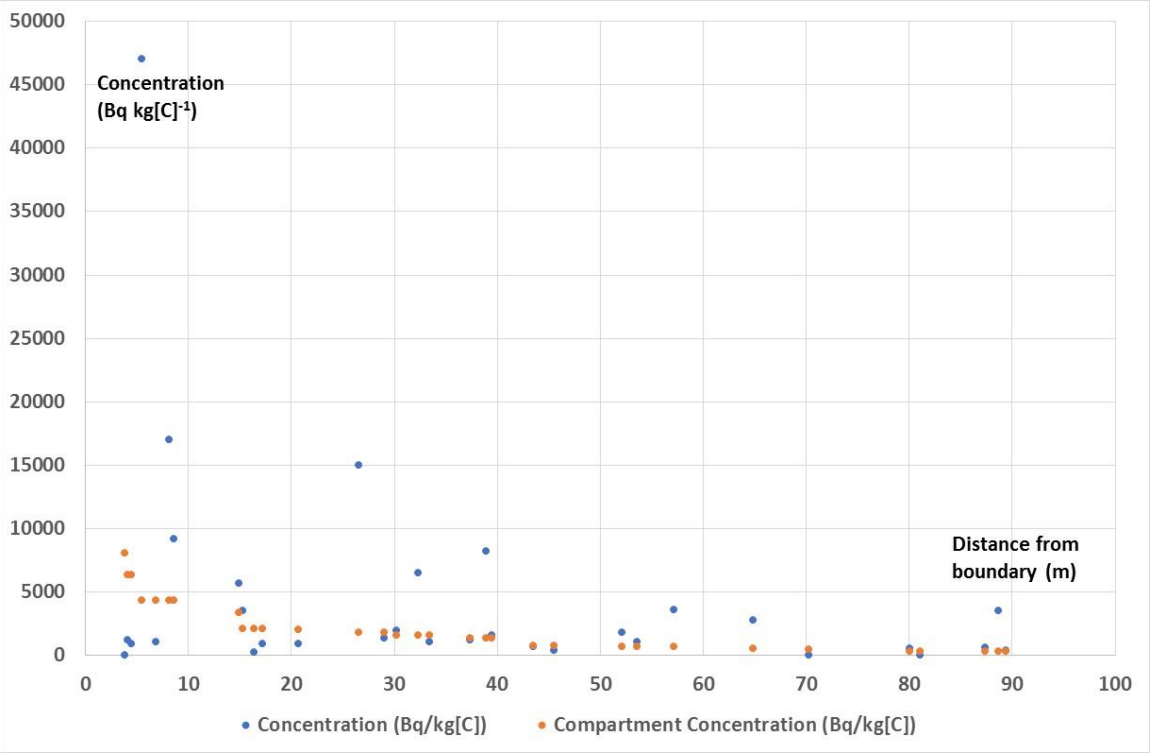

Figure 48: Observed C-14 concentrations in Duke Swamp compared with model predictions for an input flux of 1 GBq y^{-1}.

In Section 3.3 it is estimated that the C-14 flux from WMA-C in 1991 was of the order 6.5 GBq y^{-1}. Therefore, the model predictions shown in Figure 48 were scaled by a factor of 6.5 to compare with observations. The results are shown in Figure 49.

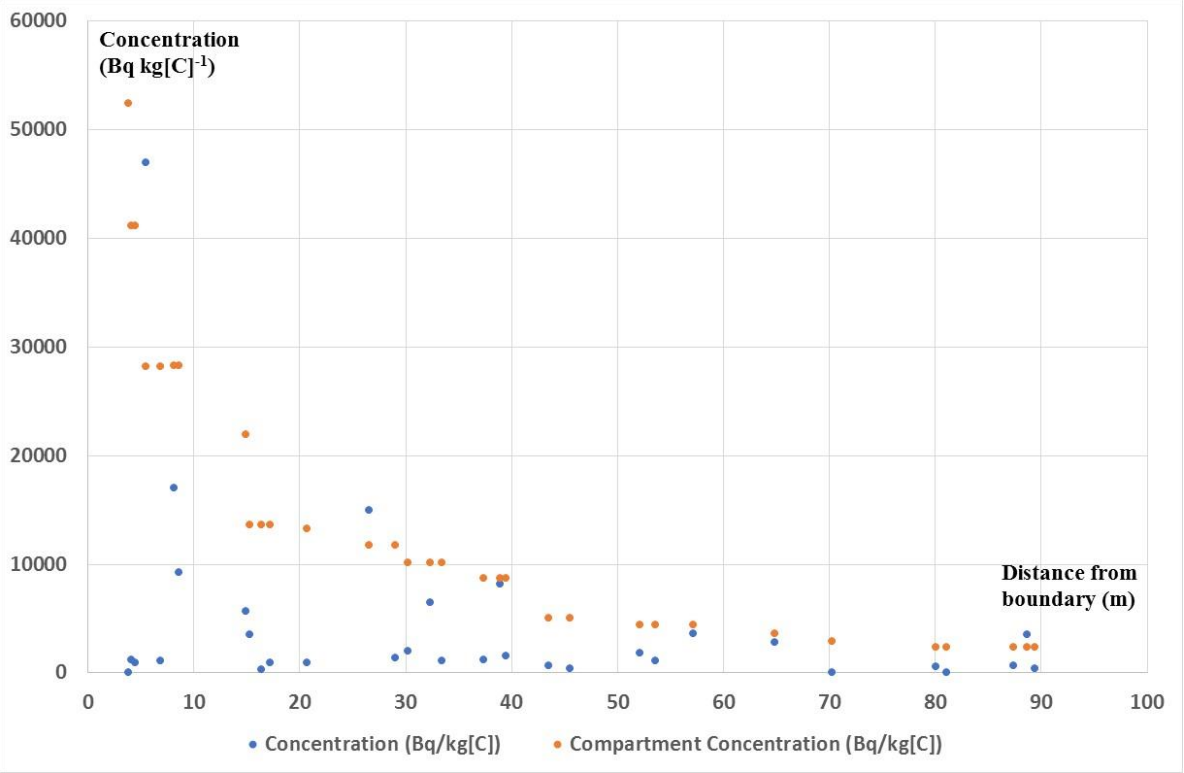

Figure 49: Observed C-14 concentrations in Duke Swamp compared with model predictions for an input flux of 6.5 GBq y^{-1}.

Bearing in mind that many of the data points are offset from the centreline of the C-14 plume impinging on Duke Swamp, the agreement between observations and model predictions is satisfactory. The appropriate comparison is between the model predictions and the upper boundary of the envelope that includes all the experimental values. A more detailed analysis would require extending the existing 1D model to 2D, but would also require a detailed understanding of the profile of the contaminated groundwater plume arriving at the swamp, and of any flow channelling of that groundwater within the swamp.

In summary, a simple two-layer model of Duke Swamp that includes the effects of groundwater flow, volatilisation and biomass uptake has been shown to provide a good quantitative description of the behaviour of a C-14 plume impinging on the swamp from WMA-C.

3.5 CONCLUSIONS RELATING TO THE DUKE SWAMP SCENARIO

The modelling study of Duke Swamp described above emphasises that C-14 transport processes in systems based on organic soils can vary greatly due to spatial distinctions in turnover rates of organic matter and in the degree of water saturation present. Whereas transport in groundwater will dominate in saturated conditions with limited biomass production and mineralisation, in unsaturated conditions and with higher rates of biomass production, uptake into biomass, followed by death and decomposition of that biomass, with a significant degree of atmospheric release of the CO_2 produced, are likely to be

the dominant processes. An interesting observation is that, at Duke Swamp, and based on the partitioning of C-14 entering the swamp in groundwater, about 20% of carbon released from organic matter by mineralisation is likely to be reincorporated in new biomass. This is a considerably larger percentage than would be expected for agricultural crops growing on mineral soils. This probably reflects differences in the vertical distribution of primary productivity and in the degree of aeration of the soil.

4. CARBON IN FRESHWATER LAKES AND UPTAKE INTO FISH

In long-term, post-closure radiological impact assessments, he uptake of C-14 from water by fish has been shown to be a dominating exposure pathway for both humans (e.g. Walke et al. [2013]; Posiva [2014a]) and non-human biota (e.g. Posiva [2014b]). If equilibrium with water is assumed in assessments, high activity concentrations in fish are calculated (largely because a low dissolved carbon content results in a high C-14 specific activity in the water that is assumed to be applicable to the total carbon content of fish present in that water). The amount of C-14 that fish will encounter will, however, be determined by where they obtain their carbon. This will vary according to the species of interest and their associated habits (e.g. benthic or pelagic). The objective of the task described in this section has been to consider from where fish obtain their carbon, taking account of different species groups and their food sources, to motivate discussion about how C-14 uptake is appropriately represented in safety assessments. It is emphasised that even if fish obtain their carbon from food rather than directly from water, that food may itself exhibit a specific activity characteristic of local water. Therefore, to address sources of C-14 in fish, it is necessary to address the whole food-web of which they are part. A further important consideration is whether an equilibrium approach to modelling C-14 uptake by fish and other aquatic biota is appropriate, or whether an alternative approach, considering the kinetics of C-14 accumulation in, and loss from, environmental media and biota, would be more suitable.

The scope of this review was limited to freshwater systems, with a specific focus on lakes, which contain a large reservoir of water compared with the input and output flows, such that residence times are long. C-14 may, therefore, be retained to a higher degree than in other freshwater systems with higher rates of exchange, such as rivers. Where possible, a distinction is made between fish with pelagic and benthic habits, since this may affect their sources of carbon. Carbon sources that are internal to lakes and those originating from associated terrestrial catchments are considered. The review then aims to consider whether the carbon taken up by fish is equilibrated with the water, sediments or the terrestrial system, or a combination of these.

The review is not intended to be an exhaustive literature research activity, but rather aims to draw together information to support consideration of whether an equilibrium approach to modelling C-14 uptake by fish is appropriate for safety assessments, or whether an alternative modelling approach may be justifiable.

4.1 SOURCE INPUTS AND CARBON CYCLING IN LAKES

At a simple level, the carbon cycle in lakes can be considered in terms of the availability of dissolved inorganic carbon (DIC) that can be sequestered into organic matter by phytoplankton and aquatic plants (macrophytes), where it is then available for transfer throughout the food web, where a food web is defined as "*a network of consumer-resource interactions among a group of organisms, populations or aggregate trophic units"* [Winemiller and Polis, 1996]. Where the photic zone extends throughout the water column, DIC may also be incorporated in benthic microalgae. The DIC may derive from atmospheric exchange of CO_2 across the air/water interface, via water exchange (e.g. riverine input), or from input via groundwater [Ascough et al., 2010]. A simple representation of the carbon cycle in a lake is provided in Figure 50.

Once incorporated within the food chain, carbon may be retained within the biomass of organisms or be cycled back to the water column in the form of respired CO_2, which is then available for photosynthetic uptake, or as dissolved organic carbon (DOC) or particulate organic carbon (POC) through processes such as excretion and death. The DOC and POC may return to the biological cycle through incorporation in bacterial biomass or direct consumption by heterotrophic biota, with respiration then returning carbon for fixation, once again, by primary producers. Depending on the state of mixing within the water column, POC may settle through sedimentation, providing a carbon source to benthic organisms. The

breakdown of dead organisms can also supply a carbon source to detrital feeding biota in littoral and benthic zones.

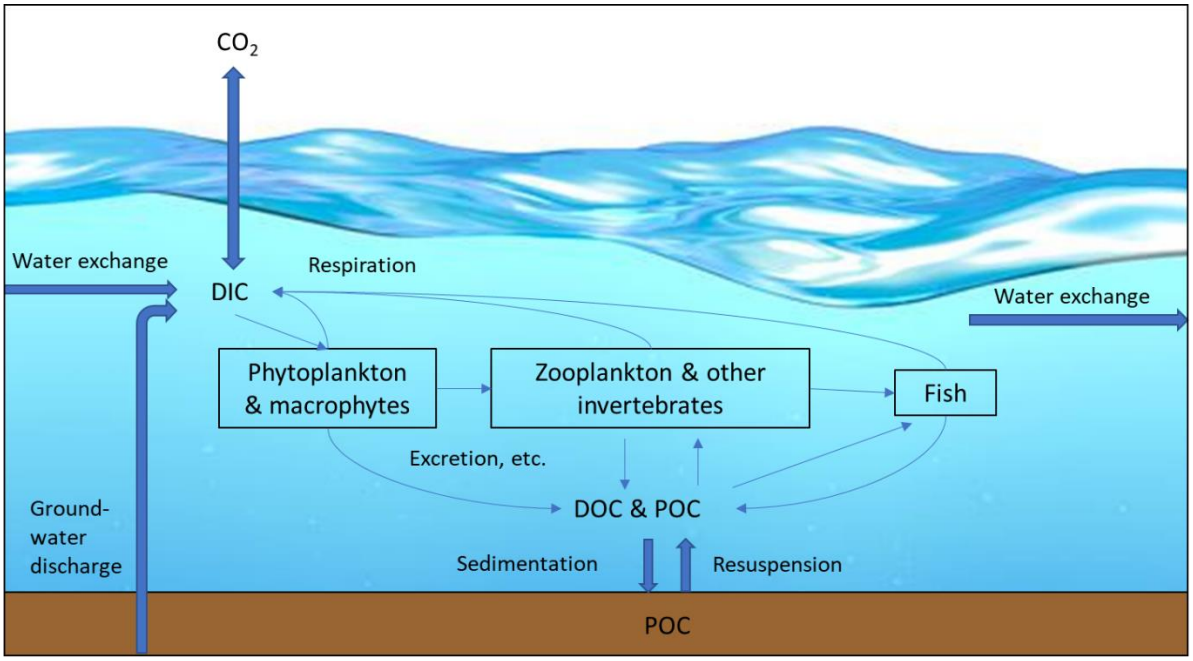

Figure 50. Example carbon cycle in a lake, illustrating the cycling of dissolved inorganic carbon (DIC), dissolved organic carbon (DOC) and particulate organic carbon (POC).

In addition to the carbon sources outlined above, the terrestrial environment can be an important carbon source for lakes. There is also increasing evidence for the incorporation of methane-derived carbon within aquatic food webs, as discussed in this report.

4.1.1 Terrestrial Support to Aquatic Food Webs

There is a growing body of evidence that the terrestrial environment subsidises the carbon demands of aquatic food webs, addressing the carbon deficit between respiration and primary production observed in many freshwater systems [Pace et al., 2004; Weidel et al., 2008; Caraco et al., 2010; Wilkinson et al., 2013; Keaveney et al., 2015a, 2015b]. Terrestrial carbon is readily degraded by biological processes within aquatic systems, with degradation being far more rapid than would occur in the terrestrial system [Lapierre et al., 2013]. This carbon supplements the aquatic carbon pools and can then be incorporated within the food web through photosynthesis, incorporation into microbial biomass [Guillemette et al., 2013] or directly consumed by aquatic consumers [Weidel et al., 2008; Caraco et al., 2010]. For example, Pace et al. [2004] found that between 20% and 50% of zooplankton biomass in two lake ecosystems could be attributed to the consumption of terrestrially-derived carbon and radiocarbon. Stable isotope analysis has also demonstrated that terrestrial organic carbon is evident at all trophic levels in lake food webs [Keaveney et al., 2015b]. It is also worth noting that there is evidence of subsequent return of aquatic carbon to terrestrial systems, for example, through the emergence of aquatic larvae [Gratton et al., 2008].

Carbon entering aquatic systems from the surrounding terrestrial environment may, for example, derive from recent photosynthesis (i.e. the current season's primary production), or have been stored in soils [Keaveney et al., 2015a]. Dead organic matter from terrestrial systems may also enter aquatic systems, contributing to the carbon pool.

Climate has been found to be an important factor influencing the transfer of terrestrial carbon to aquatic systems, with warmer climate and higher precipitation resulting in greater DOC mobility through catchments [Vuorenmaa et al., 2006; Keaveney et al., 2015a]. Catchment size is also an important factor [Vuorenmaa et al., 2006].

Jones et al. [1999] suggest that the predominant form of terrestrial carbon entering lakes is DOC. Weidel et al. [2008], however, suggest that both DOC and POC are important forms of carbon entering aquatic systems from the surrounding terrestrial environment. This is supported by the findings of Jones et al. [1999] that terrestrial DOC and POC dominated carbon pools of 12 small forest lakes in Finland. Wilkinson et al. [2013] also found that terrestrial DOC and POC were important to the overall aquatic carbon budgets throughout 39 temperate lakes in northern USA; the average contribution of terrestrial POC to the overall POC pool throughout the lakes was approximately 55%, whereas the DOC pool was strongly dominated by terrestrially-derived material with the mean over the same set of lakes being close to 100%. Only the most eutrophic of the lakes were not dominated by terrestrially-derived DOC [Wilkinson et al., 2013]. The terrestrial POC contribution is consistent with that reported by Pace et al. [2004], where 40-55% of POC was attributed to terrestrially-derived carbon. Similar results were observed for Loch Ness in Scotland, with the pelagic food web being highly dependent on detrital carbon arising from terrestrial vegetation in the catchment [Jones et al., 1998]. The proportional contribution of terrestrial carbon to aquatic food webs is, however, likely to vary seasonally, with maximum contributions coinciding with periods of lower primary productivity, such as winter. This is supported by the findings of Keaveney et al. [2015a, 2015b] that calanoid copepods within zooplankton switch between autochthonous carbon dietary sources in summer when bio-energetically-rich algal blooms are present and terrestrial-derived carbon sources in winter when phytoplankton are fewer.

Terrestrially-derived carbon, both DOC and POC, can act as substrates for bacterial production in aquatic systems, with subsequent consumption of bacteria by zooplankton and other aquatic organisms providing an alternative route into the aquatic food web from that of uptake via primary producers [Keaveney et al., 2015a, 2015b]. In addition to incorporation of this terrestrially-derived carbon into bacterial biomass, respiration of bacteria results in the release of DIC to the water column, that can then be utilised by phytoplankton [Jones et al., 1999]. Trophic transfer of this terrestrially-derived carbon then occurs via consumption by heterotrophs of phytoplankton and bacterial biomass, or through direct grazing on terrestrial POC.

In terms of DOC, research suggests that algal DOC is generally more labile and energetically rich than terrestrially-derived DOC and is, therefore, utilised more rapidly [Guillemette et al., 2013; Keaveney et al., 2015b]. Terrestrial DOC utilisation is, however, more variable with labile and recalcitrant forms being present that are utilised over short and long timeframes, respectively; the more labile terrestrial DOC being utilised in parallel with algal DOC [Guillemette et al., 2013; Keaveney et al., 2015a]. Lennon et al. [2006] suggest that, of the terrestrially-derived DOC entering lakes, up to 90% may be biologically recalcitrant with the remainder being consumed primarily by aquatic bacteria that then respire between 35% and 99% of the DOC as CO_2. This implies that the labile terrestrial DOC is available to aquatic primary producers, with that taken up into bacterial biomass being available to consumers. Keaveney et al. [2015a] suggest that the recalcitrant terrestrial carbon is more likely to enter lake sediments. This is consistent with the findings of Caraco et al. [2010] that, whilst both old (recalcitrant) and new (labile) terrestrial carbon were incorporated within aquatic food webs, the proportionate uptake into zooplankton biomass was lower for the older, recalcitrant carbon. With algal DOC being more energetically rich than the majority of terrestrial DOC, eutrophic lakes, with high algal productivity, are more likely to have less terrestrial carbon accumulated within the food web than oligotrophic lakes.

4.1.2 Methane as a Carbon Source for Aquatic Food Webs

Whereas the availability of DIC drives primary production in aquatic systems, the role of methane as a source of carbon to aquatic food webs is being increasingly recognised [Jones and Grey, 2011]. Substantial amounts of methane can be produced in anoxic sediments and converted to microbial biomass by methane-oxidising bacteria (MOB) at oxic-anoxic interfaces within bed sediments [Ravinet et al., 2010; Jones and Grey, 2011]. The MOB can be highly productive and support aquatic food webs through consumption by benthic invertebrates [Jones and Grey, 2011]. The consumption of MOB is particularly evident in benthic chironomid (non-biting midge) larvae [Deines et al., 2007, 2009; Jones and Grey, 2011; Sanseverino et al., 2012] with methane-derived carbon contributing up to 60% of chironomid carbon biomass [Jones and Grey, 2011]. This is particularly significant because chironomid larvae often dominate the benthic fauna of lakes [Deines et al., 2007]. In addition to uptake by benthic invertebrates, there is also evidence of methane-based carbon contributing to the biomass of pelagic zooplankton, although this is more likely limited to those zooplankton with vertical migratory behaviours that bring them into the vicinity of oxic-anoxic interfaces, such as may occur at the interface between the hypolimnion and epilimnion where MOB may be active [Jones and Grey, 2011]. The presence of such interfaces will largely be governed by lake-mixing regimes [Lennon et al., 2006].

The link between methane production and uptake into consumers has been suggested to be particularly important in lakes with higher terrestrial-DOC inputs, which may favour methane production [Jones et al., 1999]. This is contradicted, however, by the findings of Lennon et al. [2006], that terrestrial DOC is recycled to CO_2 through heterotrophic respiration within lake ecosystems, thus increasing the lake DIC pool available to aquatic primary producers. With more recalcitrant terrestrial POC, such as twigs and other dead wood, potentially being accumulated in the sedimentary carbon pool [Keaveney et al., 2015a], it is this component that could provide an important carbon source for methane production.

The consumption of MOB by zooplankton and/or benthic invertebrates such as chironomids, or uptake of MOB-respired CO_2 by primary producers provides the basis for methane-derived organic carbon to be further transferred through the food web. This is supported by the findings of Sanseverino et al. [2012] whereby MOB-specific fatty acids were identified in the tissues of aquatic invertebrates and fish. Bunn and Boon [1993] also argue that δC-13 depleted carbon measured in fish was most likely to result from consumption of a methane-derived carbon source.

4.2 CARBON UPTAKE IN BENTHIC AND PELAGIC FISH

Whilst there have been an increasing number of studies undertaken on terrestrial- and methane-derived carbon supporting aquatic food webs, few studies have looked specifically at the uptake of different carbon sources by fish. Nonetheless, there is evidence from stable isotopic analysis for the trophic transfer of both terrestrial carbon and methane throughout aquatic food webs. Trophic position and feeding behaviour (i.e. whether food is primarily benthic or pelagic) are both important in governing carbon uptake and are influenced considerably by lake conditions.

Within-lake biota are often considered in terms of either benthic or pelagic food webs with:

- pelagic food webs being supported by in-water primary productivity; and
- benthic food webs being supported by sediment-based primary production (depending upon factors such as water column depth and light penetration) and the sedimentation of organic matter through the water column.

There will, however, be interactions between benthic and pelagic food webs. For example, the mobility and dietary selection of fish mean that physical and functional separations between pelagic, littoral and benthic compartments in lakes can be obscured [Reynolds, 2008]. The dietary preference of fish can

also change with age, such that species may demonstrate pelagic or benthic habits at different ages [Pace et al., 2004; Weidel et al., 2008; Reynolds, 2008]. Fish may also display opportunistic feeding behaviours rather than having distinct predator-prey relationships. Some invertebrates also move between benthic and pelagic habitats: chironomid larvae are heavily preyed upon in sediments but can also provide food to pelagic consumers when pupal stages migrate through the water column to emerge as terrestrial insects [Deines et al., 2007]. Furthermore, the settlement of pelagic-derived carbon to benthic sediments and subsequent metabolism and release of nutrients and CO_2 back to the water column ensures cycling between the pelagic and benthic systems: benthic food webs influence the flow of carbon to pelagic food webs and vice versa [Reynolds, 2008].

As discussed above, terrestrially-derived carbon has been found to subsidise aquatic food webs and the utilisation of terrestrial carbon within lakes has been demonstrated. For example, Keaveney et al. [2015b], used radiocarbon analysis to demonstrate that terrestrial carbon was incorporated into fish biomass, irrespective of whether species had a pelagic or benthic feeding habit, concluding that terrestrial carbon supported the highest trophic levels in both littoral and pelagic aquatic food webs. Weidel et al. [2008] also considered the contribution of terrestrial carbon to fish biomass in a clear-water temperate lake, concluding that around half of fish biomass production could be attributed to the trophic transfer of the within-lake primary production from the current season, with the implication that the remainder may be attributable to terrestrial-carbon sources. Jones et al. [1998] also demonstrated the importance of terrestrial carbon to the pelagic food web of a lake. Terrestrial carbon was found to be the major source of carbon for zooplankton in Loch Ness and, with most fish being zooplanktivorous, fish biomass production was concluded to be highly dependent on terrestrial carbon, with up to half of the carbon flux through the food chain being attributed to terrestrially-derived carbon [Jones et al., 1998].

Terrestrial carbon inputs to lakes can be greatest in littoral zones and fish inhabiting these areas may have a greater access to terrestrial-derived carbon, both in terms of POC and terrestrial invertebrates. This may result in spatial variation in the influence of terrestrial carbon to fish biomass production within an aquatic system.

The demonstration of methanotrophic bacteria utilising methane produced in anoxic lake sediments has provided the opportunity to investigate trophic differences across fish species. Phytoplankton-derived carbon in freshwater systems typically has δC-13 values between -30‰ and -20‰, whereas very negative δC-13 values (<-30‰) are largely associated with methane-derived carbon [Deines et al., 2009]. The δC-13 values can therefore help identify whether fish carbon has been obtained from methane-derived carbon or from primary-production-based carbon, or a combination, depending on the δC-13 signal. For example, the carbon isotopic signal of pollan in a humic lake in Northern Ireland indicated a selective feeding habit, whereas that of roach and perch was indicative of more mixed pelagic and littoral foraging [Keaveney et al., 2015b]. Perch, roach and ruffe from a small, deep lake in Germany all had similar δC-13 values that were consistent with partial reliance on pelagic food resources, whereas eels, pike and bream had more enriched δC-13 signals, suggesting a greater reliance on benthic food resources [Harrod and Grey, 2006]. Whilst differences were observed, Harrod and Grey [2006] concluded that distinct pelagic or benthic habits could not be defined due to the movement of species between habitats and the integration of energy sources across these systems. Ravinet et al. [2010] found that ruffe were able to feed at depth to exploit chironomid larvae with high methanotrophic carbon signatures within a Finnish temperate lake. The percentage of methane-derived carbon in fish increased with water depth, from 0% in the littoral zone to over 28% at depth and, overall, it was estimated that 17% of the biomass of ruffe within the lake was attributable to methane-derived carbon [Ravinet et al., 2010]. Harrod and Grey [2006] also analysed the proportion of methane-derived carbon in lake fish. Large bream were caught from a small but deep stratifying lake in Germany and δC-13 analysed. Results indicated that between 10% and 21% of their diet must be based on chironomid larvae that had themselves consumed methane-derived carbon [Harrod and Grey, 2006].

Jones and Grey [2011] also estimate that fish feeding extensively on chironomid larvae in some lakes could derive up to 20% of their carbon biomass from methane. Weidel et al. [2008] found that, for a clear-water temperate lake, 74% of fish growth across a range of fish species, was supported by benthic invertebrates as compared with pelagic invertebrates, with the greater size range of benthic invertebrate prey relative to pelagic prey being suggested as an important factor, making benthic feeding more energetically attractive to fish.

The size of lakes and their depth will affect food webs. In smaller water bodies, the distinction between pelagic and benthic feeding habits of fish may not be clear, with fish exploiting a multiplicity of available foods, irrespective of trophic position [Reynolds, 2008]. In deeper lakes, differences in stable isotope signatures are more likely to be observed, particularly in lakes subject to seasonal stratification, whereby the formation of a thermocline can restrict nutrient mixing from the hypolimnion to the epilimnion and prevent oxygen within the epilimnion reaching the hypolimnion. This, in turn, can limit primary production in surface waters and largely restrict consumers, apart from those tolerant of lower oxygen levels, to the upper epilimnion where oxygen levels are maintained [Harrod and Grey, 2006]. Under stratified conditions, a stronger methane-based δC-13 signal would be expected within the benthic food web, and in those fish species, such as bream, that are able to tolerate periods of low oxygen conditions whilst foraging. The level of distinction between benthic and pelagic food webs in such lakes will, however, depend on the timing and duration of stratification. With the onset of mixing throughout the water column, the methane-based δC-13 signal would be expected to disperse as nutrients are mixed and movement of consumers less restricted. However, in temperate regions, fish biomass production is not uniform throughout the year; greater biomass production occurs in the warmer months [Harrod and Grey, 2006], which is likely to coincide with stratification in deeper lakes.

4.3 IMPLICATIONS OF REVIEW FINDINGS FOR THE MODELLING OF C-14 IN AQUATIC ECOSYSTEMS AND SUGGESTED NEXT STEPS

Based on this initial review, it is evident that terrestrial carbon plays an important role in many lakes, supporting the aquatic food web. Terrestrial carbon entering lakes may be directly utilised by aquatic bacteria or by primary producers; or be sequestered to sediments where it may be utilised by benthic invertebrates directly or by bacteria, e.g. being converted to methane in anoxic sediments. The terrestrial carbon utilised throughout the water column and bed sediments can then be recycled through the food web as a result of respired CO_2 and excretion of DOC and POC. Based on this initial review, it may be concluded that a significant fraction (50% or more) of carbon within an aquatic food web within a lake may be derived from the terrestrial catchment area. Where C-14 is discharged directly to lakes via groundwater, the input of terrestrial carbon may, therefore, dilute the uptake of C-14 within the food web. The transfer of carbon from terrestrial to aquatic systems may, therefore, merit explicit consideration when modelling C-14 in safety assessments.

The evidence of MOB being commonly present in lakes at anoxic/oxic interfaces also has implications for C-14 discharge to lakes via groundwater. Should the form of C-14 in groundwater be methane, it is likely that the action of MOB will be to sequester C-14 within the aquatic food web, either through incorporation within bacterial biomass that can then be available to consumers, or through oxidation and respiration of CO_2 that is then available to primary producers. Based on the current review, it is not feasible to estimate the proportion of methane that may be retained within the food web. However, based on the studies of methane-derived carbon within aquatic food webs reviewed to-date, it may be reasonable to consider benthic-feeding fish more likely to incorporate C-14 from methane dissolved in groundwater within tissue biomass as compared with pelagic-feeding fish, due to the activity of MOB and their utilisation by benthic invertebrates. Furthermore, there is some evidence for benthic invertebrates supporting fish biomass production to a greater extent than pelagic food sources.

The following represent topics for further discussion and potential next steps, with regards to modelling C-14 in aquatic ecosystems.

- The current review has focussed on the uptake of carbon within lake food webs, but there is also the potential for direct carbon uptake via fish gills. This may be particularly relevant for fish within rivers for which, depending on the characteristics of the discharge, uptake of carbon through the food web may be more limited. It may be appropriate, therefore, to extend the review to encompass carbon uptake by fish in rivers and to review evidence for direct carbon uptake across gills.

- Variation in stable isotopes of carbon throughout the food web may have implications for specific activity modelling of C-14. Whilst the sources of C-14 may differ from the sources of stable carbon with different isotopic signatures, information on the sources and sizes of different carbon pools, together with turnover rates, will provide the basis for any modelling of C-14. There may, therefore, be merit in developing, based on the review findings, a broader generic conceptual model for carbon pools and fluxes in lake (and river) systems and to consider timescales for turnover of the various carbon pools. It may also be useful to summarise modelling approaches that have variously been adopted and to compare these against the conceptual model for carbon in aquatic systems, providing a commentary on carbon sources, pools and fluxes considered within the different approaches.

- Finally, consideration could be given as to whether published studies on stable isotope signatures in aquatic systems provide sufficient data to enable a model scenario based on carbon pools and fluxes between them to be developed as the basis for a model-model and/or model-data comparison study.

5. CONCLUSIONS

The output of a BIOPROTA project in 2017-18 concerning C-14 in the biosphere is presented. The project encompassed behaviour of C-14 in terrestrial and aquatic ecosystems via the following activities.

- Modelling of C-14 within a Finnish boreal forest system and comparison against high resolution observational data.
- Further modelling of C-14 from an historical near-surface waste disposal facility and its migration to the Duke Swamp area within the Chalk River site in Canada, along with comparison against observational data.
- Review of carbon uptake by fish, including timescales for potential equilibrium with the surrounding water/sediment environment and their food source.

The boreal forest scenario was modelled on behalf of Posiva using a detailed, physically based model to simulate CO_2 profiles and isotopic ratio variations with height within and above the forest canopy. In most of the cases studied, the simulated vertical profiles of C-14 reasonably agree with measurements. Review of the data by the Technical Support Team demonstrated that useful insights can also be gained from sensitivity studies with a simplified model that treats the properties of the canopy to be independent of height. The analyses show that isotopic signatures arising from the boreal forest soil are rapidly damped in the first few metres of the atmosphere above the soil. This can be readily represented in a simple dispersion model using physically reasonable parameter values.

Analysis of the Duke Swamp scenario was undertaken by the Technical Support Team and focused on determining the flux of C-14 entering the swamp as well as subsequent migration and losses. The analysis shows that a two-layer model of the swamp is needed to help explain the observations, with groundwater-driven transport in the lower layer, where biological activity is limited, contrasting with dominance of uptake in biomass, effects of mineralisation and losses by volatilisation in the upper layer.

The review of carbon uptake by fish in lacustrine ecosystems emphasises the importance of terrestrial-derived carbon to the carbon cycle within freshwater aquatic systems. The review found clear distinctions in the use of different sources of carbon (e.g. of terrestrial *versus* aquatic origin) at different trophic levels and by functionally distinct components of lacustrine food-webs. Safety assessment models typically assume equilibrium between aquatic organisms and the specific activity of C-14 in lake water. There is potential to further extend the review, for example, to assess whether or not the role of terrestrially derived carbon is adequately represented in assessment models.

6. REFERENCES

Aikens AE (2012). Decommissioning in Canada. Presentation, IAEA Workshop INT9175 9001. https://www.iaea.org/OurWork/ST/NE/NEFW/WTS-Networks/IDN/idnfiles/Wkp_on_Development_WM,WasteCharacterization_Clearance/Day4/15.DecommissioningCanada_AIKENS.pdf

Ascough PL, Cook GT, Church MJ, Dunbar E, Einarsson Á, McGovern TH, Dugmore AJ, Perdikaris S, Hastie H, Friðriksson A, Gestsdóttir (2010). Temporal and spatial variations in freshwater ^{14}C reservoir effects: Lake Mývatn, northern Iceland. Radiocarbon 52: 1098-1112.

Aulagnier C, Le Dizès S, Maro D, Hébert D, Lardy R, Martin R, Gonze M-A (2012). Modelling the transfer of ^{14}C from the atmosphere to grass: A case study in a grass field near AREVA-NC La Hague. Journal of Environmental Radioactivity, 112: 52-59.

Aulagnier C, Le Dizès S, Maro D, Hébert D, Lardy R, Martin R (2013). The TOCATTA-χ model for assessing 14C transfers to grass: an evaluation for atmospheric operational releases from nuclear facilities. Journal of Environmental Radioactivity, 120: 81-93.

BIOCLIM, 2004, Deliverable D10-12: Development and Application of a Methodology for taking Climate-driven Environmental Change into account in Performance Assessments, Andra, Parc de la Croix Blanche, 1/7 rue Jean Monnet, 92298 Châtenay-Malabry, France, Available from http://www.andra.fr/bioclim/.

Bunn SE, Boon PI (1993). What sources of organic carbon drive food webs in billabongs? A study based on stable isotope analysis. Oecologia 96: 85-94.

Caraco N, Bauer JE, Cole JJ, Petsch S, Raymond P (2010). Millennial-aged organic carbon subsidies to a modern river food web. Ecology 91(8): 2385-2393.

Caron F, Manni G, Workman WJG, Haas MK (1998a). Soil CO_2 Gas-groundwater Exchange and Migration Near Waste Management Area C, Chalk River, Ontario, RC-2121, COG 98 253-I. Atomic Energy of Canada Limited, Chalk River Laboratories, Chalk River, Ontario.

Caron F, Sutton J, Recoskie CL, Haas MK (1998b). A Scoping Study of C-14 Gaseous Emissions from Waste Management Area C, Chalk River Laboratories. RC-2113. Atomic Energy of Canada Limited, Chalk River, Ontario.

CNSC (2015). Joint Convention on the Safety of Spent Fuel Management and on the Safety of Radioactive Waste Management. Canada's presentation to the 5th Review Meeting, 13 May 2015, Vienna.

Deines P, Bodelier PLE, Eller G (2007). Methane-derived carbon flows through methane-oxidizing bacteria to higher trophic levels in aquatic systems. Environmental Microbiology 9:1126-1134.

Deines P, Wooller MJ, Grey J (2009). Unravelling complexities in benthic food webs using a dual stable isotope (hydrogen and carbon) approach. Freshwater Biology 54: 2243-2251.

Donders RE, Killey RWD, Franklin KJ, Weich SJ, Strobel GS (1996). Trial Coring in LLRW Trenches at Chalk River, AECL report AECL-11681.

Evenden WG, Sheppard SC, Killey RWD (1998). Carbon-14 and tritium in plants of a groundwater-contaminated wetland. Journal of Applied Geochemistry 13, 17-21.

Gratton C, Donaldson J, Vander Zanden MJ (2008). Ecosystem linkages between lakes and the surrounding terrestrial landscape in northeast Iceland. Ecosystems 11: 764-774.

Guillemette F, McCallister SL, del Giorgio PA (2013). Differentiating the degradation dynamics of algal and terrestrial carbon within complex natural dissolved organic carbon in temperate lakes. Journal of Geophysical Research 118: 963-973.

Hardwick ML (1999). Influence of low level radioactive waste management sites on biotic and abiotic components of wetlands in Chalk River, Ontario. A Thesis submitted to the Committee on Graduate Studies in Partial Fulfilment of the Requirements for the Degree of Master of Science in the Faculty of Arts and Science. Trent University, Peterborough, Ontario, Canada.

Harman IN, Finnigan JJ (2008). Scalar concentration profiles in the canopy and roughness sublayer. Boundary-Layer Meteorol 129:323-351.

Harrod C, Grey J (2006). Isotopic variation complicates analysis of trophic relations within the fish community of Plußsee: a small, deep, stratifying lake. Archiv fur Hydrobiologie 167: 281-299.

Hart DR, McKee P, Wren C (2005). Ecological Effects Review of Chalk River Laboratories. EcoMetrix Incorporated report prepared for AECL, Ref 04-1178.

Hoch AR, Lever DA, Shaw G (2014). Uptake of Carbon-14 in the Biosphere: Summary Report. AMEC report prepared for Radioactive Waste Management Limited AMEC/004041/008 Issue 2.

Jones RI, Grey J (2011). Biogenic methane in freshwater food webs. Freshwater Biology 56: 213-229.

Jones RI, Grey J, Sleep D, Quarmby C (1998). An assessment, using stable isotopes, of the importance of allochthonous organic carbon sources to the pelagic food web in Loch Ness. Proceedings of the Royal Society of London B: 265: 105-111.

Jones RI, Grey J, Sleep D and Arvola L (1999). Stable analysis of zooplankton carbon nutrition in humic lakes. OIKOS 86: 97-104.

Junninen H, Lauri A, Keronen P, Aalto P, Hiltunen V, Hari P, Kulmala M (2009). Smart-SMEAR: on-line data exploration and visualization tool for SMEAR stations. Boreal Environment Research 14, 447–457.

Keaveney EM, Reimer PJ, Foy RH (2015a). Young, old, and weathered carbon – part 1: Using radiocarbon and stable isotopes to identify carbon sources in an alkaline, humic lake. Radiocarbon 57(3): 407-423.

Keaveney EM, Reimer PJ, Foy RH (2015b). Young, old, and weathered carbon – part 2: Using radiocarbon and stable isotopes to identify terrestrial carbon support of the food web in an alkaline, humic lake. Radiocarbon Journal 57(3): 425-438.

Killey RWD, Rao RR, Eyvindson S (1998). Radiocarbon speciation and distribution in an aquifer plume and groundwater discharge area, Chalk River, Ontario. Applied Geochemistry, 13, 3-16.

King-Sharp KJ, Benz ML, Yankovich TL, Hartwick LA (2005). Carbon-14 Contaminant Transfer in an Ecosystem Aquatic Pathway: Database and Root Uptake Experiment. AECL Technical Report, 153-121241-ENA-001 (Revision 0).

Kovalets I, Avila R (2018). Simulation of C-14 atmospheric transport for the conditions of SMEAR-II station. Memorandum provided as input to the BIOPROTA study, 28 February 2018.

Kovalets I, Avila R, Mölder M, Kovalets S, Lindroth A (2018). Verification of a one-dimensional model of CO_2 atmospheric transport inside and above forest canopy using observations at the site of Norunda research station. Boundary Layer Meteorology, doi: 10.1007/s10546-018-0340-z.

Lapierre J-F, Guillemette F, Berggren M, del Giorgio PA (2013). Increases in terrestrially derived carbon stimulate organic carbon processing and CO_2 emissions in boreal aquatic ecosystems. Nature Communications 4: 2972 doi: 1001038/ncomms3972.

Le Dizès S, Maro D, Hébert D, Gonze M-A, Aulagnier C (2012). TOCATTA: a dynamic transfer model of ^{14}C from the atmosphere to soil-plant systems. Journal of Environmental Radioactivity, 105: 48-59.

Lennon JT, Faiia AM, Feng X, Cottingham KL (2006). Relative importance of CO_2 recycling and CH_4 pathways in lake food webs along a dissolved organic carbon gradient. Limnology and Oceanography 51(4): 1602-1613.

Limer LMC, Albrecht A, Smith K, Marang L, Norris S, Smith GM, Thorne MC, Xu S (2012). C-14 Long-Term Dose Assessment in a Terrestrial Agricultural Ecosystem: FEP Analysis, Scenario Development, and Model Comparison. Report prepared within the BIOPROTA international collaborative forum and published by the Swedish Radiation Safety Authority: 2012:47. Available from www.bioprota.org.

Limer L, Klos R, Shaw G, Walke R (2013). Terrestrial Biosphere Modelling of ^{14}C Research. Swedish Radiation Safety Authority Report 2013:20.

Limer L, Les Dizès-Maurel S, Klos R, Maro D, Nordén M (2015). Impacts of ^{14}C discharges from a nuclear fuel reprocessing plant on surrounding vegetation: Comparison between grass field measurements and TOCATTA-χ and SSPAM^{14}C model computations. Journal of Environmental Radioactivity, 147: 115-124.

Limer L, Ota M, Tanaka T, Thorne M, Walke R (2017). C-14 Terrestrial Model-Data Comparisons: Final Report. Report prepared within the BIOPROTA international collaborative forum QRS-1769A-1, Version 1.0, 11 July 2017. Available from www.bioprota.org.

Mäkelä A, Kolari P, Karimäki J, Nikinmaa E, Perämäki M, Hari P (2006). Modelling five years of weather-driven variation of GPP in a boreal forest. Agricultural and Forest Meteorology, 139, 382-398.

Markkanen T, Rannik U, Keronen P, Suni T, Vesala T (2001). Eddy covariance fluxes over boreal Scots pine forest. Boreal Environment Research 6, 65-78.

Mecke M, Ilvesniemi H (1999). Near-saturated hydraulic conductivity and water retention in coarse podzol profiles. Scan. J. Forest Res. 14, 391–401.

Milton GM, King KJ, Sutton J, Enright S (1998). Tracer studies of carbon source utilization in a wetland on the Canadian Shield. Journal of Applied Geochemistry 13, 23-30.

Mobbs S, Shaw G, Norris S, Marang L, Sumerling T, Albrecht A, Xu S, Thorne M, Limer L, Smith K, Smith G (2013). Developments in modeling of C-14 in the biosphere for solid radioactive waste disposal. Radiocarbon, 55 (2-3), 814-825.

Napier JB (2015). Analysis of Carbon-14 Transport from a Contaminated Groundwater Source. PhD Thesis, Radiation Health Physics, Oregon State University.

Norris S, Albrecht A, Limer L, Cummings R, Marang L, Smith G, Smith K, Thorne M, Xu S (2011). A Comparison of Models for Assessing the Radiological Impact of 14C released to Soils in Gaseous Form

following the Geological Disposal of Solid Radioactive Wastes. International Conference of Radioecology and Radioactivity, Hamilton, Canada, June 19-24.

Pace ML, Cole JJ, Carpenter SR, Kitchell JF, Hodgson JR, Van de Bogert MC, Bade DL, Kritzberg ES, Bastviken D (2004). Whole-lake carbon-13 additions reveal terrestrial support of aquatic food webs. Nature 427:240-243.

Palonen V (2015). A portable molecular-sieve-based carbon dioxide sampling system for radiocarbon measurements. Review of Scientific Instruments 86 (12). AIP Publishing: 125101. doi:10.1063/1.4936291.

Palonen V, Pumpanen J, Vesala T. (2018). A year-long high precision atmospheric and forest soil emission $^{14}CO_2$ dataset from northern Europe. Boreal Environmental Research. *In preparation.*

Posiva [2014a]. Safety Case for the disposal of spent nuclear fuel at Olkiluoto: Radionuclide transport and dose assessment for humans in the biosphere assessment BSA-2012. Posiva Report 2012-31.

Posiva [2014b]. Safety Case for the disposal of spent nuclear fuel at Olkiluoto: Dose assessment for the plants and animals in the biosphere assessment BSA-2012. Posiva Report 2012-32.

Quintessa (2017). AMBER 6.2 Reference Manual. Quintessa Limited report QE-AMBER-1, Version 6.2. www.quintessa.org/amber

Rao RR, Killey RWD (1994). Quantitative separation and determination of inorganic and organic forms of total carbon and radiocarbon in natural waters and application at a radioactive waste management site. Radiochima Acta, 65, 63–74.

Ravinet M, Syväranta J, Jones RI, Grey J (2010). A trophic pathway from biogenic methane supports fish biomass in a temperate lake ecosystem. Oikos 119: 409-416.

Reimer PJ, Brown TA, Reimer RW (2004). Discussion: Reporting and calibration of post-bomb ^{14}C data. Radiocarbon, 46(3), 1299-1304

Reynolds CS (2008). A changing paradigm of pelagic food webs. International Review of Hydrobiology 93: 517-531.

Saetre P, Nordén A, Keesman S, Ekström P-A (2013). The Biosphere model for radionuclide transport and dose assessment in SR-PSU. Svensk Kärnbränslehantering AB (SKB) report R-13-46, updated 2017-09.

Sanseverino AM, Bastviken D, Sundh I, Pickova J, Enrich-Prast A (2012). Methane carbon supports aquatic food webs to the fish level. PLoS ONE 7(8): e42723. doi:10.1371/journal.pone.0042723.

Sheppard S, Thorne MC (2005). Model Review and Comparison for C-14 Dose Assessment. Theme 2: Task 3 report prepared within the BIOPROTA international collaborative forum. Available from www.bioprota.org.

Sheppard SC, Amiro BD, Sheppard MI, Stephenson M, Zach R, Bird GA (1994). Carbon-14 in the biosphere: modelling and supporting research for the Canadian nuclear fuel waste management program. Waste Management 14, 445-456.

Smith K (Ed.) (2015). Long-term Dose Assessment for Carbon-14: Report of an International Workshop. Report prepared within the BIOPROTA international collaborative forum, Version 2.0, August 2015. Available from www.bioprota.org.

Smith K, Smith G (Eds) (2014). C-14: Data, Ecosystems and Dose Assessment: Report of an International Workshop, Aix-en-Provence, 1 – 3 April 2014. Report prepared within the BIOPROTA international collaborative forum. Available from www.bioprota.org.

Stenström KE, Skog G, Georgiadou E, Genberg J, Johansson A (2011). A guide to radiocarbon units and calculations. Lund University, Department of Physics, Division of Nuclear Physics. Report LUNFD6(NFFR-3111)/1-17/(2011).

Stuiver M, Polach HA (1977). Reporting of 14C data. Radiocarbon, 19(3), 355–363.

Vesala T et al. (1998). Long-term field measurements of atmosphere-surface interactions in boreal forest combining forest ecology, micrometeorology, aerosol physics and atmospheric chemistry. Trends in Heat, Mass and Momentum Transfer 1998. T4. C17-35.

Vuorenmaa J Forsius M, Mannio J (2006). Increasing trends of total organic carbon concentrations in small forest lakes in Finland from 1987 to 2003. Science of the Total Environment 365: 47-65.

Walke RC, Thorne MC, Limer LMC. (2013). RWMD Biosphere Assessment Model: Terrestrial Component. Quintessa and AMEC report to NDA RWM QRS-1628A-2, Issue 2.

Weidel B, Carpenter S, Cole J, Hodgson J, Kitchell J, Pace M, Solomon C (2008). Carbon sources supporting fish growth in a northern temperate lake. Aquatic Sciences 70: 446-458.

Wilkinson GM, Pace ML, Cole JJ (2013). Terrestrial dominance of organic matter in north temperate lakes. Global Biogeochemical Cycles 27: 1-9.

Winemiller KO, Polis GA (1996). Food webs: what do they tell us about the world. In: Food webs: integration of patterns and dynamics (eds GA. Polis and KO Winemiller), pp 1-22. Chapman and Hall, New York.

Yankovich TL, King-Sharp KJ, Benz ML, Carr J, Killey RWD, Beresford NA, Wood MD (2013). Do site-specific radiocarbon measurements reflect localized distributions of ^{14}C in biota inhabiting a wetland with point contamination sources. Journal of Environmental Radioactivity, 126, 352-366.

Yankovich TL, King-Sharp KJ, Carr J, Killey RWD, Beresford NA, Wood MD (2014). Spatial analysis of Carbon-14 dynamics in a wetland ecosystem (Duke Swamp, Chalk River Laboratories, Canada). Journal of Environmental Radioactivity, 137, 173-180.

Yim MS, Caron F (2006). Review: Life cycle and management of carbon-14 from nuclear power generation. Progress in Nuclear Energy, 48, 2-36.

APPENDIX A. DUKE SWAMP DATA SET

Further information about the Duke Swamp scenario is provided below.

Description of Waste Management Area C

A photograph of the nature of the disposals is given in Figure 51. Trial coring was conducted in to WMA-C in 1995 and included analysis of groundwater contamination [Donders et al., 1996]. A description of the profile through one of the boreholes is given in Figure 52.

Figure 51: Photograph of WMA-C presented at an IAEA workshop [Aikens, 2012].

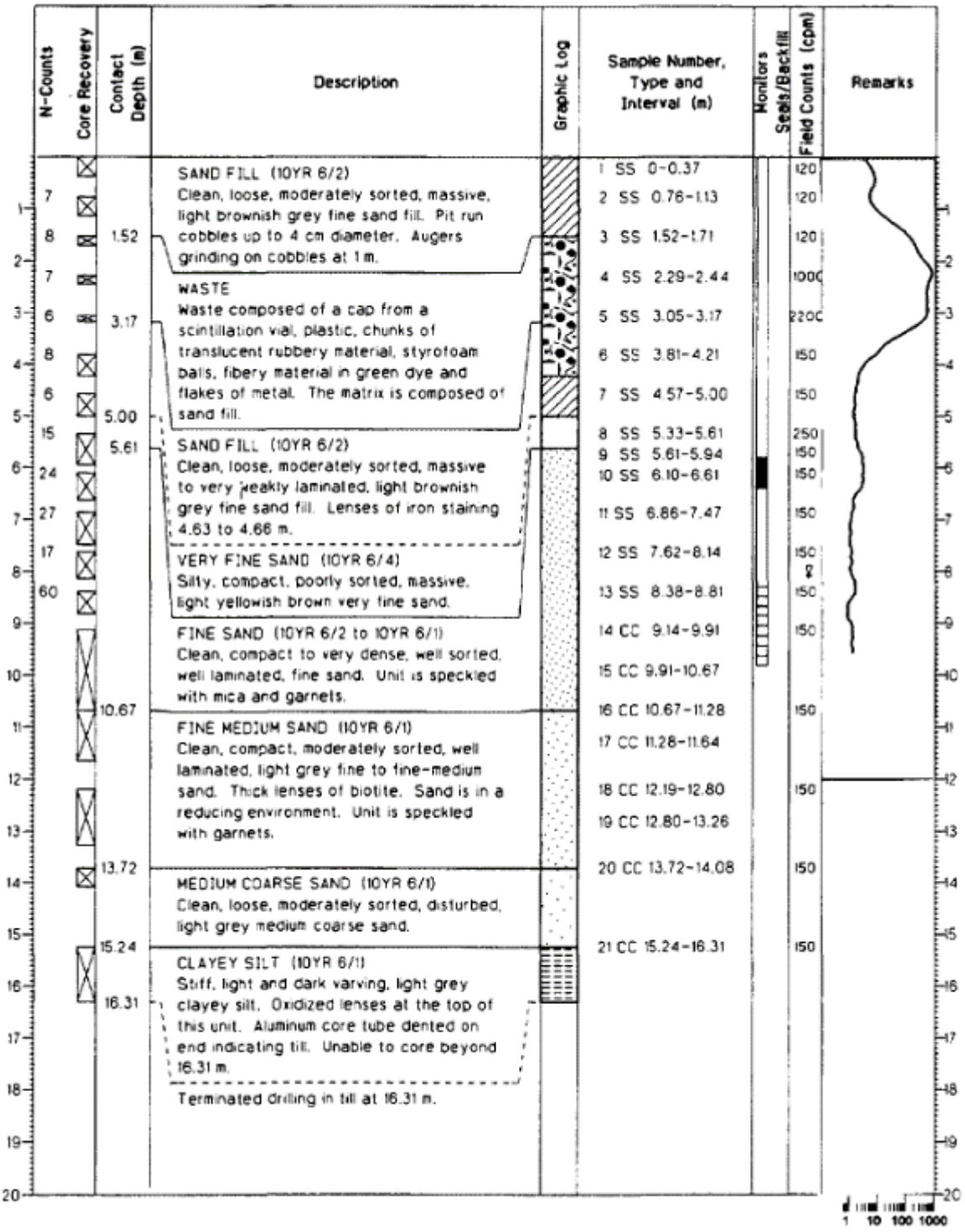

Figure 52: Borehole log for one of the trial cores into Waste Management Area C, from Donders et al. [1996].

Groundwater Interpretation for Duke Swamp

Groundwater enters Duke Swamp from Lake 233, and from Duke Swamp ultimately drains into Maskinonge Lake (Figure 53). Water leaves the swamp in two directions: to the north west, where the

water flows into Lower Bass Lake; and to the south east, where the water flows into Duke Stream [Killey et al., 1998]. Both Lower Bass Lake and Duke Stream flow into Maskinonge Lake.

Up-gradient of WMA-C, the groundwater has low redox potential and low dissolved oxygen content; reflecting its origin as recharge through the bed sediment of Lake 233. The bed sediment of the lake is generally thin but supports a substantial rate of biological activity. Groundwater beneath WMA-C has higher dissolved oxygen content in comparison to that beneath Lake 233 [Donders et al., 1996]. Groundwater beneath WMA-C flows towards the swamp at a rate of about 150 m y^{-1} [Napier, 2015].

A tentative water balance for Duke Swamp and for groundwater flow from Lake 233 to Duke Swamp beneath WMA-C is provided below. The nomenclature is illustrated in Figure 54. Meteorological data for Chalk River are given in Table 9. These are monthly averages, based on data collected between 1971 and 2000. They correspond closely to boreal continental climate conditions, EC conditions as defined in [BIOCLIM, 2004]. Annual precipitation is about 800 mm at Chalk River, of which about 190 mm falls as snow during winter months. Evapotranspiration is about 420 mm y^{-1}, which leaves a hydrologically effective rainfall of about 380 mm y^{-1} [Napier, 2015].

Table 9: Monthly average climate data for Chalk River. [Taken from http://www.eldoradocountyweather.com/canada/climate2/Chalk%20River.html].

Month	Temperature (ºC)	Rainfall (mm)	Snowfall (cm)	Precipitation (mm)
January	-12.1	14.2	43.7	56.7
February	-9.8	8.7	37.7	45.3
March	-3	31.4	30.7	62
April	5.1	51.4	9.1	60.4
May	12.6	80.2	1.4	81.6
June	17.5	88.3	0	88.3
July	20	86.8	0	86.8
August	18.7	82.1	0	82.1
September	13.7	84.6	0	84.6
October	7.3	76.7	2.7	79.3
November	0.3	48.4	24.3	72.3
December	-7.9	16.6	45.8	60.9

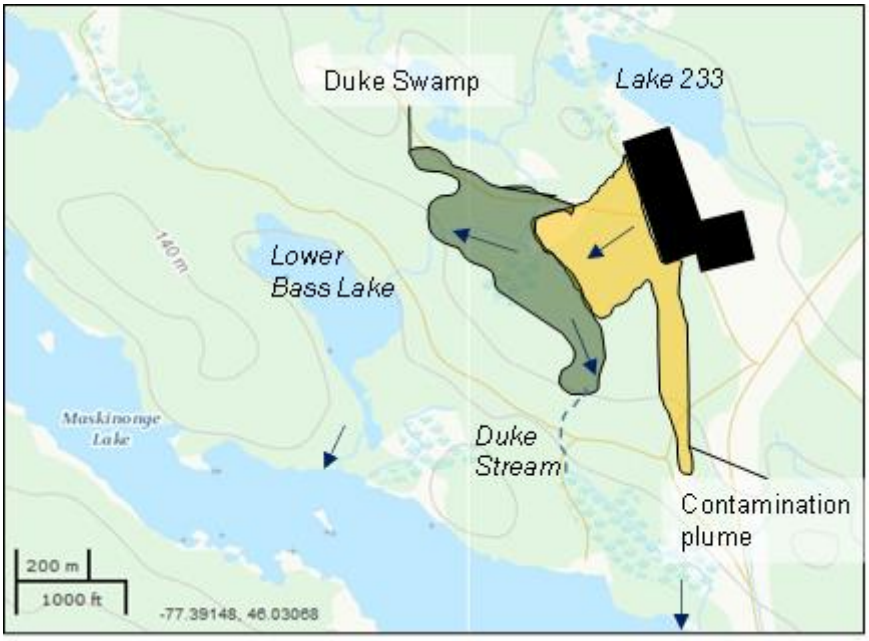

Figure 53: Indication of groundwater flow into and out of Duke Swamp. (Inspired from Killey et al. [1998]. Underlying map is ©GeoGratis – Canada Base Map.]

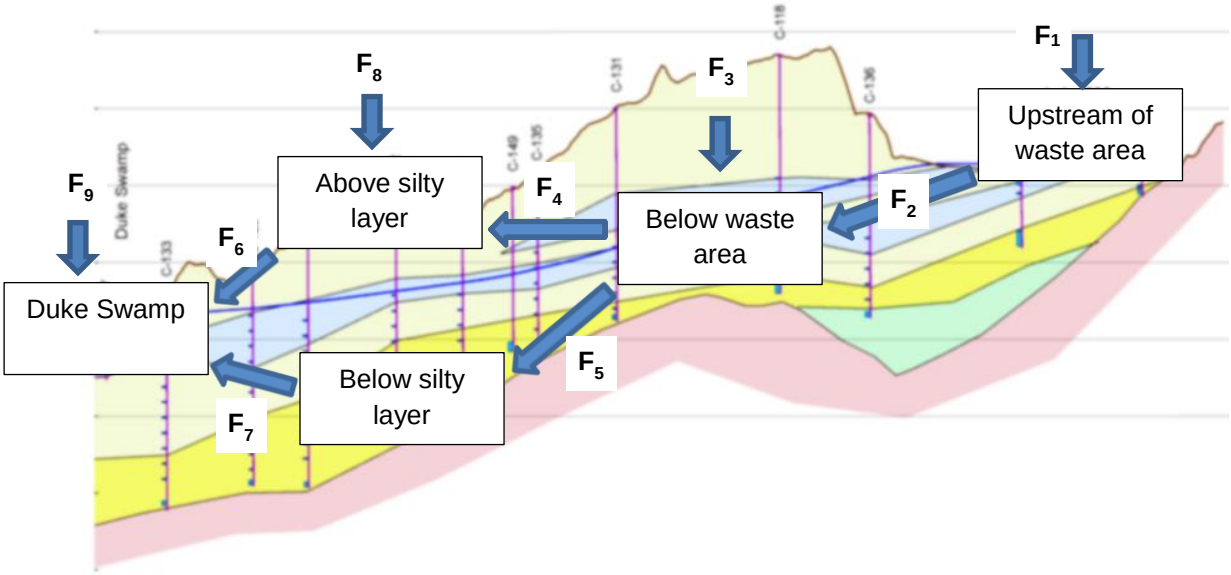

Figure 54: Water balance for groundwater flow and Duke Swamp.

For these conditions, precipitation (P) typically exceeds potential evapotranspiration (PE) by about 200 mm y^{-1}. Thus, if P at the site is taken to be 800 mm y^{-1}; PE should be taken as 600 mm y^{-1}. Over lake and wetland areas, actual evapotranspiration (AE) is taken to be equal to PE, whereas over other areas AE is taken to be 0.75*PE (i.e. 450 mm y^{-1}). Thus, P-AE = 200 mm y^{-1} over lakes and wetlands

and 350 mm y^{-1} elsewhere; the latter corresponding well with the 340 mm y^{-1} value given in Killey et al. [1998].

Upstream of the waste area, the area of Lake 233 that is taken to feed groundwater flow beneath WMA-C is taken to be the same area as WMA-C itself (i.e. 350 m x 120 m = 4.2E4 m^2; note that this is not the whole of Lake 233, since much of the lake drainage bypasses WMA-C, as shown by the water-table contours of Figure 1 of Killey et al. [1998]); other upslope contributions to groundwater flow beneath WMA-C are taken to arise from a similar area. Thus:

$$F_1 = 4.2E4 \times (0.2 + 0.35) = 2.31E4 \text{ m}^3 \text{ y}^{-1} \quad (43)$$

Hence:

$$F_2 = 2.31E4 \text{ m}^3 \text{ y}^{-1} \quad (44)$$

By similar arguments:

$$F_3 = 350 \times 120 \times 0.35 = 1.47E4 \text{ m}^3 \text{ y}^{-1} \quad (45)$$

Thus:

$$F_4 + F_5 = F_2 + F_3 = 3.78E4 \text{ m}^3 \text{ y}^{-1} \quad (46)$$

The partitioning of the total flow between F_4 and F_5 is unknown, so:

$$F_4 = \alpha (F_4 + F_5) \qquad F_5 = (1-\alpha) (F_4 + F_5) \quad (47)$$

Leakage across the silty layer is excluded, since this is likely to be a minor factor in routing C-14.

Noting that the area above the silty layer is not a lake or wetland and has a downslope length of about 250 m:

$$F_8 = 350 \times 250 \times 0.35 = 3.06E4 \text{ m}^3 \text{ y}^{-1} \quad (48)$$

$$F_7 = F_5 \quad \text{and} \quad F_6 = F_4 + F_8 \quad (49)$$

Thus, the total groundwater flow into Duke Swamp is:

$$F_6 + F_7 = F_4 + F_5 + F_8 = 6.84E4 \text{ m}^3 \text{ y}^{-1} \quad (50)$$

Killey et al. [1998] give the streamflow from Duke Swamp as 7.71E4 m^3 y^{-1} but note that runoff from precipitation falling on the rocky southwestern boundary of Duke Swamp plus direct precipitation onto the swamp contributes 1.04E4 m^3 y^{-1} to this streamflow. Therefore, groundwater discharge contributes 6.67E4 m^3 y^{-1} to this streamflow. They also give an estimate of the total groundwater input to Duke Swamp as 10.3E4 m^3 y^{-1}, which includes various contributions other than the downslope flow from WMA-C. Based on these considerations, F_9 is estimated by difference to be about 10.3E4 – 6.84E4 = 3.46E4 m^3 y^{-1}. It is assumed that some of the overall groundwater inflow into Duke Swamp is lost by subsurface flows and evapotranspiration processes, resulting in a streamflow that is rather less than the sum of the groundwater input plus runoff from precipitation falling on the rocky southwestern boundary of Duke Swamp plus direct precipitation onto the swamp (11.3E4 m^3 y^{-1}).

Description of Duke Swamp

The swamp covers an area of about 10 ha and primarily comprises fibrous sphagnum peat, which can extend to a depth of up to 3 m. Vegetation comprises plants such as sphagnum moss, lichen, ferns (bracken, ostrich ferns [Milton et al., 1998]), white spruce, and white cedar [Evenden et al., 1998].

Contamination in Waste Management Area C

As part of the trial coring conducted in to WMA-C in 1995, five boreholes were sunk into a relatively localised region of WMA-C [Donders et al., 1996]. Dissolved C-14 concentrations from those trial boreholes in WMA-C are given in Table 10.

Table 10: Dissolved C-14 concentrations in the five trial boreholes into Waste Management Area C c. 1995, from Donders et al. [1996].

Borehole	Dissolved C-14 Concentration (Bq L^{-1})
CT-1	<45
CT-2	67
CT-3	<45
CT-4	112
CT-5	720

As part of a review into the life cycle and management of C-14 from nuclear power generation in the US and Canada, Yim and Caron [2006] note that a number of AECL studies indicate that most of the C-14 (~95% or more) is released from WMA-C to the atmosphere as $^{14}CO_2$, while the smaller portion is as ^{14}C-bicarbonate in groundwater [Caron et al., 1998a,b]. Whilst methane is likely generated in the wastes, it was not detected near WMA-C in those studies, as it is readily converted to CO_2 in the unsaturated, well-aerated sand surrounding the trenches. Yim and Caron [2006] also note that Rao and Killey [1994] have measured organic C-14 in contaminated groundwater, but it was not clear whether this material was originally present in the wastes as an organic C-14 form, or if it originated from microbial conversion. Yim and Caron [2006] propose that the Rao and Killey [1994] study also suggests that most of the C-14 leaving WMA-C is inorganic. Finally, Yim and Caron [2006] note that field surveys have been performed to obtain mass balances (for C-14 and C-12) from WMA-C, to obtain current release rates.

Contamination in the Area between WMA-C and Duke Swamp

Killey et al. [1998] measured C-14 activity in groundwater in four boreholes adjacent to WMA-C, and also seven boreholes adjacent to Duke Swamp. For those locations adjacent to Duke Swamp, a 1D profile in the groundwater was obtained. The well depth, sample pH and carbon concentration (mg L^{-1}), along with volumetric concentration of C-14 as DOC and DIC (Bq L^{-1}; see Table 11) were recorded. From this information, the specific activity of C-14 (Bq gC^{-1}) in both DOC and DIC was derived. In addition, C-14 concentrations in surface water in two locations were also measured.

Four of the boreholes adjacent to Duke Swamp were also included in the field studies reported by Napier [2015]. The C-14 activity in groundwater in a further seven boreholes elsewhere in the contamination plume, plus other boreholes outside of the contamination plume and one inside Duke Swamp, were included in Napier [2015]. For each location, the depth of the well (m), CO_2 concentration (ppm), DOC (mg L^{-1}) and DIC (mg L^{-1}) concentrations were recorded. With respect to C-14 activities, these were measured in the water (Bq L^{-1}), soil gas (Bq L^{-1}) and above-ground bracken (*Pteridium*; Bq gC^{-1}). The data from those locations are presented in Table 12 and Table 13. Multi-level soil gas concentrations were taken at sample locations #8 and #369 in the centre of the contamination plume (Table 14).

Table 11: C-14 activity in groundwater (Bq L^{-1}) downgradient of WMA-C from a sampling campaign in 1995 [Killey at al., 1998].

Location	DIC (Bq L^{-1})	DOC (Bq L^{-1})
Adjacent to WMA-C		
C-104	40.3	4.5
C-105	104	6.7
C-112	259	36.9
C-114	170	32.3
Surface waters		
Duke Stream	5.1	0.6
Bulk Storage Stream	2.7	11.6

Location	DIC (Bq L^{-1})	DOC (Bq L^{-1})
Adjacent to swamp		
C-211	204	123
C-212	108	1.6
C-213	1060	26.3
C-214	321	28.1
C-216	308	4.5
C-221	59.4	2.9
C-222	70.7	9.1

Table 12: Raw 2013 data from Napier [2015].

Well	Depth m	CO_2 ppm	Plant Bq gC^{-1}	Water Bq L^{-1}	Gas Bq L^{-1}	DOC mg L^{-1}	DIC mg L^{-1}	Corrected Activity Bq gC^{-1}
8	3.58	8327	0.161	2.3	1.2662	0.67	16.47	0
10	1.62	9178	0.928	2.3	0.2668	1.67	9.1	0.678
11	3.46	5995	0.167	759.6	0.0292	1.53	7.73	0
12	2.01	5514	0.189	2.3	0.153	1.76	2.21	0
13	3.45	7214	0.124	2.3	0.0127	0.91	3.63	0
111	3.53	-	0.364	2.3	0.418	3.71	10.41	0.114
113	3.52	-	0.919	2.3	1.5259	2.32	12.85	0.669
115	3.73	8131	0.345	2.3	0.1483	1.68	11.56	0.095
210†	0	400	3.153	77.7	0	11.46	16.87	2.903
211	3.23	5119	0.254	1990	0.0158	1.91	8.53	0.004
212	2.42	4106	0.462	172.9	0.0073	12.8	14.83	0.212
213	1.79	9566	0.760	2.3	0.0239	11.3	12.06	0.510
214	1.77	4143	0.572	2.3	0.0092	7.73	9.24	0.322
215	2.4	3711	0.463	2.3	0.0042	6.47	12.6	0.213
369	3.56	-	0.172	2.3	0.0503	0.55	11.92	0

Notes: 'Corrected Activity' reflects the plant activity concentration after being corrected for background C-14.
† sample point 210 is within the Duke Swamp itself.

Table 13: Raw 2014 data from Napier [2015].

Well	Depth m	CO_2 ppm	Plant Bq gC^{-1}	Water Bq L^{-1}	Gas Bq L^{-1}	DOC mg L^{-1}	DIC mg L^{-1}	Corrected Activity Bq gC^{-1}
8	3.58	3375	0.170	2.3	0.3299	3.5	18.5	0
10	1.62	3476	0.709	2.3	0.1067	4	22	0.459
11	3.46	3003	0.148	759.6	0.0291	1.8	21.9	0
12	2.01	1403	0.167	2.3	0.312	2.5	17.8	0
13	3.45	2212	0.116	2.3	0.0115	3.2	3.8	0
111	3.53	4596	0.368	2.3	0.8345	4.4	15.2	0.118
113	3.52	426	0.653	2.3	1.9706	4	10.2	0.403
115	3.73	3595	0.373	2.3	0.3733	3.1	11.1	0.123
129	2.3	2945	0.133	2.3	0.0373	1.5	5.8	0
130	3.55	3730	0.115	2.3	0.0056	1.7	8.9	0
131	5.21	4321	0.132	2.3	0.0109	18.1	17.9	0
132	4.77	2449	0.124	950	0.003	3.3	17.4	0
133	1.32	2762	0.199	2.3	0.0219	2.3	11.5	0
134	4.06	3228	0.108	2.3	0.0032	2.7	10.1	0
135	4.05	5648	0.112	492.2	0.018	2.3	17.8	0
210†	0	400	1.751	77.7	0	7.8	16.7	1.501
211	3.23	1690	0.282	1990	0.0233	4.4	28.4	0.032
212	2.42	1980	0.462	172.9	0.1927	12.6	15.2	0.213
213	1.79	1867	0.650	2.3	0.1189	7.6	16.6	0.4
214	1.77	1159	0.893	2.3	0.016	7	13.7	0.643
215	2.4	1795	0.063	2.3	0.0849	9.8	13.7	0
369	3.56	3224	0.096	2.3	0.1115	3.1	6.4	0

Notes: 'Corrected Activity' reflects the plant activity concentration after being corrected for background C-14.
† sample point 210 is within the Duke Swamp itself.

Table 14: Soil gas activity vertical profiles from multi-level sampling at two locations adjacent to Waste Management Area C [Napier, 2015].

Sample	C-14 (Bq L^{-1})
8-A	0.000185*
8-25	0.000792*
8-50	0.001039*
8-75	0.000319*
8-100	0.000525*
8-150	0.000597*
8-200	0.023714
8-356	0.329867
8-500	2.279455

Sample	C-14 (Bq L^{-1})
369-A	0.019691
369-25	0.001862
369-50	0.00215
369-75	0.007119
369-100	0.007634
369-150	0.007387
369-200	0.00537
369-356	0.005576
369-500	0.026286

Note: The sample numbers have the format NNN-DDD, where the first component is the sample location (see Figure 10) and the second is the sample depth in cm; * The minimum detectable activity of these samples is 0.001353 Bq L^{-1}.

Contamination in Duke Swamp

Data contained in Killey et al. [1998] provides information about the 2D profile of C-14 concentrations in groundwater along a transect adjacent to the Duke Swamp boundary, and also 1D profiles of C-14 concentration in the peat at several locations in Duke Swamp. These are shown in Figure 55.

Hardwick [1999] provides C-14 concentrations in sediment samples taken in Duke Swamp in June 1995 (Table 15); note that no uncertainties in measurements are given.

Table 15: Carbon content (% by wt) and C-14 specific activities (Bq kgC^{-1}) in sediment from a sampling campaign in 1995 [Hardwick, 1999].

Location	%C (by wt)	C-14 activity
Fen		
DS1	16.3	15
DS2	44.9	31
DS3	21.4	58
DS4	7.0	36
DS5	39.7	0

Location	%C (by wt)	C-14 activity
Swamp		
DS6	47.1	1368
DS7	42.4	680
DS8	29.6	598
DS9	24.1	251
DS10	21.3	119
DS21	27.7	534
DS22	41.5	706
DS23	38.2	516
DS24	48.8	152
DS25	45.9	322

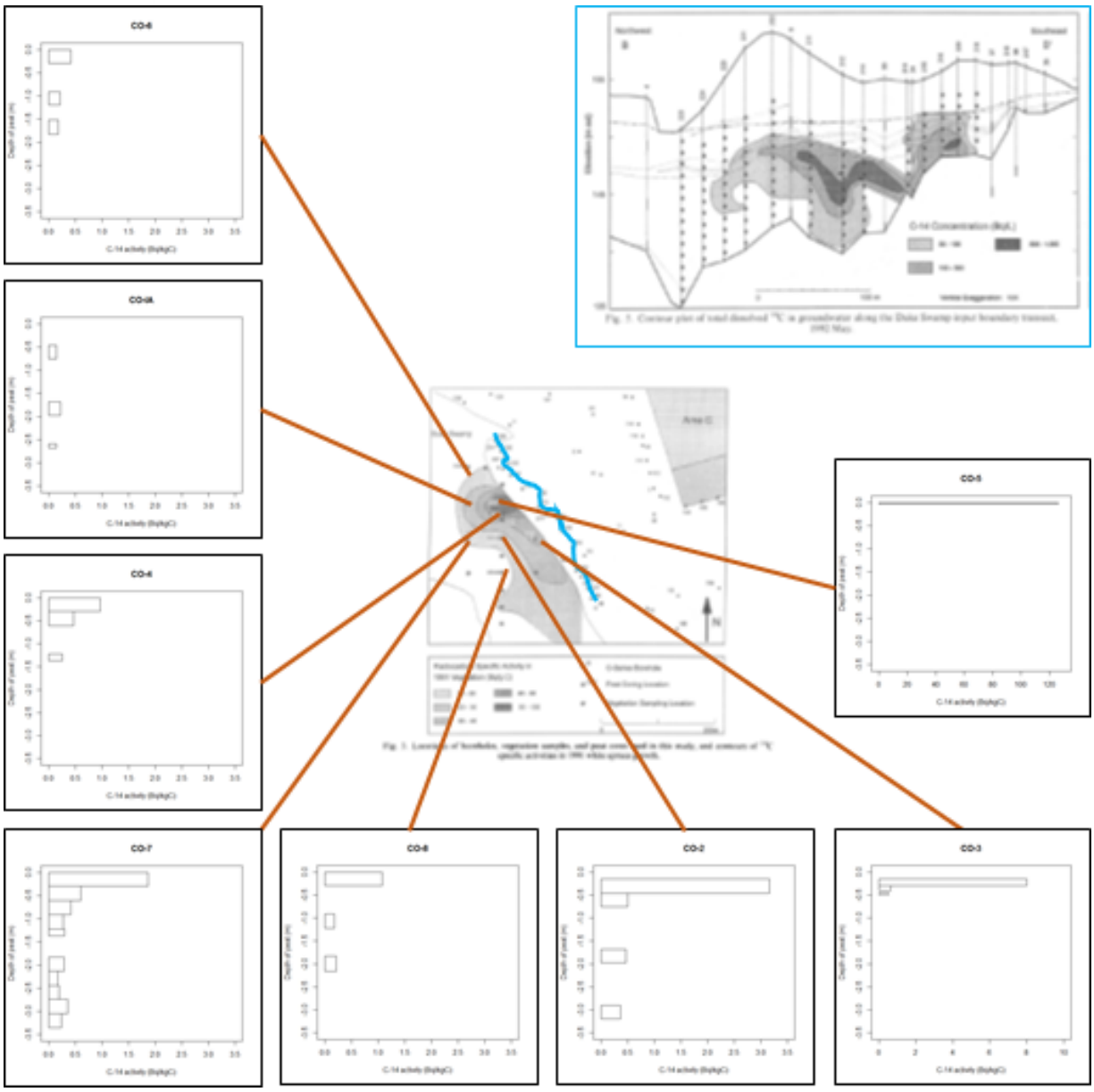

Figure 55: Spatial information about C-14 concentrations in groundwater and peat from Killey et al. [1998]. Groundwater concentrations of C-14 along the transect indicated in blue are shown in the blue box. C-14 concentrations in peat at various locations are also shown, with the brown lines used to highlight their locations. Note that the x-axes for CO-3 and CO-5 are different to the others.

Yankovich et al. [2014] provide C-14 concentrations in Sphagnum moss and sediment samples taken from Duke Swamp in 2011. The sample locations are shown in Figure 25 and the resulting concentrations are given in Table 16. The study found no significant difference between the moss and sediment concentrations. The moss and sediment were found to have water contents of 85% and 54%, respectively. The sediment samples were taken to a depth of about 5 cm at the same locations as the moss samples. The sediment samples were found to be highly organic in nature and principally consist of decaying moss. A background concentration of approximately 250 Bq kgC^{-1} is reported.

Table 16: C-14 specific activities (Bq kgC^{-1}) in Sphagnum moss and associated sediment from a sampling campaign in 2001 [Yankovich et al., 2014]

Location	C-14 specific activity	
	Moss	Sediment
Group 1		
DSS-08	960 ± 100	n.a.
DSS-11	1200 ± 120	n.a.
DSS-12	960 ± 140	n.a.
DSS-14	2000 ± 84	2400 ±180
DSS-15	1100 ± 180	n.a.
DSS-16	630 ± 120	n.a.
DSS-22	380 ± 140	n.a.
DSS-23	290 ± 160	n.a.
DSS-25	160 ± 140	n.a.
DSS-28	8200 ± 200	4200 ± 200
DSS-29	3500 ± 71	1500 ± 82
DSS-30	290 ± 41	2100 ± 57
DSS-31	720 ± 43	280 ± 95
DSS-32	420 ± 43	n.a.
DSS-36	6500 ± 250	5600 ± 250
DSS-38	1800 ± 140	n.a.
DSS-43	3600 ± 310	11,000 ± 210
DSS-45	1000 ± 36	660 ± 150
DSS-46	550 ± 79	n.a.
DSS-47	370 ± 23	n.a.
DSS-49	1800 ± 79	n.a.
DSS-50	2300 ± 110	n.a.
DSS-51	1900 ± 120	n.a.
DSS-56	2800 ± 190	**n.a.**
DSS-57	760 ± 75	n.a.

Location	C-14 specific activity	
	Moss	Sediment
Group 2		
DSS-01	270 ± 120	n.a.
DSS-02	1100 ± 84	n.a.
DSS-04	930 ± 110	n.a.
DSS-09	1600 ± 110	n.a.
DSS-17	980 ± 95	n.a.
DSS-18	690 ± 60	n.a.
DSS-27	17,000 ± 160	38,000 ± 730
DSS-35	47,000 ± 330	n.a.
DSS-42	15,000 ± 240	14,000 ± 130
DSS-48	9200 ± 220	n.a.
DSS-55	5700 ± 160	13,000 ± 250
DSS-56	2800 ± 190	n.a.
DSS-60	3500 ± 98	n.a.
DSS-61	1400 ± 100	n.a.
DSS-64	1100 ± 89	n.a.
DSS-65	1200 ± 90	n.a.
DSS-69	690 ± 69	n.a.
No group		
DSS-03	n.d. (450)	n.a.
DSS-24	n.d. (530)	n.a.
DSS-37	n.d. (860)	n.a.
DSS-39	n.d. (760)	n.a.
DSS-68	n.d. (500)	n.a.

Notes: Taken to be mean ± sigma, where sigma is described as the analytical error. n.d. indicates that detection limit was not exceeded (limit given in brackets).